



저작자표시-비영리-변경금지 2.0 대한민국

이용자는 아래의 조건을 따르는 경우에 한하여 자유롭게

- 이 저작물을 복제, 배포, 전송, 전시, 공연 및 방송할 수 있습니다.

다음과 같은 조건을 따라야 합니다:



저작자표시. 귀하는 원저작자를 표시하여야 합니다.



비영리. 귀하는 이 저작물을 영리 목적으로 이용할 수 없습니다.



변경금지. 귀하는 이 저작물을 개작, 변형 또는 가공할 수 없습니다.

- 귀하는, 이 저작물의 재이용이나 배포의 경우, 이 저작물에 적용된 이용허락조건을 명확하게 나타내어야 합니다.
- 저작권자로부터 별도의 허가를 받으면 이러한 조건들은 적용되지 않습니다.

저작권법에 따른 이용자의 권리는 위의 내용에 의하여 영향을 받지 않습니다.

이것은 [이용허락규약\(Legal Code\)](#)을 이해하기 쉽게 요약한 것입니다.

[Disclaimer](#)

Ph.D. DISSERTATION

**A Fully Implantable Neural Stimulator
for Brain Stimulation of Small Animal**

소형동물의 뇌신경 자극을 위한 완전 이식형 신경자극기

BY

SEUNGHYEON YUN

FEBRUARY 2020

**DEPARTMENT OF ELECTRICAL
AND COMPUTER ENGINEERING
COLLEGE OF ENGINEERING
SEOUL NATIONAL UNIVERSITY**

A Fully Implantable Neural Stimulator for Brain Stimulation of Small Animal

소형동물의 뇌신경 자극을 위한 완전 이식형 신경자극기

지도 교수 김 성 준

이 논문을 공학박사 학위논문으로 제출함

2020년 1월

서울대학교 대학원

전기·정보공학부

윤 승 현

윤 승 현 의 공학박사 학위논문을 인준함

2019 년 12 월

위 원 장 박 병 국 (인)

부위원장 김 성 준 (인)

위 원 장 진 우 (인)

위 원 서 중 모 (인)

위 원 정 준 수 (인)

ABSTRACT

A Fully Implantable Neural Stimulator for Brain Stimulation of Small Animal

Seunghyeon Yun

School of Electrical Engineering and Computer Science

The Graduate School

Seoul National University

In this study, a fully implantable neural stimulator that is designed to stimulate the brain in the small animal is described. Electrical stimulation of the small animal is applicable to pre-clinical study, and behavior study for neuroscience research, etc. Especially, behavior study of the freely moving animal is useful to observe the modulation of sensory and motor functions by the stimulation. It involves conditioning animal's movement response through directional neural stimulation on the region of interest. The main technique that enables such applications is the development of an implantable neural stimulator. Implantable neural stimulator is used to modulate the behavior of the animal, while it ensures the free movement of the animals. Therefore, stable operation *in vivo* and device size are important issues in the design of implantable neural stimulators. Conventional neural stimulators for brain stimulation of small animal are comprised of electrodes implanted in the brain and a pulse generation circuit mounted on the back of the animal. The electrical stimulation generated from the circuit is conveyed to the target region by the electrodes wire-connected with the circuit. The devices are powered by a large battery, and controlled by a microcontroller unit. While it represents a

simple approach, it is subject to various potential risks including short operation time, infection at the wound, mechanical failure of the device, and animals being hindered to move naturally, etc. A neural stimulator that is miniaturized, fully implantable, low-powered, and capable of wireless communication is required.

In this dissertation, a fully implantable stimulator with remote controllability, compact size, and minimal power consumption is suggested for freely moving animal application. The stimulator consists of modular units of surface-type and depth-type arrays for accessing target brain area, package for accommodating the stimulating electronics all of which are assembled after independent fabrication and implantation using customized flat cables and connectors. The electronics in the package contains ZigBee telemetry for low-power wireless communication, inductive link for recharging lithium battery, and an ASIC that generates biphasic pulse for neural stimulation. A dual-mode power-saving scheme with a duty cycling was applied to minimize the power consumption. All modules were packaged using liquid crystal polymer (LCP) to avoid any chemical reaction after implantation.

To evaluate the fabricated stimulator, wireless operation test was conducted. Signal-to-Noise Ratio (SNR) of the ZigBee telemetry were measured, and its communication range and data streaming capacity were tested. The amount of power delivered during the charging session depending on the coil distance was measured. After the evaluation of the device functionality, the stimulator was implanted into rats to train the animals to turn to the left (or right) following a directional cue applied to the barrel cortex. Functionality of the device was also demonstrated in a three-dimensional maze structure, by guiding the rats to navigate better in the maze. Finally, several aspects of the fabricated device were discussed further.

Keywords : neural interface, electrical stimulation; wireless telemetry; implantable neural stimulator; polymer packaging, energy harvesting

Student Number : 2015-20952

Contents

ABSTRACT	i
Contents	iv
List of Figures	ix
List of Tables	xiv
List of Abbreviations	xvi
Chapter 1 : Introduction	1
1.1. Neural Interface.....	2
1.1.1. Concept.....	2
1.1.2. Major Approaches	3
1.2. Neural Stimulator for Animal Brain Stimulation...	5
1.2.1. Concept.....	5
1.2.2. Neural Stimulator for Freely Moving Small Animal	7
1.3. Suggested Approaches	8
1.3.1. Wireless Communication	8
1.3.2. Power Management.....	9
1.3.2.1. Wireless Power Transmission.....	10

1.3.2.2.	Energy Harvesting	10
1.3.3.	Full implantation	14
1.3.3.1.	Polymer Packaging.....	14
1.3.3.2.	Modular Configuration.....	16
1.4.	Objectives of This Dissertation	16
Chapter 2 : Methods		18
2.1.	Overview	19
2.1.1.	Circuit Description	20
2.1.1.1.	Pulse Generator ASIC	21
2.1.1.2.	ZigBee Transceiver	23
2.1.1.3.	Inductive Link	24
2.1.1.4.	Energy Harvester.....	25
2.1.1.5.	Surrounding Circuitries	26
2.1.2.	Software Description.....	27
2.2.	Antenna Design	29
2.2.1.	RF Antenna.....	30
2.2.1.1.	Design of Monopole Antenna	31
2.2.1.2.	FEM Simulation	31
2.2.2.	Inductive Link	36

2.2.2.1.	Design of Coil Antenna	36
2.2.2.2.	FEM Simulation	38
2.3.	Device Fabrication	41
2.3.1.	Circuit Assembly	41
2.3.2.	Packaging	42
2.3.3.	Electrode, Feedthrough, Cable, and Connector.....	43
2.4.	Evaluations	45
2.4.1.	Wireless Operation Test.....	46
2.4.1.1.	Signal-to-Noise Ratio (SNR) Measurement.....	46
2.4.1.2.	Communication Range Test	47
2.4.1.3.	Device Operation Monitoring Test.....	48
2.4.2.	Wireless Power Transmission.....	49
2.4.3.	Electrochemical Measurements <i>In Vitro</i>	50
2.4.4.	Animal Testing <i>In Vivo</i>	52
Chapter 3 : Results.....		57
3.1.	Fabricated System	58
3.2.	Wireless Operation Test	59
3.2.1.	Signal-to-Noise Ratio Measurement	59
3.2.2.	Communication Range Test	61

3.2.3.	Device Operation Monitoring Test.....	62
3.3.	Wireless Power Transmission	64
3.4.	Electrochemical Measurements <i>In Vitro</i>	65
3.5.	Animal Testing <i>In Vivo</i>	67
Chapter 4 : Discussion		73
4.1.	Comparison with Conventional Devices.....	74
4.2.	Safety of Device Operation	76
4.2.1.	Safe Electrical Stimulation	76
4.2.2.	Safe Wireless Power Transmission	80
4.3.	Potential Applications	84
4.4.	Opportunities for Further Improvements	86
4.4.1.	Weight and Size.....	86
4.4.2.	Long-Term Reliability.....	93
Chapter 5 : Conclusion		96
Reference		98
Appendix - Liquid Crystal Polymer (LCP) -Based		
Spinal Cord Stimulator		107

국문 초록138

감사의 글140

List of Figures

Figure 2.1.1. A fully-implantable neural stimulator.	19
Figure 2.1.2. A cross-sectional illustration of the proposed neural stimulator.	20
Figure 2.1.3. A block diagram of the neural stimulator and the external controller	21
Figure 2.2.1. Simulation models of the antennas.....	32
Figure 2.2.2. Impedance characteristics of the inverted L antenna.	34
Figure 2.2.3. Return loss characteristics of the inverted L antenna.	35
Figure 2.2.4. Simulated models of the coils.....	38
Figure 2.2.5. Simulated coupling coefficient and power transmission efficiency of the inductive link according to the design of the receiver coil.	40
Figure 2.3.1. Configuration and the dimension of the assembled components of the neural stimulator..	42
Figure 2.3.2. Fabrication process of LCP-based devices.....	45
Figure 2.4.1. Overview of device behavior monitoring	

experiments.	49
Figure 2.4.2. Simplified inductive link schematic. Experimental conditions are specified in the figure.	50
Figure 2.4.3. Overview of power harvesting experiments of fabricated neural stimulator and biofuel cells (BFC).....	55
Figure 3.1.1. Independently fabricated modules of the neural stimulator.....	58
Figure 3.2.1. Measured SNR for ZigBee communication of the stimulator.....	60
Figure 3.2.2. Test setup of measuring the actual working distance of ZigBee telemetry between the external controller and the neural stimulator.	61
Figure 3.2.3. Experimental setup of the device operation monitoring test, measured waveforms of voltage of the energy storing capacitor of the PMIC and BFC output voltage..	63
Figure 3.3.1. Power received by the stimulator circuit as a function of the coil separation distance.	64
Figure 3.4.1. EIS measurements of the two types of fabricated electrode arrays and biphasic stimulation pulses measured in PBS	

.....	66
Figure 3.5.1. A rat in a Skinner box during the wired test for the determination of the stimulus parameters and number of lever presses versus the MFB stimulation amplitude.....	68
Figure 3.5.2. Surgical implantation of a neural stimulator in a rat	69
Figure 3.5.3. Wireless control of the movement of a rat.....	70
Figure 3.5.4. In vivo energy harvesting experiment setup with biofuel cell (BFC) and waveform of the output voltage of the BFC, and the energy storing capacitor of the PMIC	72
Figure 4.2.1. SAR simulation model.....	81
Figure 4.2.2. Electric field generated by the transmitter coil...	82
Figure 4.2.3. SAR results of the electric field generated by the transmitter coil.....	83
Figure 4.4.1. Simulated result of the placing and routing with reduced ICs and RLCs.....	89
Figure 4.4.2. Simulated models of the coils and simulated coupling coefficient and power transmission efficiency of the inductive link according to the design of the receiver coil	92

Figure 2.1.1.S. A fully-implantable neural stimulation system	114
Figure 2.1.2.S. A block diagram of the neural stimulator and the external device.....	115
Figure 2.2.1.S. Simulation models of the coils with varying shapes and number of turns.....	118
Figure 2.2.2.S. Simulation models of the coils with varying number of turns and 10 mm vertical misalignment adjusted.	120
Figure 2.2.3.S. Simulated coupling coefficient and power transmission efficiency of the inductive link according to the receiver coil design.....	121
Figure 2.3.1.S. Fabrication process of the designed neural stimulator.	123
Figure 2.4.1.S. Simplified schematic of inductive link and neural stimulator. Voltage waveform measuring points are specified in the figure.	124
Figure 2.4.2.S. Experimental setup of the EIS measurement.	125
Figure 3.1.1.S. Fabricated implantable neural stimulator.	127
Figure 3.2.2.S. Circuit examination results: measured voltage ...	

.....	128
Figure 3.2.3.S. EIS measurements of the two types of fabricated electrode arrays	129
Figure 3.2.4.S. Surgical implantation of a neural stimulator in a rat and experimental setup for Von Frey test.....	130
Figure 3.2.5.S. Verification of the spinal cord stimulation effect.	131
Figure 4.3.1.S. Experimental setup of testing fabricated ASIC, chip die of fabricated ASIC, output electrical stimulation pulse.	135

List of Tables

Table 2.2.1. Characteristics of the designed monopolar inverted-L antenna and a commercial dipole antenna	33
Table 2.2.2. Simulated characteristics of the designed coil antenna (receiver) and a commercial coil antenna (transmitter).	41
Table 4.1.1. Comparison of functionalities and performance capabilities of prior arts and this work.....	75
Table 4.2.1. Material properties of the simulation tissue model	82
Table 4.4.1. Original volume of the electrical components that consist the circuitry of the neural stimulator.....	87
Table 4.4.2. Area of the originally used ICs and reference design that minimized the area of the ICs. *The ASIC was fabricated in 0.35 μm HV-CMOS process.	88
Table 4.4.3. Power consumption of the ICs that constituting the neural stimulator circuit.	90
Table 4.4.4. Original volume of the electrical components that consist the circuitry of the neural stimulator.....	92
Table 2.2.1.S. Simulated characteristics of the designed coils.	

.....119

Table 4.3.1.S. Instruction configuration of the fabricated ASIC.

..... 136

List of Abbreviations

Abbreviation	Term
DBS	Deep Brain Stimulation
MFB	Medial Forebrain Bundle
S1	Primary Somatosensory Cortex
LCP	Liquid Crystal Polymer
BFC	Bio-Fuel Cell
ASIC	Application Specific Integrated Circuit
PMIC	Power Management Integrated Circuit
PWM	Pulse Width Modulation
MCU	Micro-Controller Unit
GPIO	General-Purpose Input/Output
IC	Integrated Circuit
ADC	Analog-Digital Converter
UART	Universal Asynchronous Receiver-Transmitter
LCD	Liquid Crystal Display
FEM	Finite Element Method
PCB	Printed Circuit Board
FFC	Flexible Flat Cable
FPCB	Flexible Printed Circuit Board
FPGA	Field-Programmable Gate Array
SNR	Signal-to-Noise Ratio
RSSI	Received Signal Strength Indicator
EIS	Electrochemical Impedance Spectroscopy
CSC	Charge Storage Capacity
PBS	Phosphate Buffered Solution
SAR	Specific Absorption Rate

◆ Note

Some part of this dissertation are extracted and adapted from the journal publications which were published or submitted during the course of the study:

- Seunghyeon Yun, Chin Su Koh, Joonsoo Jeong, Jungmin Seo, Seung-Hee Ahn, Gwang Jin Choi, Shinyong Shim, Jaewoo Shin, Hyun Ho Jung, Jin Woo Chang and Sung June Kim, "Remote-Controlled Fully Implantable Neural Stimulator for Freely Moving Small Animal," *Electronics*, vol. 8, no. 6, p. 706, 2019.

Chapter 1

Introduction

1.1. Neural Interface

1.1.1. Concept

Neural interface is a technology that can exchange information with a neural network. The basic technologies of the neural interface are neural recording, which extracts useful data from the brain, and neural stimulation, which conveys delivers the processed data to the brain [1]. The neural signals from the neural recording embody information about various physiological activities like limb movement, upcoming stroke, etc [2-4]. With adequate data processing, we can translate the signals into useful data and neural stimulation can control body activities like muscle actuation, neural firing inhibition, etc. In short, neural interface has high medical value in that we can have control and utilize the activities occurring in the body. Neural interface that can assist paralyzed patients by enabling them to operate exoskeleton with their own neural activity has been studied, and that conveys visual information to the cerebral cortex to restore vision has been developed [5-8]. Besides, the task of selectively recording brain signals and stimulating the brain nerves is the underlying technology in neuroscience research, and can be used to study many neurological phenomena, including the functions of brain regions and the mechanisms of memory. Operant learning was studied in behavior level with rats, with the electrical stimulation of the primary sensory cortex (S1) to induce virtual touching sensation such that the animals tend to turn in a direction opposite to the sensation and electrical stimulation of medial forebrain bundle (MFB) to elicit sensations of pleasure which could be used as a reward when the rat accomplishes trained motions [9, 10].

1.1.2. Major Approaches

Typical methods for implementing neural stimulation include electric stimulation, optical stimulation, and ultrasonic stimulation. Electric stimulation has been used as a neural stimulation method for a long period, and the efficacy of the electric stimulation was proven in various applications [7, 11-13]. The principle of electrical stimulation is to generate a potential difference across tissues, causing membrane potential changes in the target neuron, thereby generating action potentials [13]. Thanks to the highly developed semiconductor technology, this method can be implemented with a small and low-powered stimulation generating device, which is why this method is most commonly used in the manufacture of implantable neural stimulators [14]. Optical stimulation is a method of stimulating nerves using light emitted from light sources such as LEDs and lasers. There are two ways of implementing this method: irradiating the light directly to nerves, and stimulating biologically treated nerves with certain wavelengths of light. This method can stimulate neural cells more selectively than electric stimulation, but it is not easy to miniaturize the optical stimulation generator because of its high power [15]. Currently, it is mainly used for neuroscience research, and is expected to be used in device such as artificial retina in the future. Ultrasonic stimulation is a method of stimulating nerves using waves generated by piezoelectric transducers, the mechanism of which is known to be related to mechanical or thermal energy transfer [16]. Ultrasonic stimulation is mainly used for non-invasive stimulation using focused ultrasound [17, 18]. Like optical stimulation, high power is required and large stimulation generator is needed [19].

Neural recording technology can be classified into three types according to the

degree of invasiveness. First, non-invasive type is a method that creates no skin break when it is applied. Here includes near-infrared spectroscopy (NIRS) and electroencephalogram (EEG). NIRS is a medical imaging technique that utilizes NIR absorption spectra variation. Increased brain activity demands more oxygen, resulting in increased oxygenated hemoglobin (HbO_2) relative to deoxygenated hemoglobin (HbR) [20]. As their NIR absorption spectra differs, NIRS can detect the active region of the brain with light intensity difference. EEG is a recording technique that uses electrodes on the scalp to obtain spontaneous activity of the brain. It is impossible to record cell-level signal due to the large distance between the signal source and the electrode. Instead, event-related potentials or its spectral content is observed for diagnostic applications [21, 22]. These non-invasive methods are advantageous in that they do not require any surgical procedures, while they lack the ability to extract low level information from the brain.

Partly invasive methods obtain signals from the surface of the brain while they do not damage the brain. Electrocorticogram (ECoG) is a representative example. ECoG records local field potentials and neural spikes by reading the brain signals by placing the electrodes epidurally or subdurally. ECoG can read neural signals in the brain cortex with higher precision than EEG, and can also directly stimulate the brain regions to identify the location of electrodes and transmit information to the brain [23, 24]. However, there are disadvantages that invasive surgery is required and accessible range of the brain is limited to the cortex.

Invasive methods include all manners in which surgery is required to insert the electrode directly into the target site. In general, electrical intracortical recording is used, and electrodes with long shanks are used to reach the target area of the brain [25, 26]. In this method, a signal of the highest accuracy can be obtained by

selectively recording neural signals by direct contact to a target site, and it is also possible to selectively control the operation of a brain by stimulating the target site [27]. However, there is limitation that it requires a fairly invasive surgery, which can damage the brain while inserting the electrode to the target.

1.2. Neural Stimulator for Animal Brain Stimulation

1.2.1. Concept

Neural interface is applied to animals for a variety of neuroscience research purposes, including epilepsy control and animal behavioral learning. Animal brain stimulation is performed primarily by neural stimulators designed based on the electrical intracortical stimulation. The most basic form of neural stimulator consists of an electrode to be implanted and a connector soldered thereto. Phillips used nichrome and stainless steel wires to stimulate various brain regions in chickens [28]. Such stimulators are easy to manufacture, but the electrode is single-channeled, it is manufactured by hand, the uniformity is inferior, and stimulation is available only when a commercial stimulator is connected.

A more advanced form of stimulator consists of an electrode to be implanted and a stimulation pulse generation circuit mounted on the animal body. The electrode is percutaneously connected to the circuit through the skin, and the stimulation pulse generation circuit is controlled by an embedded microcontroller unit (MCU). The built-in MCU reads stimulation timing, parameters, etc. from external data delivered by the RF transceiver over wireless communication, and controls the generation of stimulation pulses accordingly. The circuitry is powered by a battery that is co-mounted on the animal. This design has the meaning of miniaturizing a commercial

stimulator to be mounting it on an animal, introducing wireless communication to widen the behavior radius of the animal, and automating the control of the stimulation circuit. This type of neural stimulator has been successfully applied to pigeons and rats to induce various animal behaviors [29-31]. However, there are some problems with this configuration. First, a wired percutaneous connection of electrode arrays and an external stimulator represents a simpler approach, but it impedes natural behavior of the animal. Large weight and volume of the circuitry also burdens the animals, limiting their movements. Furthermore, the percutaneous connection has potential risk of infection and the circuit is vulnerable to the external mechanical impacts or other environmental influences including animal dropping and water supply.

In order to solve the problems, a fully implantable stimulation system was proposed. The system employs an inductive link to wirelessly transmit data and power to the device that is implanted in the animal. It is also easy to miniaturize the circuit because the internal device does not require a battery. In addition, the circuitry is encapsulated with silicone elastomer to protect it from various environmental effects such as body fluids. Complementing previous problems, the design was evaluated in rats to stimulate the animal's auditory nerves [32, 33]. However, the inductive link has a short distance of wireless transmission, which causes different problems depending on the implementation of the external transmitter. In case the transmitter is implemented as a cage, the distance between the coils are large, and the size of the coils is greatly different, which lead to the low power transmission efficiency. Also, the range of animal behavior is limited to the cage size. When the transmitter is implemented on an animal, the high power of the transmitter requires a large battery, which increases the size and weight of the device, causing similar

problems as before. In addition, the elastomer is easy to handle and provides biocompatible encapsulation, but it cannot protect the device for a long time *in vivo* due to high moisture permeability. Also, its encapsulation is easily damaged for weak mechanical properties.

1.2.2. Neural Stimulator for Freely Moving Small Animal

When a neural stimulation is used for research, it is usually applied to small animals. Small animals such as rats and rabbits are less expensive and more accessible because they are commonly used for various medical studies. However, in order to apply the neural stimulation to small animals, there is a problem that the neural interfaces must also be miniaturized. Bulky devices require a lot of incisions in implantation surgery and it may cause various problems, such as large pressure on the organs or tension applied to the skin, which can lead to necrosis of the tissue. In addition, the high weight of the device burdens the animal, raising the risks of impeding normal activity and exhausting the animal. In addition, these devices require a robust package. When implanted in an animal, the circuit must be protected from the body fluids. When it is mounted on the animal, the animal tries to detach it from the body by scratching or biting the mounted device. The package must be able to protect the device from such mechanical impacts.

Studies such as functional brain mapping through brain stimulation and behavioral response should ensure the free movement of animals. In this case, the device must be designed in a small, fully implantable type and can be driven without additional device mounted on the animal. Also, in the above case a variety of brain areas are targeted. To implement it, the electrode should be easy to surgery and

designed to be specialized for the location of the stimulation.

1.3. Design Concept

The purpose of the neural stimulation system is to access various parts of the brain in real time while it is implanted in a freely moving animal. It can be inferred from section 1.2.1 and 1.2.2 that the system should be designed as fully implantable, driven without any additional device mounted on the animal, and should be miniaturized. Fully implantable device requires methods of transmitting data and power to the implanted device with long communication distance. Also, the encapsulation should be biocompatible and durable. The device should be able to stimulate multiple brain areas, while the surgery does not harm the health of the animal.

1.3.1. Wireless Communication

In devices applied to freely moving animals, wireless communication must ensure long communication distance. In addition, low communication delay and a certain data rate are required to confirm the association between neural stimulation and behavioral response.

Conventional inductive link communication has a low communication distance as low as a few centimeters with a fine data rate which is decided by its operating frequency, but it is greatly affected by environmental factors such as alignment between coils. An alternative technique to increase the communication distance is radio communication. Wi-Fi, Bluetooth, and ZigBee are some of the representing

technologies included in radio communication. It mainly uses the 2.4 GHz industrial, scientific and medical (ISM) radio band. Wi-Fi is a technology that connects electronic devices to a wireless local network area. It has a high data transmission rate and a long communication distance of up to 100 m [34], but consumes high power. Due to these advantages and disadvantages, Wi-Fi is used when a high data rate is required, such as transmitting neural recording data [35, 36]. Bluetooth is a technology that is specialized in the exchange of data between devices over short distances, enabling one-to-one communication via coupling at relatively lower speeds than Wi-Fi. In particular, since it is possible to communicate with a mobile phone, it is easy to implement various functions to help the user's convenience. However, because Bluetooth has a relatively weak output, the quality of communication is affected by the surrounding environment because of the overlap of the communication band with Wi-Fi. Also, it is difficult to implement simultaneous communication with multiple devices, and due to its high power consumption, it is hard to be applied to an implantable device. ZigBee is a low-power wireless communication technology that offers data rates up to 250 kbps and one-to-many communications [34, 37]. ZigBee has a communication distance of 10 ~ 100m, but it can easily implement long-distance communication by relaying communication through node-to-node connection [34, 38]. ZigBee's low power makes it widely used in a variety of medical devices, including implanted blood pressure monitoring devices [39, 40].

1.3.2. Power Management

Most common power supplying methods for implantable devices are inductive

link and battery. Inductive link is used when the implantable device is inserted near the skin and when an external device to wirelessly supply power can be easily and stable mounted nearby. However, in this study, which targets small animals, it is not suitable as the main power source. The battery method does not require external devices and can provide stable power within a stored power. However, the lifetime of the device is limited due to the limitation of power density, and when a primary battery is used, surgery to replace the battery is required for the reuse. In the case of neural stimulators for small animals which are currently aimed at, a battery method that can stably supply power without an external device is suitable as a main power source. To overcome the limitations of the battery-powered system, a battery charging technique using a secondary battery and an inductive link can be applied. With limited use of inductive links to charge the battery in preparation for the experiment, it can provide power that significantly exceeds the battery capacity and within the charging cycle limit of the secondary battery. In addition, an auxiliary power source may be used in case the operation time becomes long. Energy harvesting is a way to obtain power from a number of environmental factors. It is generally difficult to earn high power, but it is expected to increase the operating time of the device by assisting the power supply of the battery.

1.3.2.1. Wireless Power Transmission

Wireless power transfer has been studied as a power supply method for implanted devices. Inductive link is the most common method that can provide wide range of power wirelessly. This method transfers the power by coupling between coils through a magnetic field, thus the geometry of the coils greatly affects the

power transfer efficiency. Implantable devices are generally limited in size and constrained by magnetic field strength. That is, the structure and size of the receiving coil and the output strength of the transmitter are limited. Several studies have been conducted to maximize the efficiency of power transfer within these limits. Zierhofer theoretically showed that the coupling coefficient is maximized when the inner radius of the coil differs from the external radius by some degree [41], and Hmida presents a range of practical parameters for a system that transmits data and power simultaneously [42]. Harrison showed empirically how the coupling coefficient is maximized when the structural components of the coil and the distance between the coils are related to each other [43]. Many of the above studies have suggested that inductive links can be customized according to their requirements and provide a measure of the maximum efficiency that inductives can achieve in limited conditions.

1.3.2.2. Energy Harvesting

Energy harvesting is a technology that converts a certain form of energy in the environment into electrical energy. Various elements, such as kinetic energy, heat and light, can be converted into electrical energy. Piezoelectricity is a representative technology for converting kinetic energy into electrical energy. Certain materials like quarts cause voltage differences across their structures from mechanical stress. The voltage difference is due to the change in their molecular structure. The energy available to harvest is typically less than a few milliwatts, and it is strongly influenced by external conditions such as the strength of the applied force [44]. There is a neural stimulation devices that uses piezoelectric power, but only laboratory demonstration using finger force was evaluated [45]. In the case of thermoelectric

elements, thermal energy is converted into electrical energy using a thermoelectric phenomenon. The electrical energy is produced in proportion to the temperature difference between the two ends, but the efficiency is not good, it only harvests a few microwatts of energy in a typical environment [44]. It is rather used as a neural cooler, using reverse thermoelectric effect [46, 47]. It is hard to apply those sources to implantable medical devices. Implantable medical devices need reliable power source which is little influenced by environmental factors. Since the above technologies are affected by external force or ambient temperature, they are not good power sources for this field. Instead, there is a technology that converts bioenergy into electrical energy, called biofuel cell (BFC). It obtains electrical energy by oxidizing glucose using an enzyme called glucose oxidase (GOD). As normal animals produce glucose continuously and maintains its concentration at a constant level, BFC is a potent power source that can supply power stably in the body, though the power output levels remain below those needed for practical applications [48, 49].

The energy sources introduced above vary greatly in the power and voltage they produce depending on the environment, and also varies the design of the circuits that harvest and manage these power sources. In general, energy harvesting power sources have low output voltages, and boost regulators are typically used in power management circuits to collect electrical energy from these sources. There are two ways in which the boost regulator works. The first method is maximum power point tracking (MPPT). Energy harvesting power sources are not ideal voltage / current sources, and the output voltage decreases with the amount of output current required. As a result, the product of the output current and the output voltage is shown in the form of a curve that have a maximum point, and the output voltage value at the

maximum point is represented as a constant ratio with the open circuit voltage which varies depending on the type of power source. The open source voltage of the power source is sampled at regular intervals to control MPPT operation of the boost regulator so that the power source can operate at the point it outputs maximum power. Another method is to control the operation of the boost regulator according to the voltage level. Certain energy sources may not recover when it is overloaded. When the open-circuit voltage is constant, the load on the power source can be identified by the level of the output voltage. Based on this, the goal of voltage level control is to harvest power continuously in a safe range. The harvested power is utilized in various ways depending on the operation of the load circuit. The simplest method is to supply the load with the output voltage that is stepped up through the boost regulator or stepped down output voltage. It can be used when the power consumption of the load is very low and continuous power supply is required. Another method is to store the harvested power and then release power to the load when a certain amount of power is collected. When the power required by the circuit is high, the energy harvesting often cannot provide the required power. Circuits using this method store harvested power in a large capacitor during which the load is not powered, or is powered by other power sources such as batteries. After enough power is collected, the capacitor is connected to the load circuit to supply power. It can be applied to circuits that have high power consumption but do not have other main power source and do not require constant power supply. Depending on the type of energy harvester, various types of circuits can be combined to supply energy to the circuits.

1.3.3. Full implantation

Miniaturization and packaging are required for the fully implantable devices. Conventional neural stimulator packaging for humans uses metals such as titanium. However, the metal packaging greatly increases the weight of the device and RF shielding characteristics of the metal package interferes with wireless communication. Polymer packaging is being studied to solve these problems. Polymer packaging is a packaging technology that can be used for various purposes due to its light weight and good RF characteristics. In addition, in order to miniaturize the device, each element of the device must be miniaturized. Since elements such as batteries increase in proportion to the power consumption of the device, there is a limit to the miniaturization of the device. In this case, by modularizing each element of the device, implanting it to the different parts and connecting it in the body, the size of the device to be inserted into each part can be reduced, thereby reducing the damage by the implantation on the subject and making the entire system fully implantable. In this paper, we will explore these polymer packaging and modularization technologies.

1.3.3.1. Polymer Packaging

Packaging of implantable medical devices is largely divided into three types: metal packaging, ceramic packaging, and polymer packaging. Metal packaging is the most reliable packaging method that can protect the circuit from impact, shock, and liquid, etc. However, its RF shielding effect and heavy weight limits the miniaturization of the device and wireless communication. Ceramic packaging is also a resilient package that can block external threats to the circuit. However,

ceramic materials can break when subjected to large impacts, and breaking in the body can cause serious problems. Polymer packaging is most prominent, because it can utilize MEMS technology for polymer coating, it is light-weighted and RF transparent. Precise processes enable the formation of uniform coatings, automation of the process, ease of packaging of wireless communication circuits, and flexible mechanical properties that blend well with biological tissue. However, main disadvantage of the polymer packaging is lack of hermeticity, which limits the lifetime of the package. Various methods have been tried to increase the lifetime of polymer packaging. Material of the package is a key element that determines the hermeticity of the package. Moisture penetration rate is solely decided by the material property, and the fabrication method determines the adhesion between the interfaces.

Representative biocompatible materials used in polymer packaging include silicone elastomers, polyimides, parylene and liquid crystal polymers (LCP). Silicone elastomer is the most basic method, and it can be used in various ways, including spin coating the gel and curing it. It is easy to use with high degree of freedom, but it has weak mechanical property and low water permeability [50, 51]. It is mainly used for the production of short-term test supplies or prototypes such as multi electrode array (MEA) for *in vitro* experiments [52, 53]. Polyimides can be deposited by spin coating and have very stable chemical properties, but still have low moisture permeability[50]. Due to its flexibility and toughness, it is mainly used for manufacturing flexible printed circuit boards and experimental electrodes [54, 55]. Parylene is chemically stable and can be deposited through chemical vapor deposition. It also has a relatively low moisture permeation rate, which may be used in the manufacture of implantable devices [50]. However, due to the high

temperature of the deposition process, it is difficult to be used for packaging circuits including batteries [56]. LCP has flexible but strong mechanical properties, low water penetration, and features MEMS processes [50, 57]. It has been studied as insulating material for electrode of various applications such as retinal implant and deep brain stimulation, and also for packaging of implantable devices [25, 58-60]. Long-term stability was also tested, and the results showed that the LCP package had a life span of 8 years or more [57, 60-62].

1.3.3.2. Modular Design

There are four ways to miniaturize implantable neural stimulators: miniaturization of power supply, circuits, packages, and miniaturization of electrode parts. However, even if each part is miniaturized, the whole device gathered has a certain size or more, and reaches the limit of miniaturization. To make the device smaller, the device can be designed in multiple modules. When divided into several functional pieces, the device can be miniaturized and implanted in each part of the body with less strain on it. In addition, smaller device makes the surgery easier, and it is also possible to design different electrodes to target multiple brain regions. This modularization is based on connection technology. In order to electrically connect each module *in vivo*, a connector and a cable capable of stable connection and waterproofing are required.

1.4. Objectives of This Dissertation

The aim of this study is to demonstrate a novel wireless, fully implantable, and miniaturized neural stimulator system for brain stimulation of small animal. A

rechargeable lithium battery is employed to power ZigBee telemetry and pulse generation circuit of the implanted wireless stimulator for a greater operation range than the conventional inductive link. The battery is charged with an inductive link when the stimulator is not in use by attaching the transmitting coil on the skin above the implant. The problem of a battery-based device is a bulky size of the battery. It is enlarge to increase working time of the device, but it also limits further miniaturization of these devices. We addressed this issue by lowering the power consumption of the neural stimulator using power-saving scheme on the ZigBee-based wireless communication protocol such that a relatively small battery could be used. In addition, power managing circuit was included to support the battery with harvested energy from auxiliary power sources. Also, the implanted part of the device consists of independently fabricated smaller sub-parts of microelectrode arrays and a circuit package which are implanted separately and interconnected via flexible cables and connectors. This modular design makes the surgical implantation easier and provides more flexibility with regard to the selection of the implant location, thus reducing the “effective” size of the devices. The entire electronics is packaged by a biocompatible material that is called liquid crystal polymer (LCP), which has very low moisture absorption rate compared to conventional polymers such as polyimide, parylene or silicon elastomers. Instead of the previously reported LCP packaging process of pressing the entire area of the encapsulation [30], a new packaging method was developed which involved applying localized heat and pressure to bond the surrounding lids together to prevent the excessive heating of the battery while packaging process.

Chapter 2

Methods

2.1. Overview

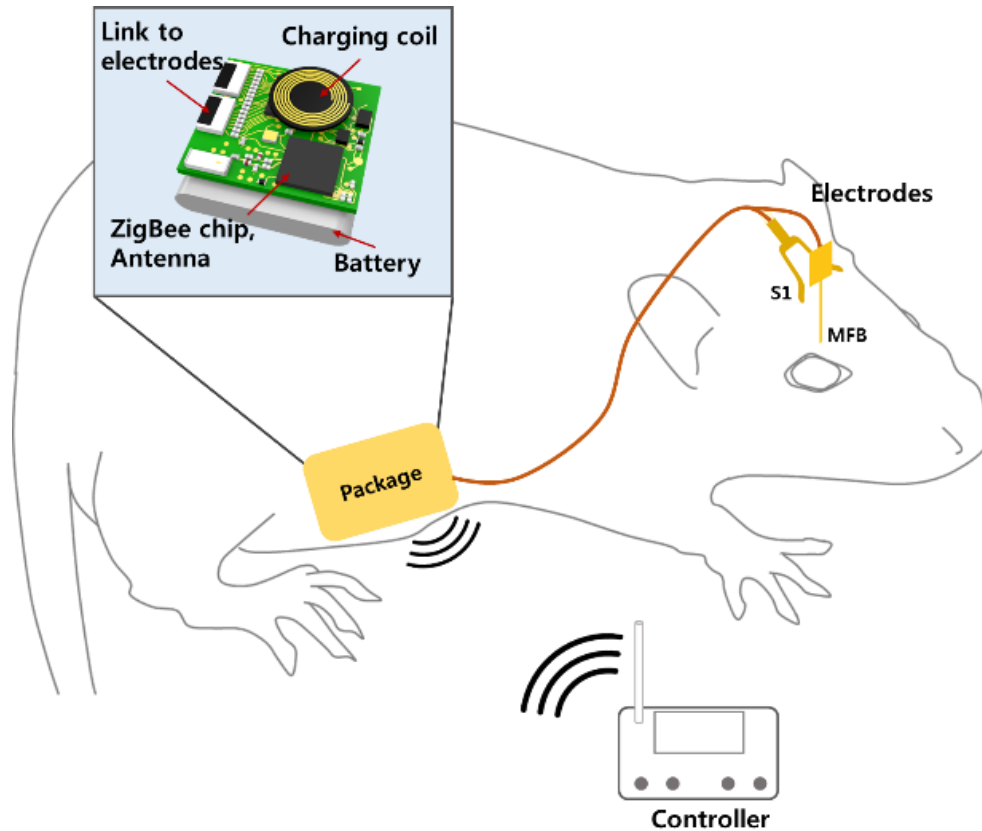


Figure 2.1.1. A fully-implantable neural stimulator: a surface array for S1 stimulation, a depth array for MFB stimulation, a package encasing the stimulating electronics and wireless module to produce stimulation pulses by means of wireless control from an external controller.

The cortical stimulating system consists of an implanted stimulator and an external controller, as shown in Figure 2.1.1. The implanted stimulator is modularly designed, which includes package, electrode, cables, and connectors. The circuitry for neural stimulation, wireless communication and power supplement including a lithium battery and a coil for inductive link charging is enclosed in the package. The implanted electronics is encapsulated by an LCP package with a microfabricated feedthrough protruding from the package for interconnections with electrode arrays and energy harvester via customized cables and connectors, as illustrated in Figure

2.1.2.

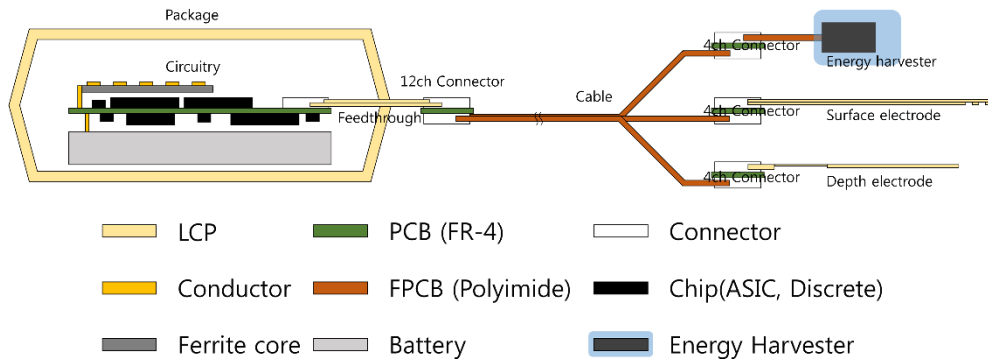


Figure 2.1.2. A cross-sectional illustration of the proposed neural stimulator.

The stimulating electrode array has two parts: a four-channel surface-type array and a four-channel depth-type array for accessing the primary somatosensory cortex (S1) and the MFB, respectively. The Y-shaped surface electrode has two arms that can target the left and the right somatosensory cortices, each with two electrodes for bipolar stimulation. The depth-type array has four electrode sites linearly positioned at the tip of the shank with a spacing of 0.25 mm, two of which can adaptively be paired for precisely targeted bipolar stimulation of the MFB to evoke a sense of reward [26].

2.1.1. Circuit Description

A pulse generation application specific integrated circuit (ASIC) is used to make electrical stimulation of neurons, and the ASIC is controlled by the external controller which sends the stimulation parameters (channel configuration, pulse amplitude, pulse width and pulse rate) and on/off commands via 2.4 GHz ZigBee telemetry. The received data is pulse-width modulated before being fed into an application-specific integrated circuit (ASIC) that generates biphasic current pulses

with the desired parameters and channel configuration. To power the ASIC and the ZigBee transceiver inside the package, a 3.7 V lithium battery (TW302020, The Han, Korea) is embedded; this battery can be wirelessly charged via an inductive link at 2.5 MHz. The charging and discharging processes of the battery and the energy harvesting process are regulated by a power management IC (BQ25505, Texas Instruments, USA).

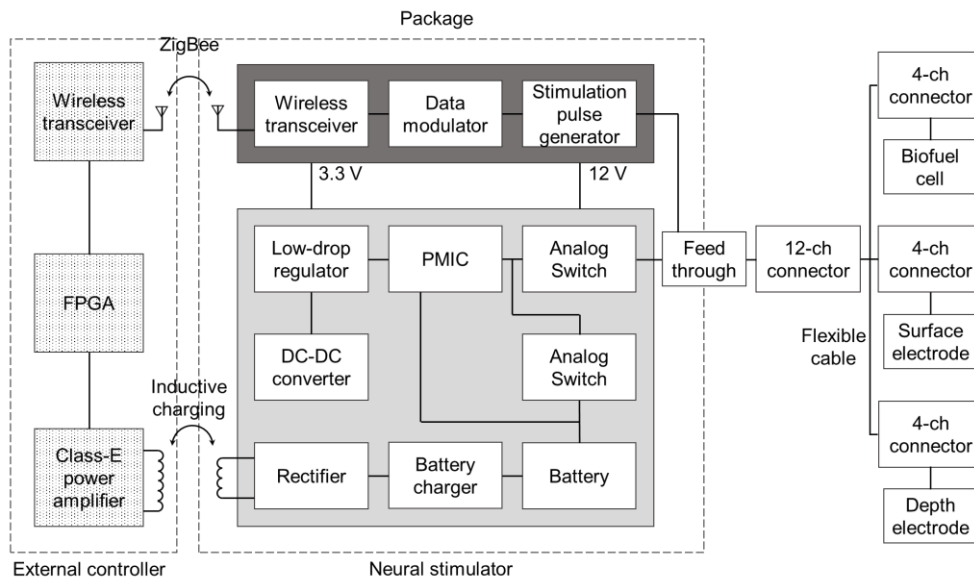


Figure 2.1.3. A block diagram of the neural stimulator and the external controller

2.1.1.1. Pulse Generator ASIC

The ASIC is an electrical pulse generator which was designed in AMS 0.35 μm HV-CMOS, for general purpose neural stimulation [63]. The clock frequency of the ASIC can be modulated with input clock signal, therefore it can generate wide frequency range of electrical pulses. Also, continuous interleaved sampling (CIS) is applied to the pulse generation circuit, enabling the electrical pulses from the ASIC to stimulate more selectively when targeting multiple brain areas. The ASIC contains

4 current sources, and each current source has 4 stimulation channels, for a total of 16 stimulation channels. Two channels that share the current source can be selected to generate bipolar pulses, or one channel and a reference channel of the current source can be chosen to generate monopolar pulses. The electrical stimulation pulses can be varied in 4 ways: pulse rate, pulse duration, current amplitude, and channel selection. These parameters are controlled by external data input, in range of 20~230 Hz, 10~630 μ s, 0.01~10.23 mA each with ASIC input clock of 100 kHz. The data is sent in form of pulse width modulation, with each pulse being comprised of multiple small pulses, representing '0', '1', and frame bit according to the number of the small pulses. The frequency of the small pulses is originally intended to be a carrier frequency of the inductive link, but as we use ZigBee telemetry to send data wirelessly, it is arbitrarily set to 2.5 MHz. As maximum number of small pulses per a bit is 20, data rate becomes 125 kbps. The ASIC is largely divided into two parts: analog circuit part and digital circuit part. Analog part is a set of digital-analog converters (DAC) in multiple H-bridge form. Each bridge end connected stimulation channel, and DAC generates stimulation pulse in accordance with control signals from the digital circuit. As the maximum output voltage of the analog circuit is limited to compliance voltage, its load impedance determines the maximum output current. The digital part, consists of data receiver, data decoder, and timing controller. Data receiver demodulate PWM signals to command set, and data decoder translate the commands bitwise to store information about the intensity and period of the stimulation pulse. Timing controller generates the control signal for adjusting pulse generation in accordance with the stored data.

In this application, 8 stimulation channels were utilized to stimulate three brain regions, left/right barrel cortex of S1, and MFB. The channels are connected to the

electrodes through a feedthrough, a flexible cable, and connectors. Input clock frequency was 100 kHz, in order to provide pulse rate near 200 Hz [9]. Power lines of 3.3 V (VDD) and 12 V (VDDH) are connected to provide required power to digital part and analog part. VDD is created with commercial step-down regulator (NCP71533, On Semiconductor, USA) from the battery voltage. It is further fed to boost converter (TPS61041, Texas Instruments, USA) to generate VDDH.

2.1.1.2. ZigBee Transceiver

The ZigBee transceiver is a mixed signal circuit which consists of an RF transceiver module and a Microcontroller Unit (MCU) that controls RF communication according to the ZigBee protocol. Here we utilized commercial transceiver CC2530 model (Texas Instruments, USA). The transceiver include flash memory that can be easily reprogrammed through C language-based interface (IAR Embedded Workbench for 8051, IAR Systems, Sweden), so that the user can change the operation algorithm of the Integrated Circuit (IC) usefully according to the intention. The RF module of the transceiver is connected with external antenna. It can transform initial data into complex signals to transmit in compliance with the IEEE 802.15.4 standard, and receive over-the-air data to store in radio RAM [64]. The module provides the interface between the MCU and the radio, so that the radio events are controlled by the user programming. The MCU, running at 32 MHz, can receive wirelessly retrieved data and process it with basic instruction sets that also is programmed through C language-based interface. Also, it can control various peripheral circuit integrated in the IC, including general-purpose input/output (GPIO), Analog-Digital Converter (ADC), universal asynchronous receiver-

transmitter (UART), etc.

In this application, the transceiver inside the package of neural stimulator is programmed to receive data from the transceiver of the external controller. The received data is output serially through a GPIO as PWM. The generated PWM signal is modulated with 2.5 MHz oscillator and 2-bit AND gate to be sent to the stimulation ASIC. Also, in combination with large-resistors-made voltage dividers, the 12-bit ADCs measures output voltage of battery, energy harvester, and power management integrated circuit (PMIC). The measured data is sent to computer through external ZigBee receiver circuit, which is connected to computer via UART.

2.1.1.3. Inductive Link

The inductive link is used to charge the lithium battery embedded in the package of the neural stimulator. The transmitting circuit consists of a conventional class-e amplifier and a commercial coil, mounted on the external controller as shown in Figure 2.1.3. The receiving circuit includes a receiver coil, a rectifier, a Zener diode and a battery protection IC. The carrier frequency is 2.5 MHz, and the parallel capacitor of the coil was connected to the receiver coil to tune the resonance frequency. The value of the capacitor was determined by the following equation:

$$C_p = \frac{1}{\omega^2 L_R}$$

where ω is the resonance frequency and L_R is the inductance of the receiver coil. The output of the rectifier was connected with Zener diode, which clamps the voltage not to exceed the maximum input level of the battery protection IC. The battery protection IC limits charging current, and stops charging when the battery voltage is higher than 4.2 V, protecting it from being overcharged.

2.1.1.4. Energy Harvester

The package contains PMIC (bq25505, Texas Instruments, USA) to utilize retrieved energy from low-power energy harvester. The circuitry of the PMIC can work alone with energy harvester, not requiring any secondary power sources. When an energy harvester is first connected, the boost charger of the PMIC charges output capacitor to above 0.6 V, so that the other parts of the circuitry of PMIC could be powered (cold start). After, it charge output capacitor, storing the energy from the energy harvester[65]. The charging operation is optimized with maximum power point tracking (MPPT). Generally, energy harvesters have a condition that can output maximum power. As they are not ideal sources, their output voltage decreases as required output current increases. Therefore there is some point that their multiple of their output voltage and current is at its maximum. The ratio of the open circuit voltage (OCV) and the output voltage where the power is maximized differs with the type of energy harvester. If the value is specified, the PMIC samples OCV of the energy harvester and control the operation speed of the boost charger so that the maximum energy could be earned from the energy harvester. In this way, when the voltage of the capacitor reaches high voltage, then the capacitor is connected to the circuit load to supply power. If there is a battery connected, it can switch the source that supplies power to the load using external MOSFET switch so that the load is powered continuously. When the voltage of the capacitor reaches low voltage, the capacitor is disconnected from the load, and begins to be charged again. The operation of the PMIC, like ratio of MPPT, low and high voltage of the capacitor, etc., can be programmed with externally connected resistors.

In this application, a biofuel-cell (BFC) was used as an energy harvester. BFC is a device that obtains energy by oxidizing glucose in the body. Energy harvesters require special conditions (temperature differences, constant mechanical stress, etc.) but these environments are generally difficult to retain in the body. On the other hand, since glucose is an easily obtained element in the body, BFC can continuously receive the necessary requirements in the body. Therefore, it is suitable for an energy harvester that is implanted with a neural stimulator and continuously replenish the power. When it is connected to the neural stimulator, BFC is harvested in 80 % OCV condition. As shown in Figure 2.1.3, it is connected to PMIC via an analog switch, which is controlled by ZigBee transceiver. It is disconnected when the stimulator is off so that it can recover its energy by mass transfer.

2.1.1.5. Surrounding Circuitries

Surrounding circuitries include an external controller and a ZigBee receiver circuit. The external controller was designed and fabricated by Shinyong Shim in Department of Electrical and Computer Engineering, College of Engineering, Seoul National University [66]. The external controller consists of a class-E amplifier for inductive charging, a custom programmed field-programmable gate array (FPGA; SPARTAN3A, Xilinx, USA) that configure the user interface and pass information to the ZigBee transceiver, and ZigBee transceiver for wirelessly sending ASIC commands to the neural stimulator [66]. The ZigBee transceiver on the controller receives data that contain battery voltage level and it is indicated by the lighting of the light-emitting diodes (LEDs) that the user can intuitively check the battery level.

The ZigBee receiver circuit is a commercially available circuit to test the

functionality of the ZigBee transceiver of CC2530 model. It consists of detachable ZigBee module, programming interface, liquid crystal display (LCD), UART interface, and other user-friendly components. In this application, the ZigBee transceiver retrieves the measurement data and outputs it to the LCD. Also, it communicates with a computer via an UART so that the data can be stored and processed with the computer.

2.1.2. Software Description

Customized software controls the operation of the ZigBee transceivers in the neural stimulator, the external controller, and the ZigBee receiver. The software is programmed through C language-based interface (IAR Embedded Workbench for 8051, IAR Systems, Sweden).

Sleep mode was adopted to minimized power consumption of the transceiver, especially the one in the neural stimulator. The power consumption of the transceiver in active mode is about 96 mW, which is too large for the use in implantable devices given that the power of the stimulation ASIC is at the microwatt level. When the transceiver is in sleep mode, it can turn off all circuit parts including RF module and MCU, except for sleep timer, so that interrupt signal from the timer turns on the circuit after a certain time. In this way, the power consumption of the transceiver is lowered to about 3 μ W when it is in the sleep mode. The transceiver in the neural stimulator was programmed to alternate between the active mode and the sleep mode at the duration of 100 ms and 10 ms respectively, resulting in reduction of power consumption to nearly a tenth of that when it is fully active. The RF module of is deactivated in the sleep mode, the transceiver cannot use ZigBee telemetry for 100

ms out of 110 ms, in average. Therefore the cost of the sleep mode is a latency of communication up to 110 ms. The average latency of the command initiation in the external controller and the pulse generation is about 60 ms, which is sum of half the cycle of two alternating modes and ZigBee communication delay of about 5 ms. In this application, it is in acceptable range when considering that it is less than 10 % of the whole time for animal to be stimulated and to respond.

A command instruction is 17 bit word, including one frame bit. It is split in half, frame bit removed, then stored in the transmission buffer. When the command data from the controller is received, it is stored in 8bit radio registers. MCU recovers original 17 bit instructions from the stored data, and output the instructions serially using GPIO. The instructions are sequentially expressed as PWM. The duty cycle of '1', frame bit, and '0' are 75 %, 50 %, and 25 %, respectively. The duration of high and low for each bit is controlled using preset idle instructions of MCU. The instructions consists of 14 type commands, which are one for stimulation frequency setting, four for duration setting of each current source, four for stimulation amplitude setting of each current source, four for stimulation channel setting of each current source, and one for stimulation on command. Since the stimulation in this application requires 0.5 s burst stimulation, stimulation off command is sent to ASIC after that. Each bit of the instruction requires 8 μ s, and maximum required time for command transfer is about 1.9 ms.

While in active mode, the transceiver in the neural stimulator performs two tasks. One is to check whether there is data from the controller and send the data to the ASIC. The other is the measurement function described below. After the implantation, the user needs a way to check that the implanted device is ready for normal operation. Generally, power source verification is the easiest way to figure it

out. The ADC in the transceiver can measure voltage between 0 V and 1.25 V versus ground. The voltage dividers in the circuit modulate the amplitude of the voltage of the battery and the BFC, and other measuring points. The MCU controls the ADCs to sample them in 12 bit form, and fit them into 8 bit radio registers to send to the external controller and the ZigBee receiver circuit. In the receiver circuit, the data are modulated according to the preset calibration, and averaged to remove thermal noise. The data are displayed on the LCD, and transmitted to computer through UART.

The transceiver in the controller communicates with two device, the FPGA on the controller and the transceiver in the neural stimulator. It exchange data with the FPGA using handshaking method. One request pin (REQ), one acknowledge pin (ACK), and four parallel data pins (DATA) of total six GPIO pins are utilized. First, the transceiver sets REQ high and wait for the DATA and ACK. When the FPGA reads it, FPGA prepares the DATA and sets ACK high when DATA is stabilized. The transceiver reads the ACK, stores the DATA, sets REQ low, and wait for ACK. FPGA reads the REQ, and sets the ACK low, which means one cycle of the handshaking is finished.

2.2. Antenna Design

Antennas for ZigBee telemetry and inductive link was designed and simulated. Antenna size is one of the important factors in determining the size of the implanted neural stimulator, while it is critical factor that determines efficiency of the communication. A common design goal is to miniaturize the size of the antenna while keeping performance within the available range. It is assumed that the size of

the package is about 25 mm x 25 mm x 10 mm or less, and there must be space for the circuit and the battery inside.

2.2.1. RF Antenna

Size of the implantable device affects device design, implantable location, user discomfort, surgery, etc. Therefore the most important point in the application of RF communication to implantable devices is the size of the RF circuit. In implementing RF communication, the most important part in determining the size is its antenna. The size of the antenna is proportional to the wavelength and has a major influence on the frequency characteristic and gain of the antenna. In order to apply the antenna to the implantable medical device, various studies for miniaturization of the antenna have been conducted. Various structures, such as patch type, chip type, and cylindrical type, have been investigated, and have shown its performance at or above the commercial antenna level in the industrial, scientific and medical bands (ISM) [67-69]. However, the size of the antenna is still larger than the size of state-of-the-art implantable devices [40, 70], and its fixed structure cause it difficult to deform into a shape suitable for the target device to be applied. For example, four main types of wire antennas are usually used: straight, inverted-L, intermediate-fed, and inverted-F. Intermediate-fed antennas and inverted-F antennas have the advantage that the impedance of the antenna can be adjusted by the length of the line connected to the ground plane [69, 71, 72]. However, multiple lines are required and the required area is large, making it difficult to apply to the implantable devices.

Monopole inverted L-type antennas can be a good way to reduce the volume of antennas. The antenna of this structure is easy to implement and test as it can be

easily fabricated using a commercial wire, and its floating structure on the substrate does not occupy much area/volume. In addition, it is advantageous in that it is easy to manufacture a structure suitable for the target device by adjusting the length ratio of conductor lines [73].

2.2.1.1. Design of Monopole Antenna

The center frequency of ZigBee communication is 2.45 GHz and the channel bandwidth is about 2 MHz, distributed at 5 MHz intervals [34]. Accordingly, the wavelength length λ is about 12.5 cm, and the standard length of the antenna is determined as $\lambda / 4$ considering the size of the package of the neural stimulator. The structure of an inverted L-type antenna is determined by the length of the L-type, the ratio of the width and height of the conductor, and the radius of the conductor. Among them, the ratio of width and height to the bending point is an important factor in determining the resonance frequency and directionality of the Inverted-L antenna [73]. Also, the length of the antenna is expected to critically determine the resonance frequency, and its conductor radius is expected to affect its impedance.

2.2.1.2. FEM Simulation

The characteristics change according to the structure of the inverted L antenna was analyzed by computer simulation software (ANSYS Electronics Desktop, ANSYS Inc., USA). The return loss, impedance, and the gain of the antenna along direction were investigated according to the variation of the length (l) of the antenna, the length ratio (width (a), height (b)) of the conductor, and the radius (r) of the conductor with target frequency of 2.45 GHz. The models of the antenna was built

as shown in Figure 2.2.1.

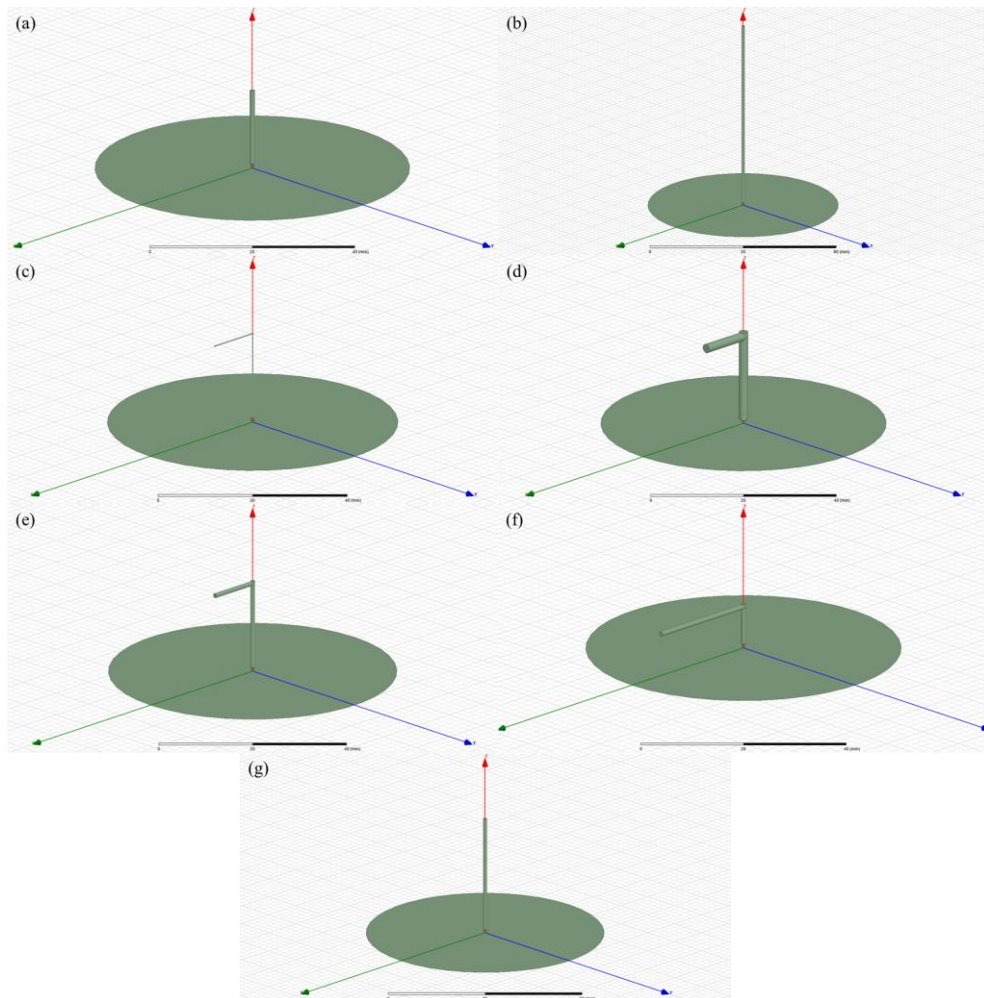


Figure 2.2.1. Simulation models of the antennas. (a) $l = 0.125 \lambda$, $a:b = \text{control}$ (straight), $r = 0.5 \text{ mm}$, (b) $l = 0.5 \lambda$, $a:b = \text{control}$ (straight), $r = 0.5 \text{ mm}$, (c) $l = 0.25 \lambda$, $a:b = 3:5$, $r = 0.125 \text{ mm}$, (d) $l = 0.25 \lambda$, $a:b = 3:5$, $r = 1 \text{ mm}$, (e) $l = 0.25 \lambda$, $a:b = 2:6$, $r = 0.5 \text{ mm}$, (f) $l = 0.25 \lambda$, $a:b = 6:2$, $r = 0.5 \text{ mm}$, (g) $l = 0.25 \lambda$, $a:b = \text{control}$ (straight), $r = 0.5 \text{ mm}$.

Figure 2.2.3 shows the return loss of the antenna according to the length of the inverted L antenna, the ratio of each conductor, and the radius of the conductor. It can be found in Figure 2.2.2 (a) that the frequency of the minimum return loss varies greatly with the length of the antenna, and the minimum return loss is at 2.29 GHz where the antenna length is 1/4 of the wavelength. Based on the result, the antenna length was set to 1/4 of the wavelength, and the simulation was performed according

to the length ratio of the conductors. As a result, the return loss was decreased and the resonance frequency of the antenna was increased slightly as the height ratio of the antenna declined. Also, it was confirmed that the radiation pattern of the antenna changes evenly as the width ratio of the antenna length increases. As the radius of antenna lead increased from 0.125 mm to 1 mm, the resonant frequency and return loss did not show much difference. Instead, as shown in Figure 2.2.2 (e-f) and Figure 2.2.3 (c), the absolute value of the impedance increased by about 8.7% and the bandwidth increased from about 140 MHz to 220 MHz. Considering the results, the length ratio of 3:5 for least return loss in 2.4 GHz, and the radius of the conductor of 0.125 mm that the bandwidth covers the whole ZigBee frequency range was selected, as shown in Table 2.2.1. It is shown that the performance of the designed antenna is slightly lower than the commercial antenna, and the antenna volume is about 13.9% of the commercial antenna, which can be inferred that the antenna were successfully miniaturized, with greater structural tunability.

Antenna Specification	Designed Monopolar Inverted-L Antenna (Implant Side)	Commercial Chip Antenna (Controller Side)
Center Frequency (MHz)	2400	2450
Bandwidth (MHz)	150	265
Length (mm)	31.25	5
Length Ratio (Width: Vertical)	3:5	Not Available
Radius (mm)	0.125	2 (width, rectangular)
Volume (mm ³)	1.53	11
Weight (g)	0.015	0.04
Return Loss at Center Frequency (dB)	-11.5	-25.384

Table 2.2.1. Characteristics of the designed monopolar inverted-L antenna and a commercial dipole antenna.

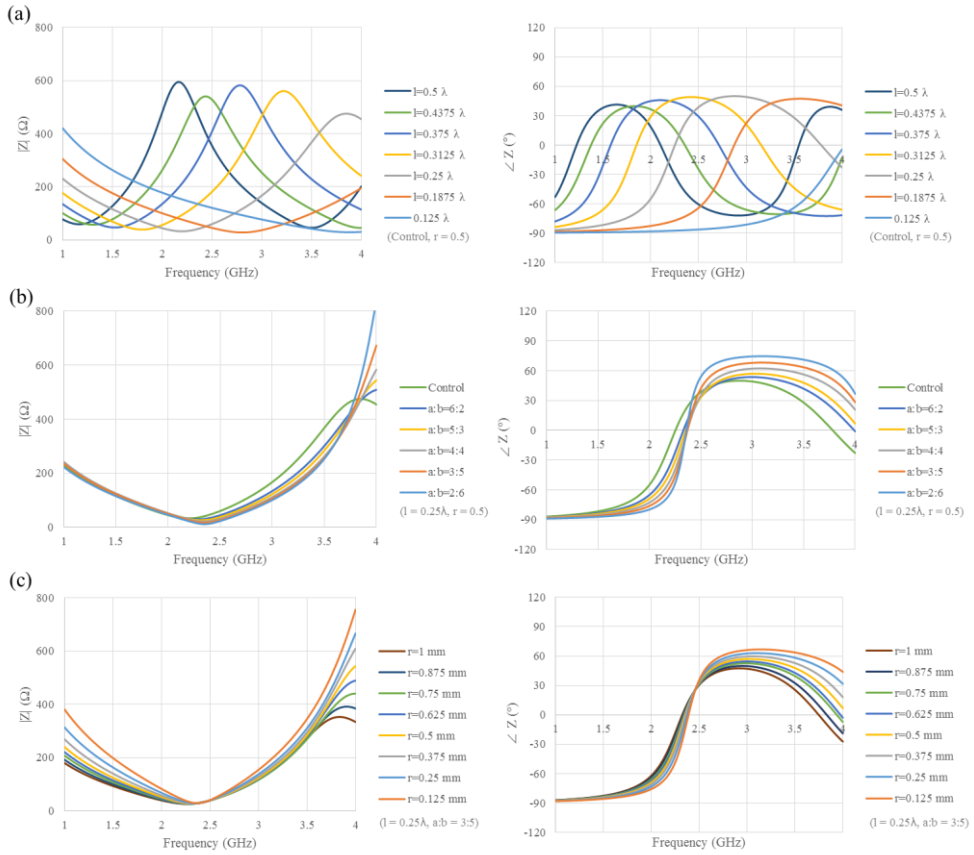


Figure 2.2.2. Impedance characteristics of the inverted L antenna according to (a) length, (b) length ratio of the conductor lines, and (c) the radius of the conductor. A straight antenna was set as a control of the length ratio simulation.

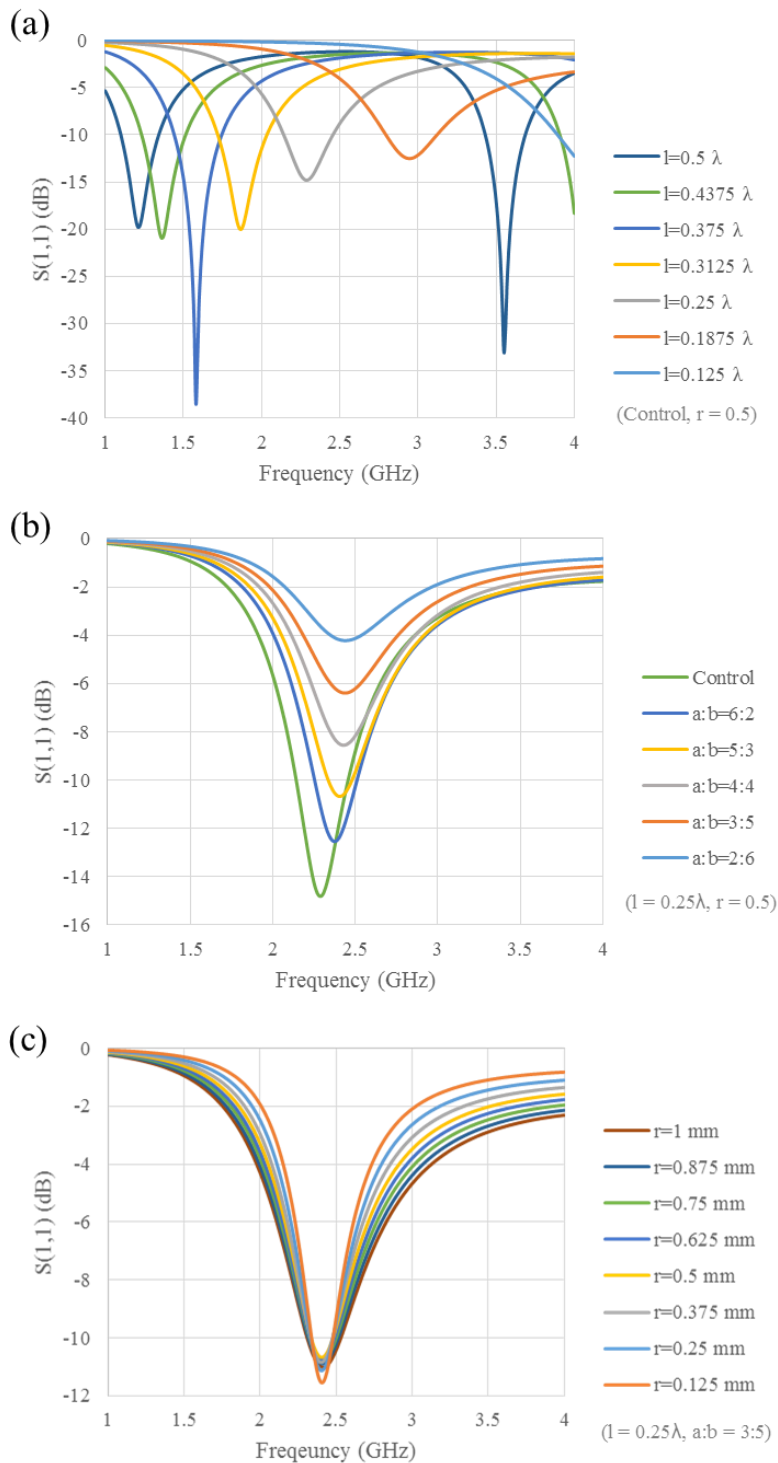


Figure 2.2.3. Return loss characteristics of the inverted L antenna according to (a) length, (b) length ratio of the conductor lines, and (c) the radius of the conductor. A straight antenna was set as a control of the length ratio simulation.

2.2.2. Inductive Link

Wireless power transfer is one of the technologies used to power implanted neural stimulators. An inductive link method using mutual induction between coils is widely used [59, 74]. The inductive link is a method of transmitting power at a short distance of several cm or less. The inductive link consists of an amplifier, transmitting coil, tuning RC as transmitter part, and a receiving coil, tuning RC, and a load circuitry as receiver part. If the distance between the coils increases, the power transmission efficiency decreases drastically[43]. Therefore, the coil parts of the power transmission device is designed to be fixed as close as possible to the receiver. Their coupling is also a critical factor which is determined by geometric properties of the coils. Circuit design is also an important issue. An amplifier with high efficiency is required, and the load impedance that receives the transmitted power also can affect the Q factor of the circuit. Based on the direction of increasing the power transmission efficiency, when data is transmitted together, it is designed to consider the bandwidth or reduce the influence of misalignment according to the environment. As an example, Ali designed a coil with an inductance of 8 μH and an outer diameter of 6.3 mm, based on the criteria for setting the outer / inner diameter ratio of the coil to 0.4 and limiting the coupling constant to 0.4 or less for stable transmission of data, achieved the power transmission efficiency of approximately 40% [75].

2.2.2.1. Design of Coil Antenna

When applying it to an implantable device, the size of the receiving coil is limited for the small device volume. The size and the structure of the receiving coil

and the transmitting coil are closely related to the power transmission efficiency, and studies have been conducted to design more efficient coils [43, 75, 76]. Coil type is mainly adopted as a planar, spiral coil with advantages of reliable production and magnetic coupling. Coupling coefficient is an important characteristic of the coils that determines the power transmission efficiency. It is calculated with self-inductance and mutual inductance of the coils, which are mainly determined by ratio of internal radius and external radius of the coil, radius of coil, number of turns, and their shapes. It had been shown that the ratio between internal radius and external radius that maximizes coupling coefficient is nearly 0.4 [41, 77]. The radius of the receiver coil is generally limited by the device size, and it should be smaller than the transmitter coil [78]. High number of turns is usually a better option, but it is limited by physical restrictions like line width and line spacing, which also affect the resistance of the coil. The resistance of the coil is mainly affected by material of the line, line width, line thickness, line length, and if any, number of vias. Q factor of the coil is reversely proportional with the resistance, and proportional with frequency, and self-inductance. High Q factor is preferred, but effect of misalignment of the coil is amplified in high-Q-factor circuit. Effect of the misalignment is expected to change according to the shape of the receiver coil. Operating frequency of the coil is also carefully determined. Electromagnetic field (EM) absorption changes according to the operation frequency and dielectric constant, conductivity of the absorbing material. EM absorption rate in log scale frequency was previously investigated, and the lowest absorption rate was observed between 1 MHz and 10 MHz [79]. In this application, the operation frequency of 2.5 MHz which is compatible with the readymade controller device was selected.

2.2.2.2. FEM Simulation

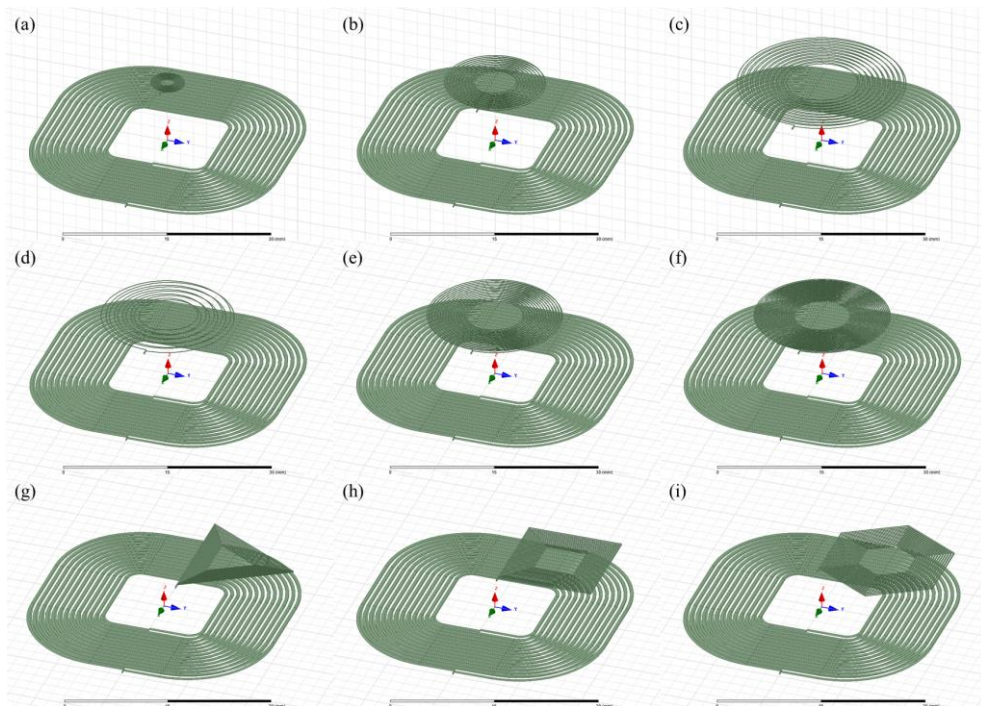


Figure 2.2.4. Simulated models of the coils with varying external radius (a~c, 5 mm, 15 mm, and 25 mm in sequence are shown), number of turns (d~f, 10 turns, 30 turns, and 50 turns in sequence, are shown), shape(g~i, triangle, square, and hexagon in sequence are shown)/10 mm misalignment horizontally.

The characteristics of the two parallel coils according to the structure of the receiver coil was analyzed by computer simulation software (ANSYS Electronics Desktop, ANSYS Inc., USA). The goal of the simulation was to find the receiver coil design that fits the assumed size of the package and maximizes the power transmission efficiency. First, two-layer coil models with diameter of 5 mm to 25 mm in 5 mm increments as receiver coils and a transmitter coil model with 40 mm \times 40 mm area which were fabricated for the practical use [66] were created. Numbers of turns of the coils were controlled as 10, and the ratio of the external radius and the internal radius were maintained at 0.4 to maximize their coupling coefficient. The receiver coil and the transmitter coil were aligned with a 10 mm center distance. The

models used for the simulations are shown in Figure 2.2.4. Self-inductance and resistance of each coil and coupling coefficient at 2.5 MHz were simulated according to the radius of the receiver coil. Their power transmission efficiency were calculated as follows:

$$Q_T = \frac{\omega_0 L_T}{R_T},$$

$$Q_R = \frac{\omega_0 L_R}{R_R},$$

$$Q_R' = \frac{(Q_R^2 R_R) \parallel R_L}{\omega_0 L_R},$$

$$\eta = \frac{(k^2 Q_T Q_R')}{(1 + k^2 Q_T Q_R') \left(1 + \frac{R_L}{Q_R^2 R_R}\right)}$$

where ω_0 is an operation frequency, L_T is a self-inductance of the transmitter coil, R_T is a resistance of the transmitter coil, L_R is a self-inductance of the receiver coil, R_R is a resistance of the receiver coil, Q_T is a quality factor of the transmitter circuit, Q_R is a quality factor of the receiver circuit, Q_R' is a modified quality factor of the receiver circuit with load, and η is a power transmission efficiency when the amplifier is ideal [43]. Equivalent resistance of the stimulator circuit (1 k Ω) was applied as the load resistance.

As shown in Figure 2.2.5 (a), calculated power efficiency increased with larger external radius of the coil. Considering fabrication process margin, radius of 20 mm was selected.

Based on the results, the effect of the number of coil turns was simulated. The number of turns was increased by 10 and maximum number of the turns was 50. The coil with turn number of 40 were simulated to have the highest power transmission efficiency, as shown in Figure 2.2.5 (b).

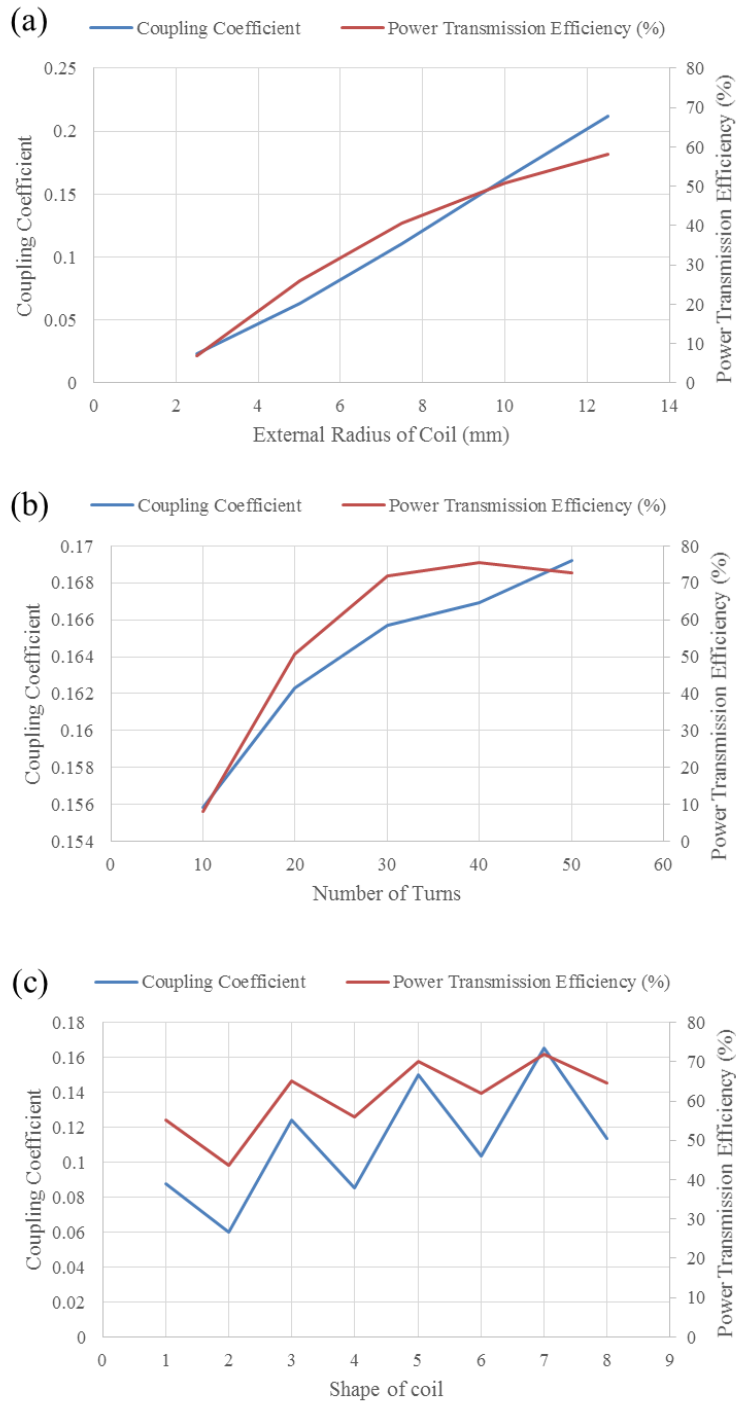


Figure 2.2.5. Simulated coupling coefficient and power transmission efficiency of the inductive link according to the design of the receiver coil: (a) the external radius, (b) number of turns, (c) shape of coil. In (c), 1~8 in x axis represents shape/status of triangle (1), triangle/misaligned (2), square (3), square/misaligned (4), hexagon (5), hexagon/misaligned (6), circle (7), circle/misaligned (8).

Coil shape effects were also simulated. Coil models with the same inner, outer diameters of triangles, squares, hexagons, and circles were created. The case where the horizontal distance between the centers of coils was 0 and 10 mm was compared. Normalized reduction ratio of the transmission efficiency were calculated. Each shape showed the efficiency reduction rate by the misalignment of 0.206 (triangle), 0.143 (square), 0.116 (hexagon) and 0.104 (circle), which can be calculated from Figure 2.2.5 (c). It is shows that the circular coils were most insensitive to misalignment. Considering above simulation results, the characteristics of the receiver coil were designed as Table 2.2.2.

Antenna Specification	Designed Coil Antenna (RX)	Model of Commercial Coil Antenna (TX)
Size (mm ³)	20 × 20 × 0.2	40 × 40 × 0.2
Shape	Circular	Rectangular
Number of turns	20 × 2 layers	13 × 2 layers
Inductance (μH) @ 2.5 MHz	25.3	23.6
Resistance (Ω) @ 2.5 MHz	8.16	5.11
Line width/Spacing (mm)	0.1/0.2	0.45/0.45

Table 2.2.2. Simulated characteristics of the designed coil antenna (receiver) and a commercial coil antenna (transmitter).

2.3. Device Fabrication

2.3.1. Circuit Assembly

A four-layer FR-4 printed circuit board (PCB) was fabricated in size of 20 mm × 18 mm × 0.4 mm. All IC components including the pulse generation ASIC, the ZigBee transceiver and the PMIC were first mounted. ZigBee transceiver was pre-

programmed by a specially customized board that can hold quad flat nonleaded package (QFN) and connect them to the computer via universal serial bus (USB) before being mounted on the stimulator PCB. RLC components were mounted, and a 90 mAh lithium battery (TW302020, The Han, Korea) and a coil (WR202020-18M8-G, TDK corporation, Japan) which fits the simulation results were connected to the PCB through via holes. A monopole, inverted-L antenna was fabricated, and mounted in the simulated structure using the wire with conduction line diameter of 0.6 mm.

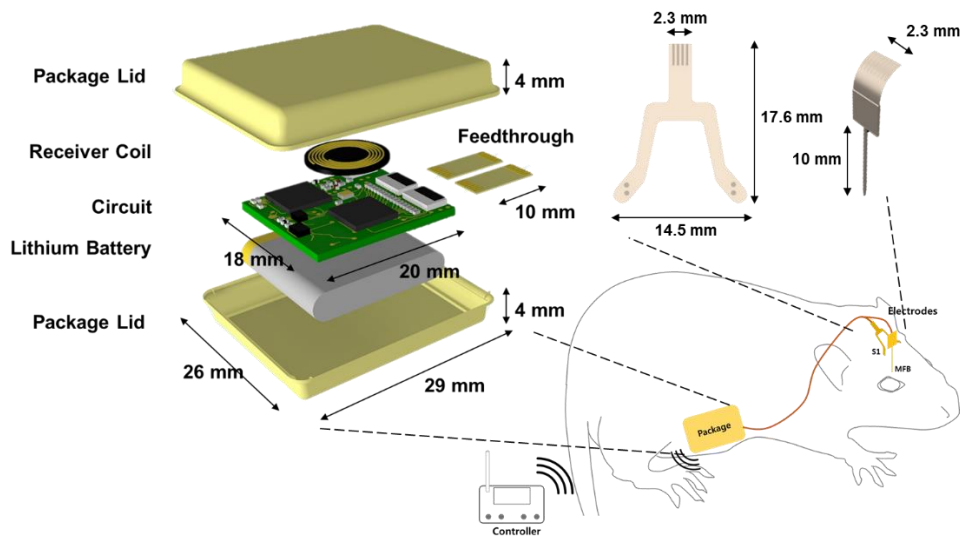


Figure 2.3.1. Configuration and the dimension of the assembled components of the neural stimulator.

2.3.2. Packaging

100 μm -thick low temperature LCP films (LT-LCP; 280 $^{\circ}\text{C}$, Vecstar CT-F series, Kuraray, Japan) and 100 μm -thick high temperature LCP films (HT-LCP; 330 $^{\circ}\text{C}$, Vecstar CT-Z series, Kuraray, Japan) were cut in size of 60 mm \times 60 mm with a laser machine (355 nm UV, Samurai system, DPSS, USA). Three HT-LCP films and two LT-LCP films were alternately aligned in a pair of custom-designed aluminum jig,

laminated and deformed at 295 °C for 10 min with a load of 2 Kg/cm² in a heat press (Model 4330, Carver, USA) to prepare 500 µm-thick LCP package lid in desired nonplanar shape. The assembled stimulator circuit board with the feedthrough board plugged into the connector was placed between two three-dimensionally deformed LCP package lids with the feedthrough extruded at the center of the lid edge. The circuit board was fixed at the lid with double-sided polyimide tape. This was followed by thermal pressing on the edge of the package with a 2 mm margin for biocompatible encapsulation of the electronics to protect them from body fluids. The edge of the package was trimmed by a laser and smoothed by applying small amount of dental cement.

2.3.3. Electrode, Feedthrough, Cable, and Connector

The fabrication of the electrodes, feedthroughs, cables, and connectors are assisted and performed by Seung-Hee Ahn and Gwang Jin Choi in Department of Electrical and Computer Engineering, College of Engineering, Seoul National University. Depth and surface electrode arrays were microfabricated using LCP films generally following the procedures in previous publications on LCP-based neural interfaces [26, 80]. First, LCP substrate for the microfabrication was prepared. An elastomer (MED 6233, Nusil Silicone Technology, USA) layer was spin-coated on a 4-inch silicon wafer. A 25-µm-thick LCP film (Vecstar CT-Z series, Kuraray, Japan) was cut into a 4-inch-wafer-sized pieces by using a UV laser system (Samurai System, DPSS, USA). The LCP piece is attached to a 4-inch silicon wafer using a roller. As the first procedure of metal patterning, the LCP substrate is placed under O₂ plasma condition for 180 seconds using an etcher (Oxford Etcher 80Plus, Oxford

Instruments, UK); then a 50-nm-thick titanium layer and a 100-nm-thick gold layer were deposited on the prepared LCP substrate by evaporation. A photoresist layer (AZ4620, Clariant, Switzerland) was spin-coated on the metal layer, and patterned using an aligner (MA6/BA6, SUSS MicroTec, Germany) and a developer (AZ300, AZ Electronic Materials, Luxembourg). An 8- μm -thick gold layer was electroplated on the areas without photoresist. The photoresist was removed with a stripper (AZ700, AZ Electronic Materials, Luxembourg). Remaining thin metal layer on the LCP was etched with aqua regia and HF. It was then encapsulated with a 25- μm -thick lower melting-point LCP film (Vecstar CT-F series, Kuraray, Japan) by thermal bonding using a heating press (model 4330; Carver, USA). The exposure of the electrode sites and connection pads, and the outlining process were performed by lasers-machining using the UV laser system. Finally, iridium oxide (IrOx) was electroplated onto the electrode sites to improve the electrochemical characteristics. The fabrication of the depth-type electrode only differs from the above process for the surface array in that four sheets of metal-patterned LCP films were laminated with a cover layer as well as additional padding layers to reach a total thickness of 250 μm to ensure suitable mechanical strength of the shank during implantation into the cortex. All parts of the depth probe that are not inserted into cortex were thinned down to 100 μm by means of laser ablation for greater flexibility.

The LCP-based 8-channel feedthrough board 4.5 mm by 10 mm in size provides an electrical bridge between inside and outside of the LCP package, or stimulating circuit and electrode arrays, respectively. It was microfabricated through a similar process of patterning, insulation and laser machining of LCP films to have eight gold tracks running between the exposed pad areas at both ends.

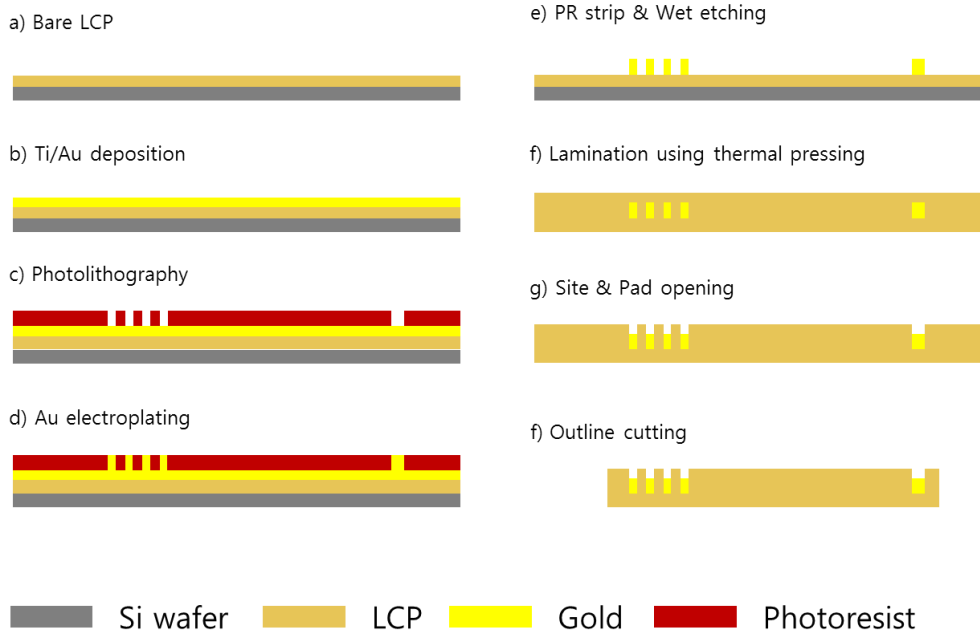


Figure 2.3.2. Fabrication process of LCP-based devices. Metal patterning process on the Si-wafer-bonded LCP is first described, and insulation making/device shaping methods are depicted.

The flexible cables used were custom-made on a polyimide substrate by a manufacturer of flexible PCBs. The 4ch/12ch connectors interconnecting the feedthrough, flexible cable, and the arrays were fabricated by mounting two commercial Flexible Flat Cable (FFC)/Flexible Printed Circuit Board (FPCB) connectors on custom-made FR-4 PCBs.

2.4. Evaluations

The functionality of the device was evaluated with regard to four aspects: operation of wireless communication test, wireless power transmission, electrochemical measurements, and animal testing *in vivo*.

2.4.1. Wireless Operation Test

The following are required in order for the established ZigBee communication to be used effectively in this application. First, the communication distance must be secured. The circuit must be able to acquire good quality communication signals in order for the animal to be effectively controlled even far away from the experimenter, or in certain structures or environments that interfere with communication. Signal-to-Noise Ratio (SNR) tests can be applied to verify the signal acquiring capabilities of circuits, and communication range tests can be applied for more practical evaluation.

The measurement function for monitoring the neural stimulator operation in this application is implemented in conjunction with the ZigBee communication. The capability of the communication is an important factor for the performance of the measurement function since all measured signals are transmitted to the external controller and the computer through ZigBee communication. Here, a test on the stability and utility of the measurement function can be performed.

2.4.1.1. Signal-to-Noise Ratio (SNR) Measurement

SNR is the ratio of the strength of the acquired signal to the noise strength of the environment. SNR is a measure of how much signal quality can be obtained at the location where it is measured, and its value varies depending on signal generation strength, signal transmission path, the number of surrounding noise sources, etc. Here, the SNR measurement was performed with the distance from the signal source as a variable. SNR of the ZigBee communication link between the controller and the LCP-encapsulated stimulator was evaluated. The received signal strength indicator

(RSSI) of the background noise and the received packets was used to calculate the SNR. The measurement was performed in a long, straight space while varying the communication distances and directions between the controller and the LCP-encapsulated stimulator. The ZigBee module of the controller was connected to the ZigBee receiver circuit, which was programmed to receive data from the ZigBee module and output the measured RSSI value on the LCD. The ZigBee module of the controller was programmed to continue to communicate spontaneously with the neural stimulator, and to measure the RSSI for each communication and average each two-hundred results to update the LCD output. The RSSI on the LCD was recorded for each meter of distance, and measured for three orthogonal directions. The SNR measurement were performed twice with the neural stimulator using commercial chip antenna (2450AT42A100, Johanson Technology Inc., US), and the neural stimulator using the designed inverted-L antenna.

2.4.1.2. Communication Range Test

The experiments were conducted by simulating the actual use situation in a large space to verify the realistic operation of ZigBee communication when the distance between communication devices is far. The neural stimulator was packaged and wrapped in pig meat to simulate the animal testing environment, and the coated wires connected to the stimulation pulse generator were protruded from the meat and connected to the oscilloscope. The controller was controlled to deliver a pulse generation command signal wirelessly to the neural stimulator once every second. Experiment were conducted with increasing the distance by 5 m to find the maximum distance that the command signal can be transmitted stably without delay or error in

communication.

2.4.1.3. Device Operation Monitoring Test

The purpose of the experiment is to check the quality of operation when the data transmission of the measurement using the transceiver's ADC was performed by the ZigBee telemetry. The measured target is a 100 μF capacitor connected to the PMIC, which stores the power retrieved from the energy harvester and discharges when powering the load. Therefore, the operation status of PMIC can be identified by measuring the voltage change across the capacitor. To establish an experimental environment in which data is streamed continuously, the transceiver of the neural stimulator was programmed to measure the capacitor voltage once every 15 ms and transmit the results to external ZigBee receiver. The ZigBee receiver circuit received the measurement data, displayed the value on the LCD, and sent it to the computer through the UART. The data transmitted to UART is a string connected with decimal time information and hexadecimal measured voltage values, and hexadecimal data is a concatenation of voltage of energy harvester and voltage of PMIC capacitor. The measured data were converted to decimal data using a custom-made Matlab (Mathworks, US) program. Based on the converted data, the noise intensity and the sampling rate were derived.

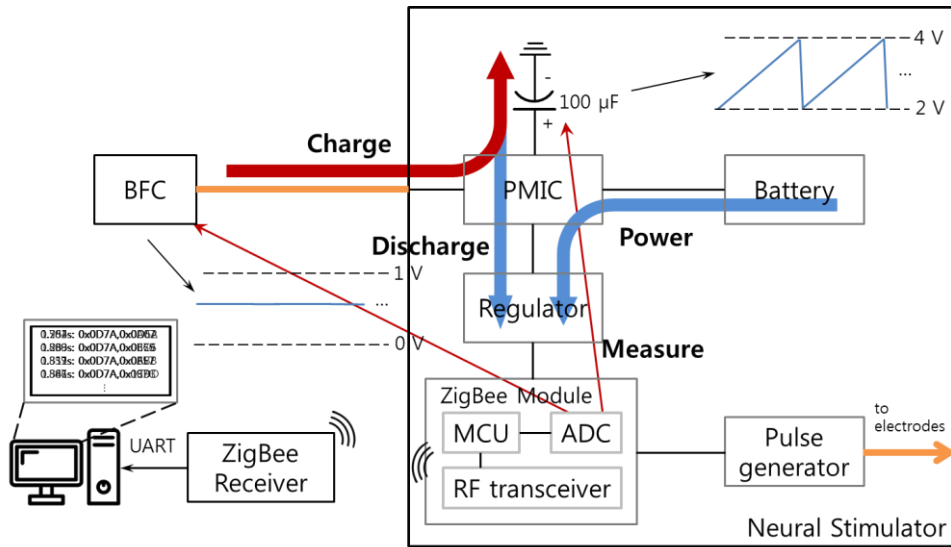


Figure 2.4.1. Overview of device behavior monitoring experiments. ADC and communication functions of ZigBee transceiver are used to check the operation status of PMIC and BFC.

2.4.2. Wireless Power Transmission

The purpose of this experiment is evaluate the power that the inductive link can transmit through the designed coils. As mentioned above, the power transmitted over the inductive link is affected by the load resistance of the receiver. The fabricated neural stimulator has a power mode to reduce power consumption. There are active mode and sleep mode, and each mode has a large difference in power consumption. Therefore, when the neural stimulator circuit in each mode is replaced with an equivalent resistance, the values of the two equivalent resistances are not the same. In this experiment, in order to measure the power delivered through the inductive link when the fabricated neural stimulator is in each mode, the load of the inductive link receiver was replaced with the equivalent resistance of each mode as shown in Figure 2.4.2. The power received at varying distances was measured to confirm

inductive behavior in various situations. The operating distance was increased from 2mm to 2mm, and the received power was calculated by measuring the voltage applied to the load resistance through the oscilloscope.

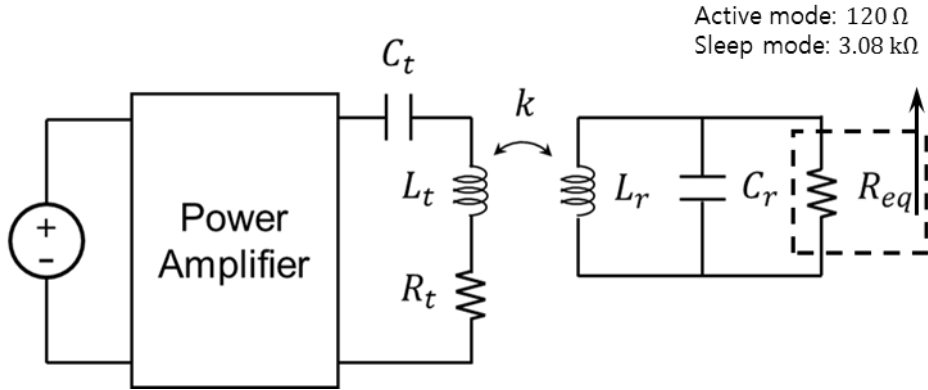


Figure 2.4.2. Simplified inductive link schematic. Experimental conditions are specified in the figure.

2.4.3. Electrochemical Measurements *In Vitro*

The aim of this experiment is to confirm whether the fabricated neural stimulator can effectively deliver the stimulation pulse to the target in the body. Electrical stimulation is delivered to the flexible cable through a connector in the stimulation pulse generation ASIC, and the pulse is delivered from the cable to the electrode, and to the living body at the electrode site. The path impedance of most of these paths is negligible in the order of a few ohms, and the interface impedance between the electrode and the living body occupies most portion of the path impedance. The voltage between the two stimulus channels that the pulse generation ASIC can provide is limited, so if the voltage across the interface rises above a certain level, it is impossible to apply sufficient electrical stimulation to the target. Therefore, in the case of the stimulation electrode, the interface impedance should be below a certain magnitude. In addition, the amount of charge that an electrode

site can store without damaging the electrode is limited, and this value is expressed as the charge storage capacity (CSC). The CSC generally increases as the surface area of the interface increases, which in turn reduces the resistance of the interface. Thus, electrodes with large sites can flow higher currents. However, when the site is widened, the area electrical pulse is delivered is also widened, which may cause stimulation to unintended parts. Therefore, the electrode site is designed as a trade-off between selectivity and CSC / impedance. In this experiment, we evaluated the interfacial characteristics of the fabricated electrode and simulated the situation in which the stimulation pulses were delivered *in vitro* to confirm the stimulation transmission capability of the neural stimulator in the actual situation.

First, the EIS of the stimulating electrode arrays was measured using a potentiostat (SI 1287/Si1260, Solatron, UK) for frequencies ranging from 1 Hz to 100 kHz. Sinusoidal waves with a varying amplitude of 10 mV, ranging -0.8~0.6 V were applied in a phosphate buffered solution (PBS; 1X, Gibco) and the current flowing through the electrode was recorded.

A voltage transient of the electrode triggered by the external controller was measured in a PBS solution while the pulse parameters and operation distances were varied. The pulse generation ASIC was controlled to generate a burst of biphasic current pulses for 0.5 second per stimulation. The pulse parameters of the pulse rate, pulse duration and amplitude was varied through the wireless ZigBee communication to deliver 17-bit stimulation instructions into the package. The test was conducted using a fully assembled stimulator and electrode array but without packaging to have the access to the voltage nodes for measurement.

2.4.4. Animal Testing *In Vivo*

Animal care and surgical procedure were performed by Chin Su Koh in Department of Neurosurgery, College of Medicine, Yonsei University. Three male adult Sprague-Dawley rats (200–250 g) (Orientbiod, Osan, Korea) were individually housed in polycarbonate cages with wood chip bedding while free access to food and water was allowed. A 12 h light/dark cycle (08:00 to 20:00) was maintained at $24 \pm 2^\circ$ and $55 \pm 5\%$ humidity. The Institutional Animal Care and Use Committee of Yonsei University (IACUC no. 2016-0161, date of approval 2016.09.26.) approved the study. Rats were anesthetized via an intraperitoneal injection of pentobarbital (40 mg/kg) (Hanlim Pharm, South Korea) and positioned in a stereotaxic frame. The rats were injected with 0.1 mL of atropine (Huons, South Korea) 10 min before the injection to insure the stability of anesthesia. The midline of the scalp was incised, and the surface of skull was scraped. Three small burr holes to anchor the screws were drilled into the skull (AP +4.0 mm, ML \pm 3.0 mm and AP -7.0 mm, ML +4.0 mm). Screws (tip diameter 1.0 mm) were inserted into the holes.

One burr hole for positioning the depth of the electrode to stimulate the MFB was drilled (AP -2.3 mm, ML -1.8 mm), and two parallelogram-shaped skull sections were removed to position the surface electrode to contact the barrel field (approximately AP -2.0 mm, ML -5.0 mm). The surface electrode was positioned through the parallelogram-shaped hole and fixed with dental resin to facilitate the positioning of the electrode. The dura mater was not penetrated during the positioning of the surface electrode. The depth electrode (AP -2.3, ML -1.8 mm) was vertically inserted (DV 8.6 mm, [9]) using a micromanipulator (SA-25A, Narishige, Japan) and fixed with dental resin. Electrode arrays were plugged into two 4-channel

connectors and cables after insertion, followed by the application of dental resin around the connectors for encapsulation. The cables were threaded to the subcutaneous pocket at the abdominal skin via a subcutaneous tunnel that was created from the neck to the abdomen. The flexible cable and the feedthrough of the package were connected by the 12-channel connector. After connection of the cables to the package, dental resin was applied to the connector to secure the sealing. The package was placed in the subcutaneous pocket. The wounds were closed with sutures and the stimulation test commenced three days thereafter.

Prior to the *in vivo* evaluation, a set of wired stimulation tests was performed using the same electrode array that was wire-connected to a stimulator circuit board identical to the wireless stimulator. This was done to find the optimized implantation location and to tailor the stimulation parameters of both the surface array and the depth array to induce directional movement by eliciting a virtual touch sense via S1 and to evoke a reward sense at the MFB region, respectively.

For both the MFB and S1 stimulation and for both the wired and wireless experiments, a single stimulus consists of a burst of 50 charge-balanced biphasic current pulses. The stimulus is produced when one of the three stimulation buttons (S1 left, S1 right and MFB) on the external controller is pressed.

For the MFB stimulation, rats (n=3) implanted with two arrays were placed in a Skinner box with a lever which triggers electrical stimulation on the MFB when pressed [81]. The MFB stimulation was given as a reward only when the rat voluntarily pushed the lever without operator's intervention such that the rat could learn to correlate the lever push and the compensation stimuli [81]. The number of lever pushes per minute was observed depending on the amplitude of the current pulses while the pulse rate and duration were fixed at 250 Hz and 0.2 ms, respectively,

based on results from the literature [9, 10].

For the S1 area to control the directional changes of the locomotion of the rat, electrical stimulation was applied to the right S1 as a virtual touch sensation of the left whisker, causing the rat to turn to the right, while stimulation was given to the left S1 to make it turn to the left [82, 83]. The proper range of the stimulation amplitude that stably evoked visually observable behavioral responses was determined to be a fixed pulse rate and duration of 0.5 ms and 180 Hz, respectively [9, 10].

After full implantation of the whole system, rats (n=3) were trained for movement control in two phases through which they learned to correlate the directional cue given as the virtual somatosensory touch sense at S1 to the MFB reward. First, the rats learned to obtain a MFB reward by moving forward and turning toward the correct direction following the left- or right-turning cues in open space. A custom-built remote controller was used to deliver the stimulation parameters and the onset command wirelessly for both S1 and MFB in real time. After this initial training phase, the rats were subsequently placed in a 3D maze consisting of a 30-degree ramp, a 45-degree ramp, a square maze, an obstacle and a tower cave maze. The rat was navigated through the designated path in the maze using a combination of directional cues and rewards.

Control experiments were conducted to rule out any possibility of animal behaviors induced by environmental factors such as the clicking of the button on the remote controller as opposed to the electrical stimulation applied to the cortex. To do this, during the wireless experimental setup, rat behavior was observed when 1) S1 stimulation was given without a subsequent MFB reward, 2) MFB stimulation was applied alone, and 3) the stimulation buttons were pressed with the remote

controller turned off.

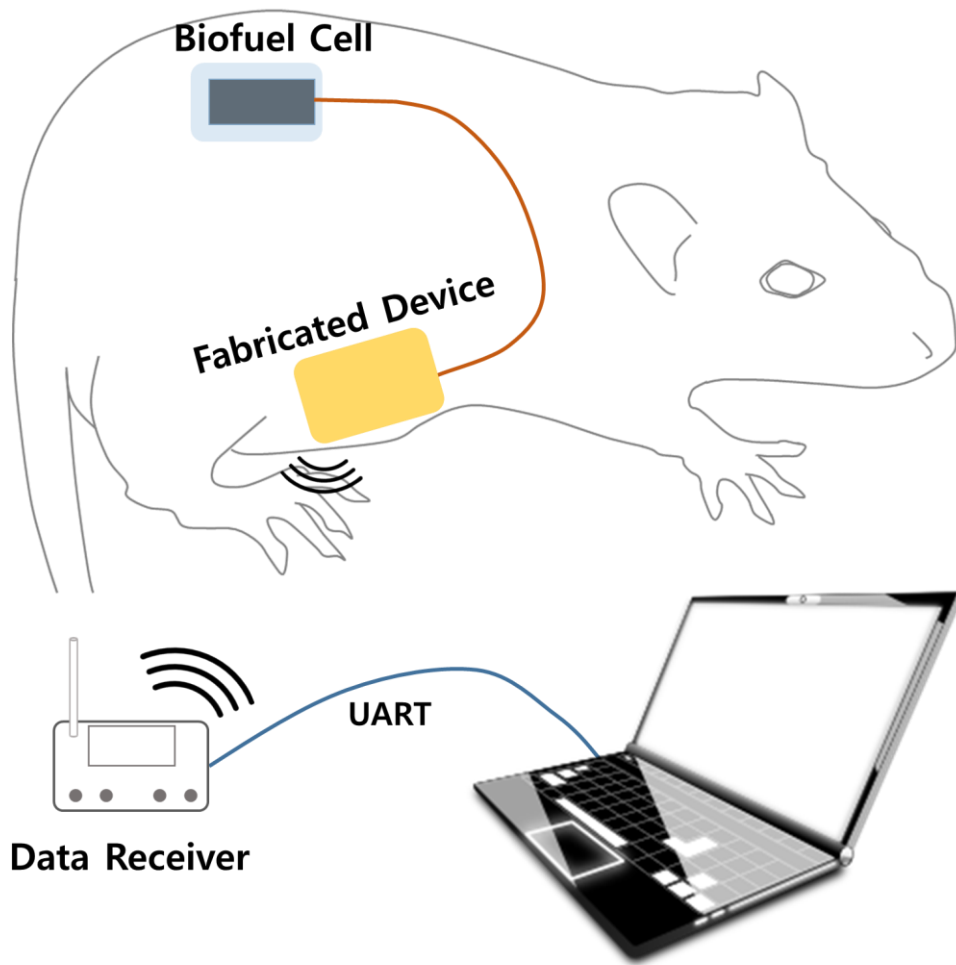


Figure 2.4.3. Overview of power harvesting experiments of fabricated neural stimulator and biofuel cells (BFC).

In vivo energy harvesting experiment with biofuel cell (BFC) co-implanted with the neural stimulator was conducted. The fabrication of the BFC was conducted by Dahye Lee and Sung Hee Jeong in Graduate School of Convergence Science and Technology, Seoul National University. The electrodes of the BFC were coated with carbon nanotubes, and glucose oxidase/bilirubin oxidase were attached to the surface of the anode and cathode, respectively. The BFC was fabricated with polyimide flexible cable connection. Rats were anesthetized using the procedure described

above. The middle of the back was incised, and the BFC were inserted in the subcutaneous pocket. The cables were threaded to the subcutaneous pocket at the abdominal skin via a subcutaneous tunnel that was created from the back to the abdomen. The flexible cable and the feedthrough of the package were connected by the 4/12-channel connector. After connection of the cables to the package, dental resin was applied to the connector to secure the sealing. The package was placed in the subcutaneous pocket at the abdomen. The wounds were closed with sutures and the measurement test was conducted one hour thereafter to adjust BFC at the biological environment. Measurement of the experiment were recording with a laptop connected with ZigBee receiver circuit via UART, as shown in Figure 2.4.3. The neural stimulator was programmed to start the measurement with the activation. Voltage of the BFC and the capacitor of the PMIC were recorded while power harvesting at the BFC was continued.

Chapter 3

Results

3.1. Fabricated System

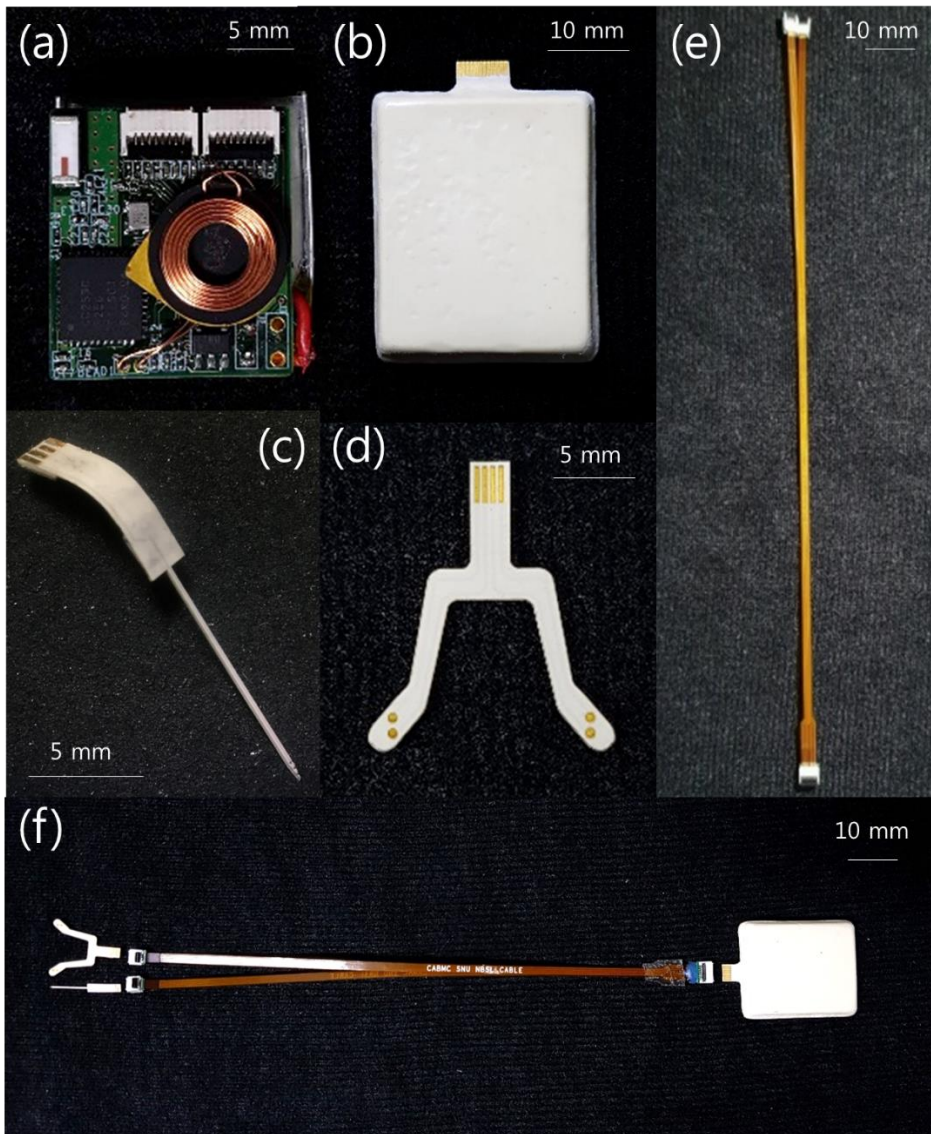


Figure 3.1.1. Independently fabricated modules of the neural stimulator: (a) package, (b) depth-type electrode array, (c) surface-type electrode array, (d) cable and connectors, and (e) assembled whole device

The fabricated fully implantable neural stimulator is shown in Figure 3.1.1. A rectangular-chip-shaped LCP package (29 mm × 26 mm × 8 mm size, 5.9 g weight) encasing the wireless stimulation pulse generator circuit board is assembled with independently fabricated surface and depth electrode arrays, a feedthrough,

connectors and a flexible cable. The Y-shaped surface array is 50 μm thick, minimizing the damage to the brain by the insertion of the electrode. The shank of the depth-type electrode has a cross-section of $250 \times 250 \mu\text{m}^2$. The middle part of the shank that needs to be bent after implantation was thinned down to a thickness of 100 μm by laser ablation for greater flexibility.

3.2. Wireless Operation Test

3.2.1. Signal-to-Noise Ratio Measurement

Figure 3.2.1 (a) shows the measured SNR of the ZigBee telemetry depending on the distance between the external controller and the neural stimulator with chip antenna on three orthogonal directions. The SNR values for each point on the graph were obtained by averaging repeatedly measured four SNR values. The SNR was observed to decrease below 25 dB at a distance greater than approximately 10 m for all three directions, in good agreement with a previous study reporting that ZigBee can maintain reliable communications when the SNR is higher than 25 dB [84].

The measured SNR of the ZigBee communication of the stimulator using the designed monopolar inverted-L antenna is shown in Figure 3.2.1 (b). This was measured with the same process as the above result. The SNR measurement of the ZigBee telemetry with designed antenna was maintained above 25 dB to about 20 ~ 25 m. The lowest SNR value measured was 10 dB, and it was shown in Figure 3.2.1 (b) that the measured value converged to this point as the distance increased in both cases. This value is considered the minimum strength of the signal for ZigBee telemetry to succeed in communication. The reason is that since the measured SNR was calculated based on the signal strength of the received data, the signal that failed

to receive did not affect the results. The minimum distance to reach this value is about 15 m when using a chip antenna and about 25 m when using a designed antenna.

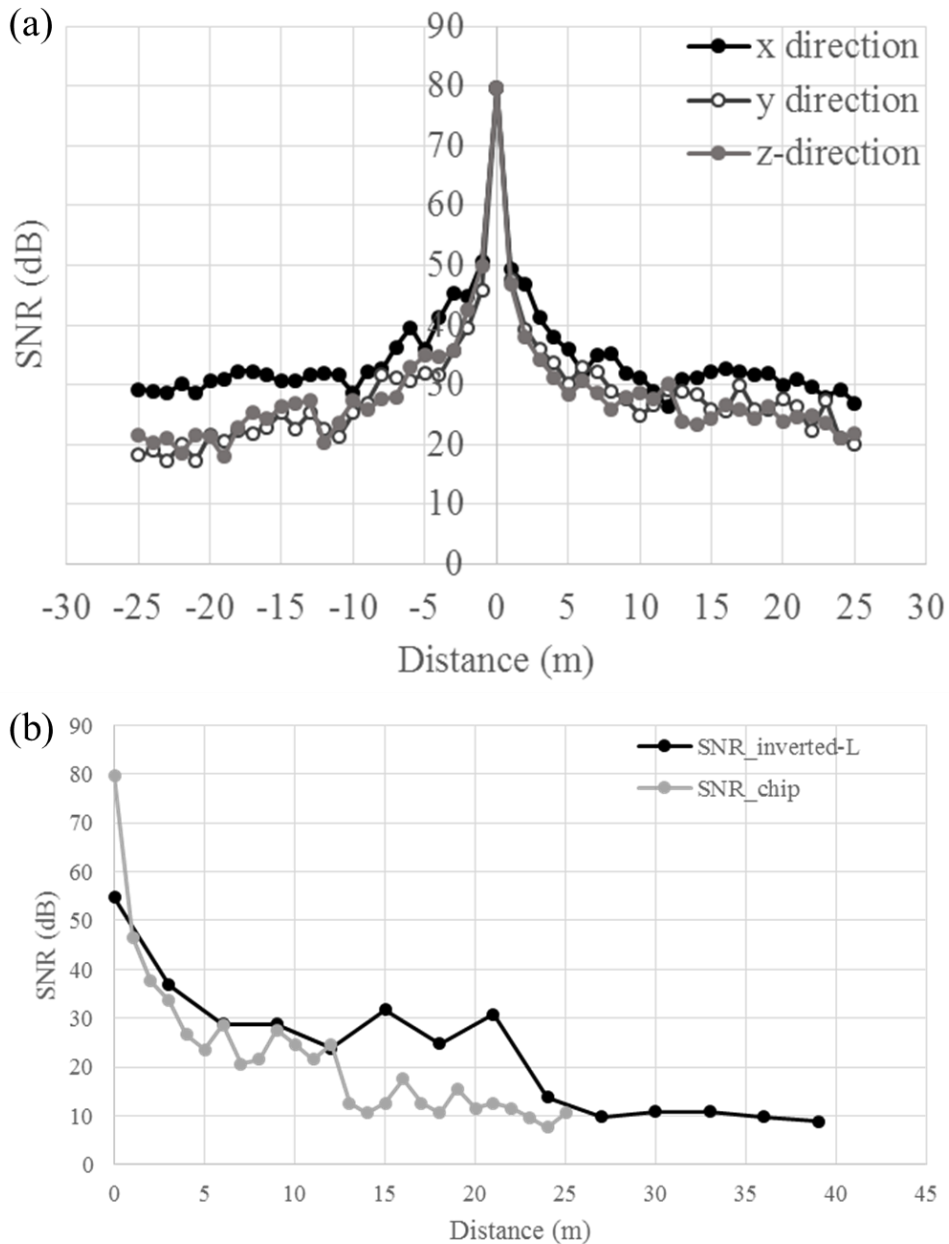


Figure 3.2.1. (a) Averaged SNR for ZigBee communication depending on the distance between the external controller and the stimulator using chip antenna in three directions, (b) Measured SNR for ZigBee communication of the stimulator using chip antenna and designed monopolar inverted-L antenna depending on the distance from the external controller.

3.2.2. Communication Range Test

The actual working distance of ZigBee telemetry was measured in the bio-mimicking environment. Test videos on the controller side and neural stimulator side were taken and the two videos were combined and synchronized based on the clapping sound recorded at the beginning. Figure 3.2.2 is a part of the merged image, showing that the stimulation pulse generation is normally controlled without any communication delay noticed at 30 m of distance between the controller and the neural stimulator. The level of communication delay was checked based on the LEDs on the controller. The leftmost one of the controller's LED was programmed to turn off at the start of the communication and on after 0.5 seconds. Simultaneous stimulation pulse and LED-off shown in the Figure 3.2.2 mean that the communication delay is less than 0.5 seconds.



Figure 3.2.2. Test setup of measuring the actual working distance of ZigBee telemetry between the external controller and the neural stimulator.

3.2.3. Device Operation Monitoring Test

Device monitoring tests using wireless communication were performed in an *in vitro* environment. As shown in Figure 3.2.3 (a), the experiment was prepared with the ZigBee receiver circuit connected to the notebook via a UART and the neural stimulator to the biofuel cell *in vitro*. Figure (b-c) shows measured waveforms of the voltage of the energy storing capacitor of the PMIC and BFC output voltage. In Figure 3.2.3 (b), a triangle wave is a charging/discharging cycle of 100 μF capacitor, and the value of the exchanged power is calculated to be 526 μJ . The average voltage of the BFC output is 0.232 V and the total harvested energy is 11.1 mJ. Calculated average harvested power is 91.0 μW .

The measured data was analyzed to evaluate the stability and functionality of the measurement. First, the sampling rate of the measurement was calculated. The inverse of the time between each measurement point was calculated as the momentary sampling rate. As a result, the average sampling rate was 33.1 Hz, the maximum was 52.6 Hz, and the standard deviation was calculated to be about 6.39 Hz. The measurement function is designed to operate at a sampling rate of 67 Hz, indicating that an average of 15.2 ms of delay occurred during the actual measurement. As a result, the sampling rate has been reduced to about 50% of the intended level. Also, based on the observation that data streaming was interrupted intermittently or suddenly a vast of data was transmitted, it is suspected that the cause is in the process of performing experiments such as instability of ZigBee communication environment and problems of UART transmission programming.

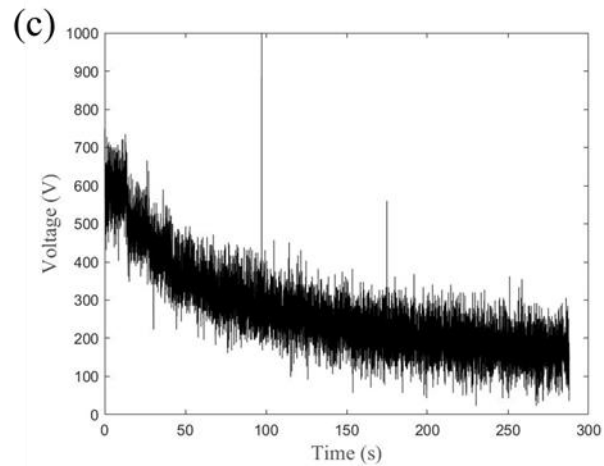
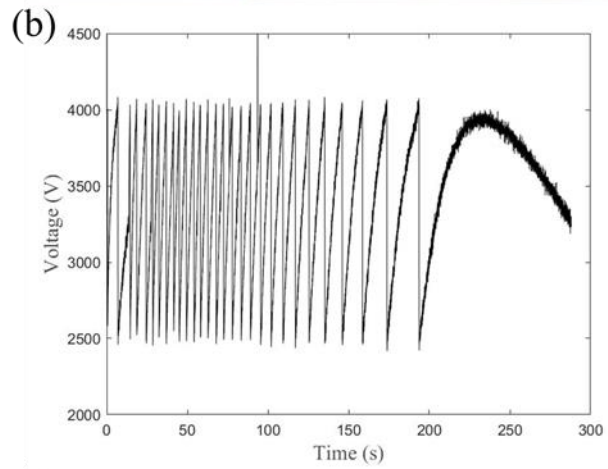
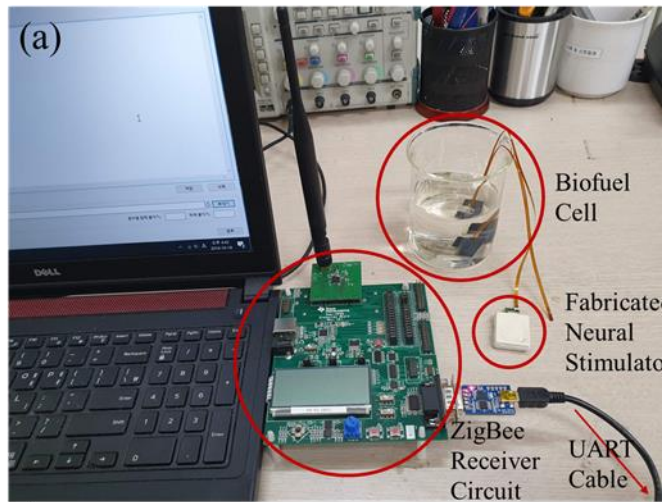


Figure 3.2.3. (a) Experimental setup of the device operation monitoring test, measured waveforms of (b) voltage of the energy storing capacitor of the PMIC and (c) BFC output voltage.

3.3. Wireless Power Transmission

The wireless power transfer test with the varying distance between the coils was conducted. The calculated equivalent loads for the circuits in the sleep mode and active mode are $3.08\text{ k}\Omega$ and $120\ \Omega$, respectively. The measured power value for each load value is shown in Figure 3.3.1. Received power at active mode, sleep mode and time-weighted average received power (100 ms for sleep mode and 10 ms for active mode) is shown in Figure 3.3.1. The maximum power received in the active mode was about 24.0 mW at a distance of 4 mm , about 89.9% less than the 238 mW in sleep mode, and the average maximum power was calculated as 217 mW . The received power in the sleep mode was higher than that in the active mode. It is assumed to be due to the higher equivalent load resistance in the sleep mode that resulted in the higher power transfer efficiency of the inductive link [43, 85]. The maximum power transfer at a separation distance of 4 mm is the result of the external coil tuned to match the mutual inductance at an inter-coil distance of $3\text{ to }5\text{ mm}$, which is the most typical range for charging of this stimulator in rats.

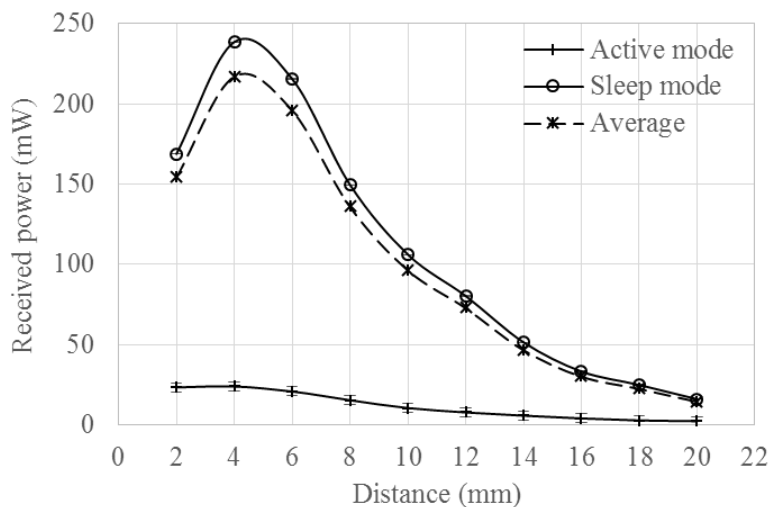


Figure 3.3.1. Power received by the stimulator circuit as a function of the coil separation distance for both the active mode and sleep mode.

3.4. Electrochemical Measurements *In Vitro*

The means and the standard deviations of the EIS measurements are plotted in Figure 3.4.1 for the magnitude (a) and phase (b) at each frequency in the range from 0.1 Hz to 100 kHz. The average impedance magnitude of the surface-type and depth-type electrodes with the IrOx deposition were $1.67 \pm 0.387 \text{ k}\Omega$ and $33.6 \pm 24.7 \text{ k}\Omega$ each at 1 kHz, respectively. The impedance of the depth-type electrodes were about 30 times larger than previously fabricated ones [26]. Considering the size of the depth-type electrode site was $1500 \text{ }\mu\text{m}^2$ ($20 \text{ }\mu\text{m} \times 75 \text{ }\mu\text{m}$) and the previously fabricated electrodes had site of approximately $7000 \text{ }\mu\text{m}^2$ ($150 \text{ }\mu\text{m}$ radius), the difference of the impedance between two independently fabricated electrodes is due to the difference in site area.

In a stimulation pulse generation test with wireless control, the stimulator could generate biphasic current pulses with varying pulse parameters in accordance with the incoming data from the external controller. The measured waveforms of the generated stimulation pulses are shown in Figures 3.4.1 (c) and (d) for corresponding pulse rates, pulse durations, and amplitudes of 100 Hz, 500 μs , 1 mA and (d) 50 Hz, 250 μs , and 2 mA. The adjustable ranges of the stimulation parameters are 0.01 mA to 10.23 mA for the pulse amplitude, 10 μs to 630 μs for the pulse duration, and 20 Hz to 230 Hz for the pulse rate. The stimulator could generate pulses up to a distance of approximately 30 m between the stimulator and the external remote controller. The produced pulses maintained the desired parameters throughout the operation range before abruptly disappearing at the maximum distance.

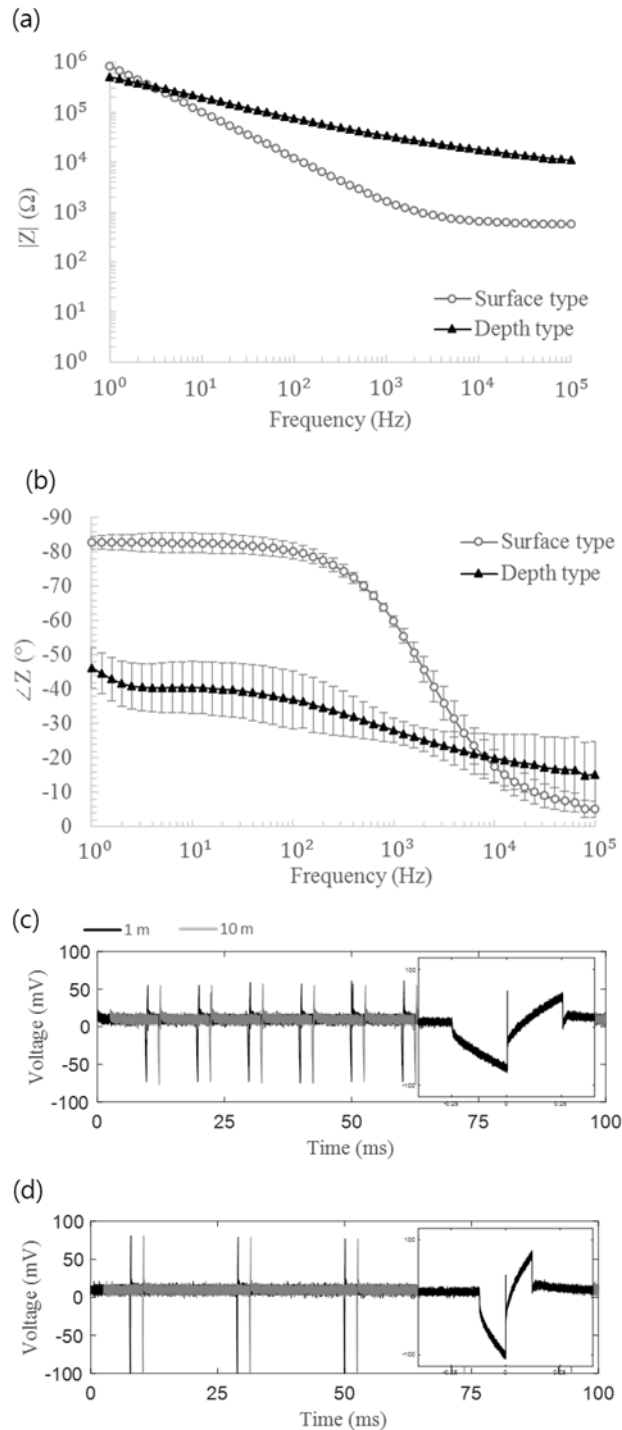


Figure 3.4.1. EIS measurements of the two types of fabricated electrode arrays: (a) magnitude and (b) phase, (c-d) biphasic stimulation pulses measured in PBS with the various parameters by the remote controller at distances of 1 m and 10 m: (c) at pulse rates, pulse durations, and amplitudes of 100 Hz, 500 μ s, 50 μ A and (d) 50 Hz, 250 μ s, and 100 μ A, respectively (inset shows the magnified view of a biphasic pulse).

3.5. Animal Testing *In Vivo*

Animal care and surgical procedure were performed by Chin Su Koh in Department of Neurosurgery, College of Medicine, Yonsei University. Figure 3.5.1 (a) shows a rat in a Skinner box while electrical stimulation to the MFB is being triggered when the rat presses the lever. The number of times the lever is pressed per minute was recorded as a function of the increasing current amplitude of the stimulation pulses to the MFB, as shown in Figure 3.5.1 (b). Greater strength of the stimulation induced the rats to push the lever more frequently, but with a decreasing slope. Based on this observation, we chose 200 μA to 400 μA as the stimulation intensity levels for the following wireless experiment, as these values fall in a range comparable to that in a previous report [9]. As described earlier, the pulse frequency and the pulse width were fixed at 250 Hz and 0.2 ms, respectively, where a burst of 50 pulses constituted a single stimulus.

In the case of wired S1 stimulation, behavioral responses of rats were observed while varying the pulse amplitude with a fixed pulse width of 0.5 ms and pulse duration of 180 Hz. Here, we chose the appropriate amplitude range of 100 μA to 350 μA , which could elicit consistent and natural turning behavior of the rats while not causing the rats twitch or jerk due to an excessively strong stimulation. This is also in good agreement with the results from previous publications [9, 10].

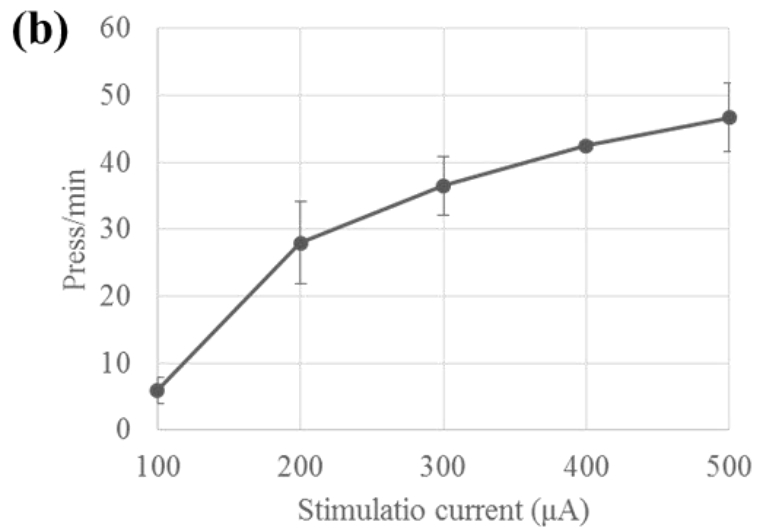


Figure 3.5.1. (a) A rat in a Skinner box during the wired test for the determination of the stimulus parameters; a MFB stimulation is triggered by lever pressing, and (b) number of lever presses versus the MFB stimulation amplitude.

Figure 3.5.2 (a) shows the surgical implantation of the stimulator by implanting the depth probes into MFB and the surface array into barrel cortex. After placing the package in the abdomen, as shown in Figure 3.5.2 (b), all of the modules were interconnected by connectors and cables. Subsequently, we closed the wound, as shown in Figure 3.5.2 (c).

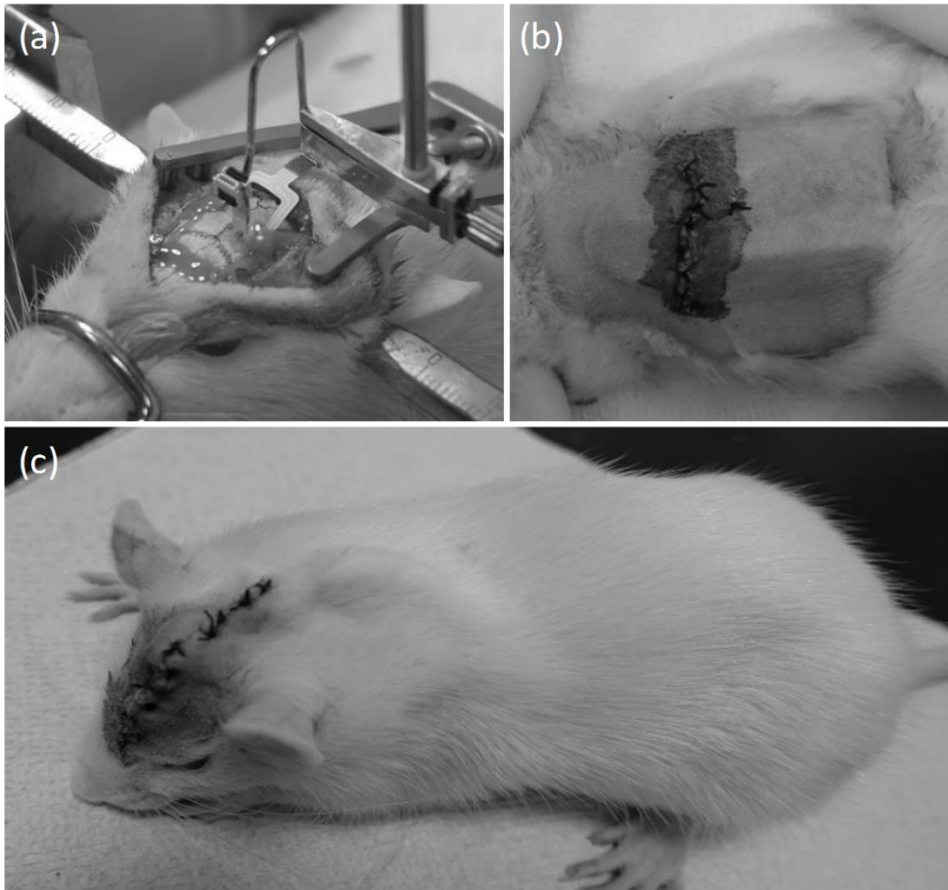


Figure 3.5.2. Surgical implantation of a neural stimulator in a rat: (a) electrodes inserted in the brain, (b) package implanted in underneath the abdominal skin and (c) a rat after surgery.

Test procedures were partly performed by Chin Su Koh in Department of Neurosurgery, College of Medicine, Yonsei University. First, the rats were trained to turn left or right in response to a combination of the stimulus on S1 as a directional cue and a subsequent MFB stimulus as a reward for a correct response. Figure 3.5.3 (a) shows the behavioral response of the rat over the course of one second. The rat with the implanted stimulator turned left following the virtual sensation on the right whisker that was elicited by left S1 stimulation. The external remote controller is also shown in Figure 3.5.3 (a) with the stimulation button pressed between $t = 0.2$ to 0.4 sec. Similarly, the stimulation could induce the rat in this case to turn right, as shown in Figure 3.5.3 (b).

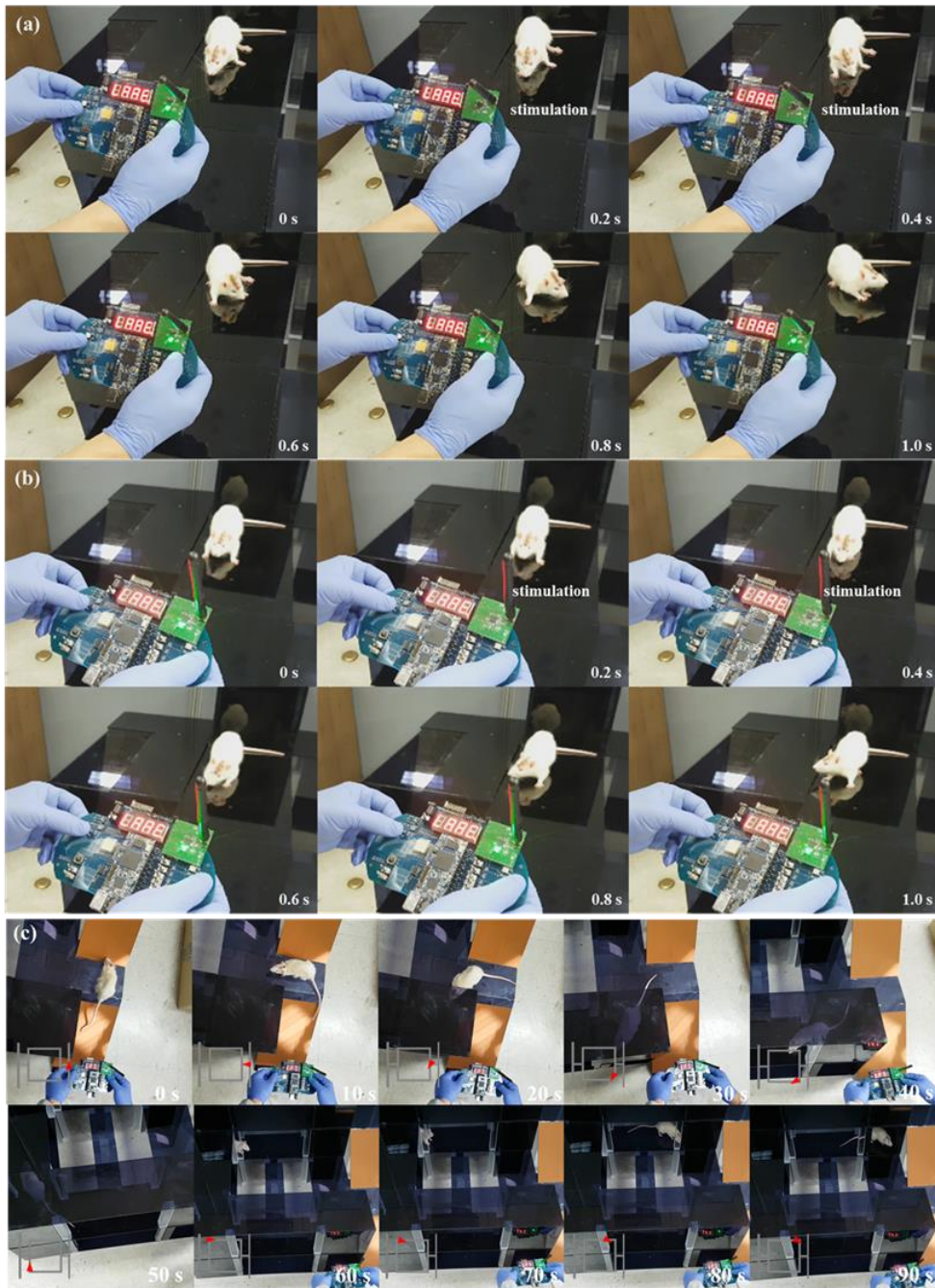


Figure 3.5.3. Wireless control of the movement of a rat: rats were induced to turn to the left (a) or right (b) following directional cues from the remote ZigBee-based controller, showing the movement in a 3D maze, and (c) returning to the origin after travelling through a rectangular corridor (drawing at the left bottom corner indicates the current position of the rat in the map of the maze).

After conditioning, the rat was remotely controlled to navigate through a 3D maze (Figure 3.5.3 (c)). We could induce the rats to climb a 30-degree ramp, enter a square maze, and return to the original point after travelling through rectangular corridor while making four turns. Despite some lingering behaviors, two rats could complete the task without failing to follow the induced direction. One rat was not trained, as it showed unexpected response to the MFB stimulation, presumably due to the depth electrode inserted deeper than intended, which stimulated the nigrostriatal pathway.

A control test was conducted to confirm that the cortical stimulation indeed induced behavioral changes of the rat. When the S1 stimulus was applied without a subsequent MFB reward, the rat turned toward the correct direction, implying that the S1 stimulus alone is sufficient to induce movement of the rat after the conditioning process. When the MFB stimulus is applied, the rat showed a probing response, such as rapid vertical movement of the head [11] without any effective turning behavior. The rats did not respond to the clicking sound of the stimulation buttons on the remote controller.

In vivo energy harvesting experiment with biofuel cell (BFC) co-implanted with the neural stimulator was conducted. Figure 3.5.4 (a) shows the experimental setup that consists of the fabricated neural stimulator co-implanted with BFC in the rat, and the ZigBee receiver circuit connected to the laptop via an UART cable. Figure 3.5.4 (b-c) shows measured waveforms of the voltage of the energy storing capacitor of the PMIC and BFC output voltage. In Figure 3.5.4 (c), a triangle wave is a charging/discharging cycle of 100 μ F capacitor, and the value of the exchanged power is calculated to be 526 μ J. The average voltage of the BFC output is 0.355 V and the total harvested energy is 4.8 mJ. Calculated average harvested power is 41.6

μW , which supplements 0.16 % of the power consumed by the fabricated neural stimulator.

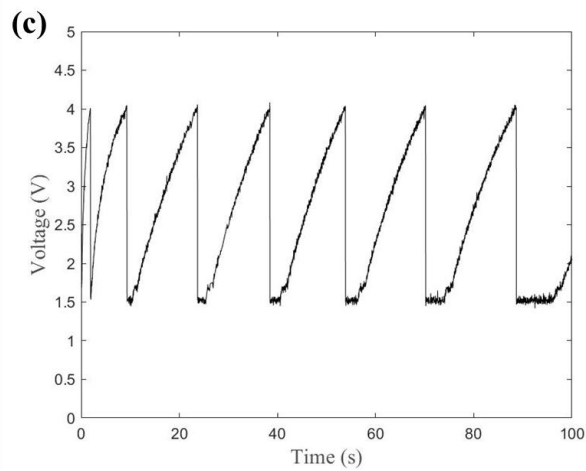
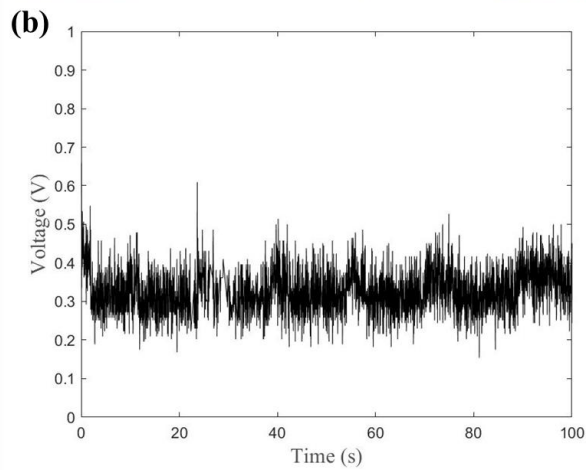
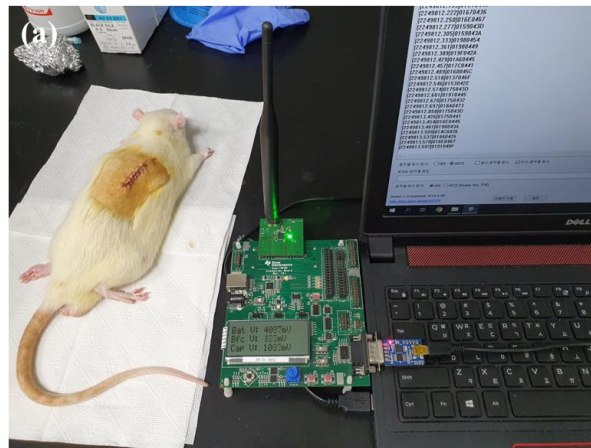


Figure 3.5.4. (a) *In vivo* energy harvesting experiment setup with biofuel cell (BFC) co-implanted with the neural stimulator, (b) waveform of the output voltage of the BFC, (c) waveform of the voltage of the energy storing capacitor of the PMIC.

Chapter 4

Discussion

4.1. Comparison with Conventional Devices

A fully implantable wireless neurostimulator was developed for brain stimulation in small animals. The fabricated neural stimulator was designed modularly and packaged with LCP, a biocompatible polymer, for easy and reliable surgery, complete implantation to animals, and device miniaturization. Most devices that has been developed for small animals are devices that are not miniaturized and packaged. These include large communication circuits and stimulation circuits, and the power consumption of the circuits is large in the range of 199% ~ 854% of the present study [30, 31, 86]. Large batteries are used to supplement the power to the circuits. In some cases, the size of the battery is smaller than that used in this study but the continuous experiment time is expected to be less than 2 hours [29]. The devices are implanted percutaneously, and the packages are covered with dental cement yet some wires connecting the electrodes are not protected [29-31, 86]. Devices that are miniaturized and packaged have also been developed. These devices have been designed based on inductive linking, mimicking cochlear implant devices [32, 33]. The device is powered through a cage covered with coils. Because the device cannot be powered from outside the cage, the range of operation is limited to the inside of the cage. These limitations impede the free movement of animals and do not guarantee stable experiments. Animals are susceptible to infection due to percutaneous implantation of the device and are burdened by the weight of the device, the device does not guarantee long test times and can easily be damaged by external environmental factors. These problems interfere with the stable performance of the experiment, and the results are deteriorated because the experiment is influenced by factors other than control variables. In this study, to solve the above problems, a

programmable RF transceiver was used and the power mode was applied to reduce the power consumption and improve the operation time of the device. In addition, the RF antennas were newly designed to minimize the size of the device, and the circuit size was minimized. The customized polymer packaging technology that can be performed at low temperature was developed to enable battery packaging and minimize the size margin required for packaging.

	[30]	[86]	[29]	[31]	[32]	[33]	This work
Size (mm)	48 x 23 x 19	36 x 22 x 7.5	32 x 25 x 6	26 x 16 x 9	14 x 12 x 6	N/A	29 x 26 x 8
Weight (g)	28	40	20	9	2.5	N/A	5.9
Packaging	None	None	None	None	Silicone	Silicone/Parylene	LCP
Stimulation electrode	stainless steel wire	stainless steel wire	Unknown	stainless steel wire	Pt electrode array, Pt/Ir wires	Pt electrode array, Pt/Ir wires	microfabricated LCP array
Stimulation method	Constant voltage	Constant voltage/current	Constant current	Constant voltage	Constant current	Constant current	Constant current
Stimulation target	MFB, S1	MFB, S1	dIPAG, S1, VTA	PAG, DIVA	Cochlea	Cochlea	MFB, S1
Configuration	Head-mounted, percutaneous connection	Head-mounted, percutaneous connection	Head-mounted, percutaneous connection	Head-mounted, percutaneous connection	Fully implanted, monolithic	Fully implanted, monolithic	Fully implanted, Modular
Communication	FM	Bluetooth	Bluetooth	FSK	N/A	2.4 GHz radio link	ZigBee
Powering	Li battery (160 mAh)	Li battery (120 mAh x 2)	Li battery (80 mAh)	Li battery (120 mAh)	3-axes Inductive coils on cage	3-axes Inductive coils on cage	Li battery (90 mAh), Inductive charging
Avg. power consumption (calculated)	82.5 mW	222 mW	148 mW	51.8 mW	N/A	N/A	15.2 mW
Target animal	Long-Evans rat	Sprague-Dawley rat	Sprague-Dawley rat	Pigeon	Mouse, rat	Hooded Wistar rat	Sprague-Dawley rat

Table 4.1.1. Comparison of functionalities and performance capabilities of prior arts and this work. Our device is characterized by fully-implantation, low power consumption, and wireless telemetry.

An additional advantage of this study is the design and fabrication of electrodes specific to the stimulation target. Previous studies have frequently used basic

stainless steel wire electrodes [30, 31, 86]. However, these electrodes are generally difficult to increase the number of channels, lack of flexibility which leads to damaging biological tissues, and there is a limit to minute targeting. Polymer-based Pt electrode arrays have also been tried [32, 33], but these electrodes are manually assembled, limiting the miniaturization of the size, inferior manufacturing precision, and disadvantageous in producing a large number of electrodes. In this study, the MEMS process was used to fabricate electrodes based on polymers, thereby improving the channel density of the electrodes enabling fine targeting, securing flexibility, and thin electrodes to prevent damage to biological tissues. In addition, a large amount of electrodes can be easily produced through a batch process.

4.2. Safety of Device Operation

The developed device was designed to use electrical current to stimulate neurons and electric field to charge the device's battery. Since the operation of the device inevitably involves the direct Energy transfer to the body, the question may be raised whether such operation is safe. This section describes the safety evaluation of the device by analyzing the effects of electrical stimulation and wireless power transfer on the body.

4.2.1. Safe Electrical Stimulation

The stimulation method of the fabricated neural stimulator is biphasic constant current stimulation. The stimulation current ranges from 10 μA to 10230 μA , and the stimulation voltage changes up to 12 V, the maximum compliance voltage,

depending on the impedance of the stimulation target. Stimulation parameters are determined in the range that effectively activates target neurons but minimizes damage to tissues and electrodes. Before discussing safe neural stimulation, we first establish the conditions for effective neural stimulation. Effective neural stimulation requires a stimulation amplitude above the threshold of the target tissue. The amplitude of the neural stimulation is generally adjusted based on the magnitude of the stimulation voltage or the magnitude of the stimulation current. They are called constant-voltage stimulation and constant-current stimulation. Constant-voltage stimulation makes circuit design easier because it constantly limits the voltage used for the stimulation. If the stimulation voltage is kept low, the voltage across the electrode is also small, minimizing the oxidation of the electrode. However, constant voltage stimulation is unable to control the amount of charge delivered to the stimulation target, which is one of the important parameters that involving the threshold of neural stimulation [87-89]. Since the impedance of the tissue to be stimulated may vary depending on the subjects, and the voltage applied to the tissue may vary depending on the impedance of the electrode, it is difficult to control the intensity of the stimulation delivered to the tissue when the constant-voltage stimulation is performed. In addition, when the total amount of charge transferred to the tissue is not maintained at 0, charge may accumulate in the tissue inducing damage, and the electrode may be damaged when excessive charges are momentarily transferred to the electrode. Constant-current stimulation is a widely used method because it controls the total amount of charge delivered to the tissue and thus can manage the above problems. As described above, the amount of charge delivered through the stimulation is the standard of the threshold of the stimulation, so the stimulation parameters are usually determined by adjusting the stimulation current

and the time. This is expressed as the charge per phase, and as the magnitude of the current decreases, more charge is required to achieve the same effect [88]. In order for the charge required for the stimulation to be transferred normally, the electrode must be able to carry that amount of charges [87]. Such characteristics of electrodes are represented as charge storage capacity (CSC). In this study, stimulation currents ranging from 200 to 400 μA and stimulation pulse durations of 0.5 ms were used to stimulate MFB and S1 of rats. These values can be interpreted as charge per phase, ranging from 50 to 100 nC/phase. The CSCs of the fabricated depth-type and surface-type electrodes are about $101 \pm 27.1 \text{ mC/cm}^2$ and $5.68 \pm 2.74 \text{ mC/cm}^2$, respectively. The surface area of each electrode is $15.0 \times 10^{-6} \text{ cm}^2$ and $707 \times 10^{-6} \text{ cm}^2$, with a maximum charge density of 6.67 mC/cm^2 and 0.142 mC/cm^2 delivered to each electrode when stimulation parameters are applied. The calculated charge density is less than 10% of the CSC value of the electrodes, it can be seen that the stimulation parameters in this study were effectively transmitted by the fabricated electrodes.

The cause of tissue damage by electrical stimulation is known as followings: the change of the surrounding environment due to excessively frequent stimulation, high charge per phase/high charge density of the stimulation, and stimulation outside the water window [13, 87, 90, 91]. However, as little is known about the proportion or exact mechanism of each affect, generally safe stimulation intensity is largely determined by experience. Through empirical studies on the charge per phase or charge density per phase of a stimulation, the maximum stimulation intensity formula has been established as follows:

$$\log \frac{Q}{A} = k - \log Q,$$

7 8

where Q/A is charge density per phase ($\mu\text{C}/\text{phase}$), Q is charge per phase ($\mu\text{C}/\text{phase}$), and $2 > k > 1.5$, that fits the empirical data [92]. Applying it to this study, the stimulation intensity is limited to $155 \mu\text{A}$ for the depth-type electrode and $1064 \mu\text{A}$ for the surface-type electrode when assuming that the phase length is $250 \mu\text{s}$. The results indicate that the current design of depth-type electrodes can be dangerous for safe stimulation. The design can be modified to increase the electrode site area at the expense of selectivity, or the stimulation parameter can be changed to shorter duration and larger current.

The water window refers to the voltage range at which the electrolysis of water does not occur at the electrode. The water window of the Ir oxide electrode was reported to be -0.6 to 0.8V [87, 90]. This voltage is formed by the electrode-tissue interface impedance, and increases in proportion to the amplitude of the stimulation current according to Ohm's law. In other words, the impedance of the electrodes limits the stimulation current range that can be applied on the tissue without electrolysis of water. The impedances of the surface-type electrode and the depth-type electrode were $1.67 \text{ k}\Omega$ and $33.6 \text{ k}\Omega$ on average, respectively. The results show that the impedance of the fabricated depth-type electrode is in a range that is difficult to perform safe stimulation. Improvement of the geometric surface area through the size improvement and plating of the electrode site is required. The improvement can be performed in various ways. Pt black can be used as a site material, which was investigated as the material with the lowest area-specific-impedance (ASI) [93]. There are methods to improve the ASI by applying additional treatment on the base metal layer. CF_4 plasma treatment on the thermally evaporated Au was developed to reduce ASI to 2.26%, etching Ag after co-sputtering Au with Ag have been studied

to obtain porous Au layer [94, 95]. Moreover, various methods of metal layer deposition and plating have been studied to obtain a porous electrode structure [1, 96-98].

Safe electrical stimulation is also related to corrosion of electrode. Corrosion of the electrodes produces a variety of materials, which are often biotoxic. The main cause of electrode corrosion is excessive anodic current, which oxidizes the metal electrodes. In fact, electrode corrosion is known to be less when using monophasic pulses or unbalanced ideal pulses with relatively low anodic currents and when cathodic currents are first formed. However, the change in the stimulus waveform may affect charge transfer, which may reduce the efficiency of the stimulus and cause tissue damage.

4.2.2. Safe Wireless Power Transmission

Inductive link uses the electromagnetic wave generated by the transmitting coil to transmit power to the receiving coil. The generated electromagnetic waves pass through the living tissue, and in the process, some of the electromagnetic waves are absorbed by the body. Excessive exposure to electromagnetic waves can adversely affect the body, which is the specific absorption rate (SAR). SAR is the amount of energy absorbed by the body per unit mass, and the unit is W/kg. In US code of federal regulation (CFR), The SAR limits for general population/uncontrolled exposure are 0.08 W/kg, as averaged over the whole body, and a peak spatial-average SAR of 1.6 W/kg, averaged over any 1 gram of tissue (defined as a tissue volume in the shape of a cube)[99]. The SAR of the electromagnetic wave is computed as follow:

$$\text{SAR} = \frac{\sigma |E|^2}{2\rho} \text{ [W/kg]}$$

where σ is conductivity, E is electric field, and ρ is mass density [100]. That is, if the magnitude of the electric field generated by the coil of the inductive link can be identified, SAR can be calculated.

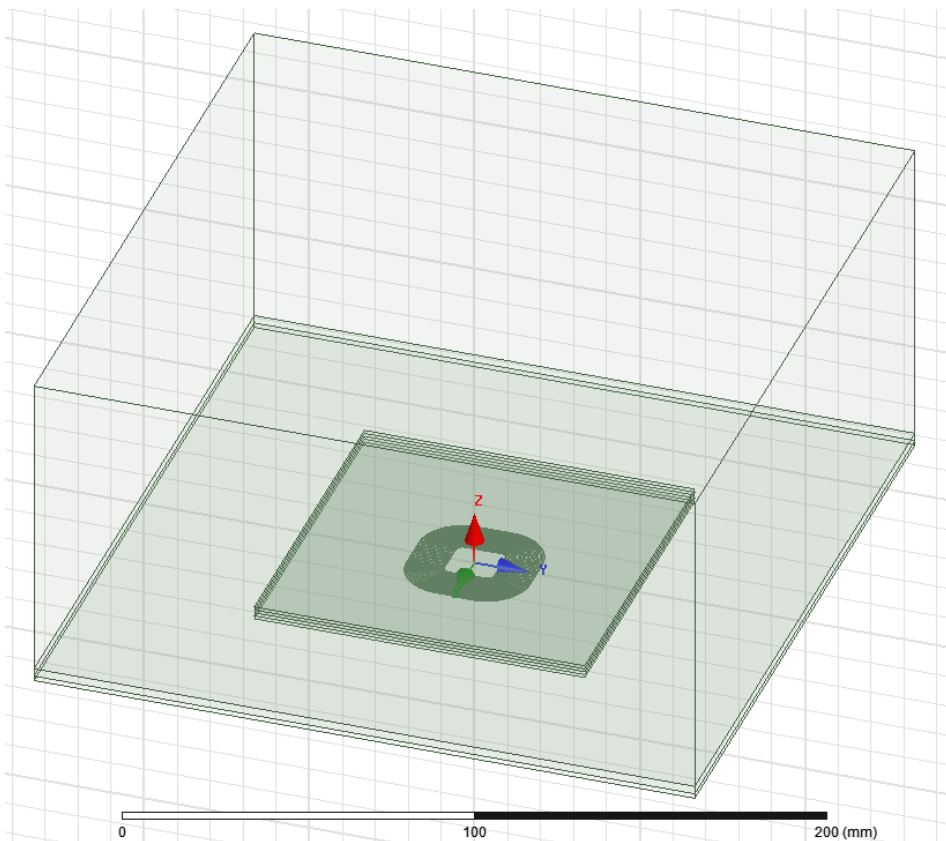


Figure 4.2.1. SAR simulation model: transmitter coil of inductive link and biological tissue consisting of skin, fat, and muscle layer.

Simulations were performed to evaluate the safety of the inductive links used in this study. A biometric model consisting of skin, fat, and muscle layers and a model of the transmission coil used for the inductive linkage were generated, and the transmission coil was located 0.1 mm from the skin, as shown in Figure 4.2.1. The

designed model was analyzed by computer simulation software (ANSYS Electronics Desktop, ANSYS Inc., USA). Material properties shown in Table 4.2.1 was applied to the model [101-103].

Tissue	Mass density (kg/m ³)	Permittivity (F/m)	Conductivity (S/m)	Thickness (mm)
Skin	1109	799	0.0501	1.5
Fat	919.6	49.9	0.0452	2.5
Muscle	1060	640	0.559	96

Table 4.2.1. Material properties of the simulation tissue model.

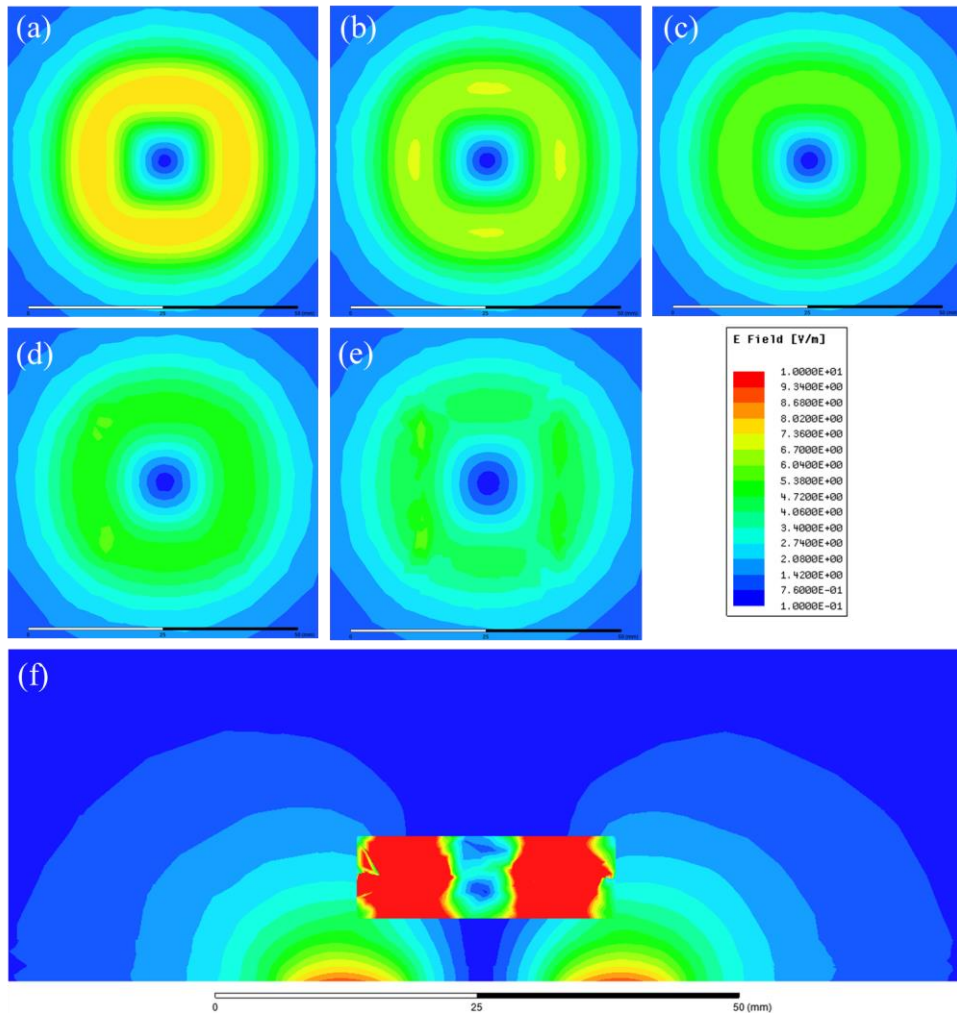


Figure 4.2.2. Electric field generated by the transmitter coil. (a) Electric field displayed at 1 mm, (b) 2 mm, (c) 3 mm, (d) 4 mm, and (e) 5 mm distance from the coil, and (f) electric field displayed along vertical plane at coil center.

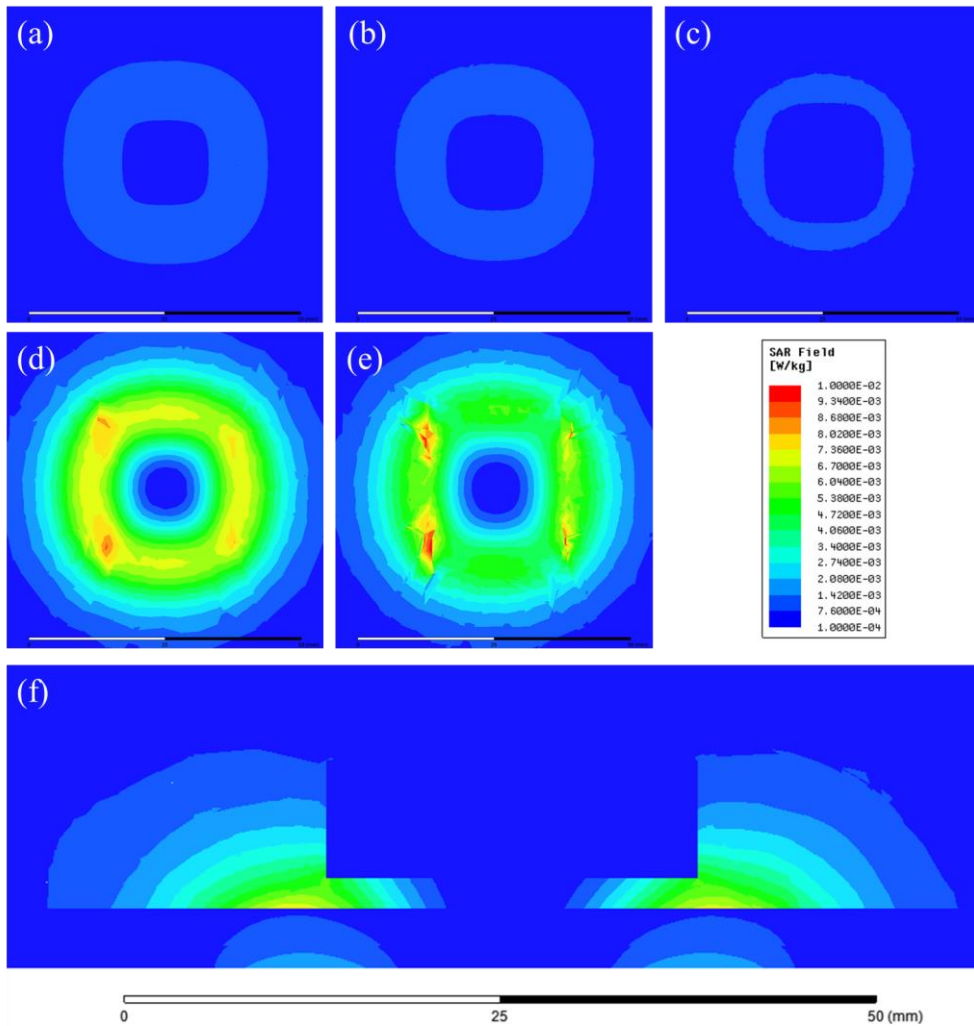


Figure 4.2.3. SAR results of the electric field generated by the transmitter coil. (a) SAR field displayed at 1 mm, (b) 2 mm, (c) 3 mm, (d) 4 mm, and (e) 5 mm distance from the coil, and (f) SAR field displayed along vertical plane at coil center.

As shown in Figure 4.2.2, the electric field generated by the transmitter coil decreases with the distance from the wire of the coil. The electric field has maximum value of 8.39 V/m in the skin layer, 7.26 V/m in fat layer, and 6.24 V/m in muscle layer. SAR computed based on the above results is shown in Figure 4.2.3. Since the conductivity of the muscle is approximately ten times greater than that of the fat and skin, the calculated SAR is shown greatest at the muscle. The maximum value of the SAR is 1.52 mW/kg in skin layer, 1.24 mW/kg in fat layer, and 12.4 mW/kg in

muscle layer, which is less than 0.775 % of the peak spatial-average safety limit and 15.5 % of the exposure limit averaged over the whole body when assuming that the maximum SAR is applied to the whole body.

4.3. Potential Applications

We described here the development and evaluation of a fully implantable neural stimulator to control the movement of unrestrained rats remotely. Full implantation of the device was achieved by modular design and LCP packaging that could contribute to miniaturization of the implantable neural stimulator. The key technologies developed for this device, including a microelectrode array, neural stimulation circuit, inductive link charging, ZigBee telemetry, circuit integration/packaging, electrophysiology and animal experiments, can be readily extended and utilized for a much wider range of implantable neural interfaces such as those used in deep-brain stimulation (DBS), spinal cord stimulations (SCS), for BMI and other sensory and motor prosthetics. The device developed here may also be applied for accessing locations where humans or mechanical robots cannot reach. Examples of these cases are a nuclear disaster, a collapsed building due to a natural disaster, and land mine searches.

While the current system was utilized only for stimulation in this paper, this system can be easily extended to recording applications as the system structure has a lot in common with the recording devices including wireless communication, neural electrode arrays, and the packaging technology. The recording function can be readily implemented by three minor modifications: addition of an amplifier, reprogramming of the RF transceiver, and addition/tuning of the electrode array. An

amplifier chip is required to match the amplitude of the recorded signal to the input range of the analog-digital converter (ADC) included in the ZigBee transceiver chip. The RF transceiver needs to be programmed to include an uplink communication for sending out the acquired neural data to the ZigBee receiver circuit which then can be sent to a computer via UART for data collection and storage. Lastly, the stimulating arrays can be turned into recording arrays after redesign of the electrode size and material for appropriate electrochemical characteristics but using the same fabrication process. The electrode array can be tuned to simultaneously record neural signals and convey stimulation pulse. Addition of new electrode array is also possible with minor modification in channel numbers of the feedthrough and the connectors.

The metered system can be used as a closed loop neural stimulator with added neural recording capabilities. Closed-loop neural stimulation extracts useful information from neural recording data and adjusts the parameters and timing of neural stimulation. For example, in case of epilepsy, it can be used to identify the precursors before the occurrence of seizure through the neural recording and then it can prevent the occurrence of seizure through neural stimulation, and the effect of the neural stimulation can also be confirmed with neural recording [104-106]. In addition to the epilepsy, this technique can also be used for a variety of neuropathic disorders, including neuropathic pain, Parkinson's disease (PD), obsessive-compulsive disorder (OCD), and tremor [107-110]. The developed system may also be used in conjunction with the sensor. Various application is possible; a glucose sensor can be used instead of the recording electrode to control hormone secretion through neural stimulation [111-113], bladder control with a pressure sensor [114-118], and gait control using an acceleration sensor [119-124].

There is also the potential for application in low power systems. The developed neural stimulator reduces its power consumption by using power mode, and it is also possible to further reduce its power consumption by adjusting the time ratio between sleep mode and active mode. As the power decreases, the overall time in the active mode is reduced, so the device can be used for applications that is used by long cycle or applications that do not require long active times. In addition, it is possible to supply power by using the energy harvesting function. If the power efficiency of the energy harvester that can be used in the body is improved, and the power of the system is reduced, self-powering is also possible. Therefore, we are seeking an alternative power source to replace the battery in the package, as it limits the operation time and limits device miniaturization as well. Rapidly evolving energy harvesting technologies such as piezoelectricity, thermoelectricity or BFCs could be adopted as a means of the self-powering of the implanted device. Energy harvesting for implantable devices has been pioneered in several publications [44, 45, 48, 49, 125, 126], though the power output levels remain below those needed for practical applications.

4.4. Opportunities for Further Improvements

4.4.1. Weight and Size

The implantation site of the package was also an issue when designing the neural stimulator and *in vivo* experiments. We tested the feasibility of package implantation in both the back and abdominal space. A relatively large space is available in the back, but when a dummy device was implanted in the back, it hindered the movement of the spine with constantly applied mechanical stress. When

the package was implanted underneath the abdominal subcutaneous pocket, it was much easier for the rat to move around. But it also had risk that the organs in the abdomen can be affected by breathing, moving or sleeping motion. We attempted to minimize the discomfort of the rat by sophisticatedly customizing of the system based on the rat anatomy, including the cable length, electrode shape, and the surgical procedure. However, when the neural stimulator was implanted, the rats sometimes showed the signs of discomfort such as scratching the sutured area, which resulted in the exposure of the implanted package in the worst case. Therefore next version of the device with size reduction was required.

Component s	Circuit				Coil	Batter y	Packagi ng space	Sum (assemble)
	RLC s	ICs	Anten na	PCB				
Volume (mm ³)	12.0	102	11.0	144 (20×18×0.4)	189	1200	4354	6032 (29×26×8)

Table 4.4.1. Original volume of the electrical components that consist the circuitry of the neural stimulator.

The current version of implanted stimulator has a package with size of 29 mm long, 26 mm wide, and 8 mm thick. Table 4.4.1 shows the volume that each electrical components occupies. The battery is the largest component of all, and the packaging space occupies the largest volume (72.2%) in the package. It shows that the design of the packaging should be minimized. The package was designed in four steps. First, the area of the circuit was determined. All required functional modules including ZigBee telemetry, Stimulation ASIC, PMIC were integrated in a single PCB. A four-layer PCB with electrical components being mounted on both top and bottom sides was designed. Since the assembly of components in the package was intended to be stacked to minimize the area, circuit area was the standard that decided the area of the other parts. The radius of the coil was limited to 10 mm, and the battery with

similar area and lowest thickness was chosen. Then the packaging lids were designed. The packaging lids were designed as simple rectangle that is contoured at the edges. The two lids combine to form a cube, in which the electrical components are placed. Since the assembled circuitry does not shaped as a cube, it does not fit the lids well. Also, the assembled circuitry contains lots of empty space therein. The empty space comes from the areas for the placing and routing of the ASIC/RLCs, area different among the coil, the PCB, and the battery, and packaging margin that leaves 2 mm at each side, and 0.5 mm at top and bottom. These should be considered when designing new package.

To design a new package, minimization of the circuit area should be examined first which determines the maximum area the other components can utilize. Circuit minimization can be performed in two ways: reduce the size of the RLCs and ICs, and optimize the placing and routing in the PCB. First, ICs can be minimized by single-chip integration. When designing an IC, significantly large areas are occupied by package and output pins. If they are integrated together, useless pinouts can be minimized, and the areas wasted by packaging and routing can be saved.

Components	Fabricated ASIC *			RF transceiver [127]	Boost converter [128]	Rectifier [129]	Sum (assembly)
	Pulse generator	Oscillator	Regulator				
Area (original, mm ²)	30.3	8.12	4.2	36	16.2	6.96	102
Area (reference, mm ²)	4.56	0.436	0.669	3.86	3.9	0.0055	13.4

Table 4.4.2. Area of the originally used ICs and reference design that minimized the area of the ICs. *The ASIC was fabricated in 0.35 μm HV-CMOS process.

Table 4.4.2 shows the area of the ICs in the reference designs. The total area occupied by the ICs can be reduced to 13.1 % of the previous area. Also, RLCs can

be minimized. The total area occupied by RLCs is reduced to 76.3 % of the previous design when removing redundant components or unnecessary components due to IC design changes. Placing and routing was simulated with reduced ICs and RLCs. Figure 4.4.1 shows the resulting circuit board area of $12.9 \times 9.8 \text{ mm}^2$. PCB can also be miniaturized. It can be fabricated based on the copper-cladded LCP films with high melting temperature (HT-LCP; $330 \text{ }^\circ\text{C}$, ULTRALAM 3850, Rogers Corporation, USA) to utilize microfabrication process, while minimizing its thick to $150 \text{ }\mu\text{m}$.

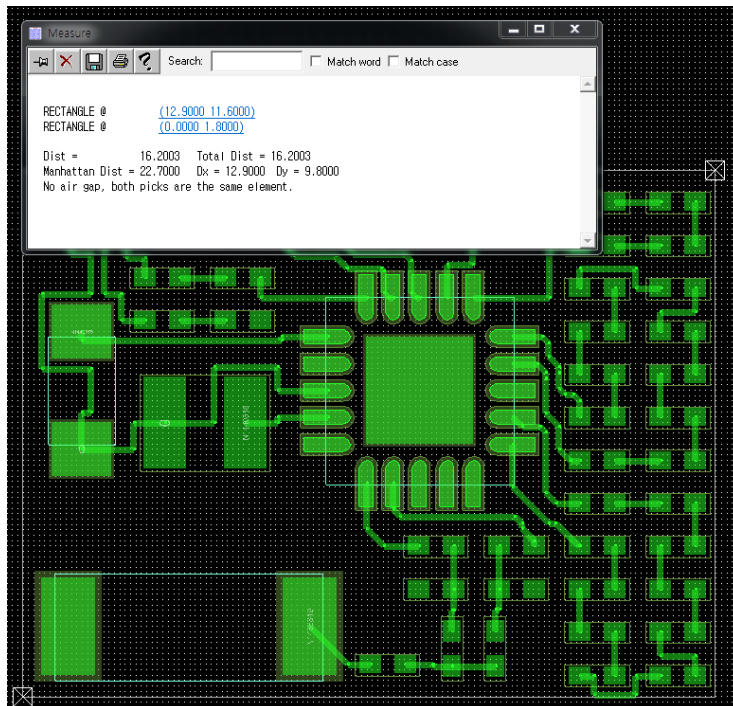


Figure 4.4.1. Simulated result of the placing and routing with reduced ICs and RLCs.

After the area of the circuit is determined, battery should be designed. The main reasons that the large batteries are used are high power consumption of the circuit and limited energy density of the batteries. Table 4.4.3 shows the power consumed by each electrical components in the neural stimulator circuit. The major power consuming part is ZigBee transceiver which consumes 83.7 % of the total power.

Therefore, the battery can be miniaturized further if the power consumption of the ZigBee transceiver is reduced. We previously devised a special power-saving scheme which automatically alternates between an active mode and a sleep mode, which could reduce the power consumption by a factor of 10. The power of the ZigBee transceiver can be further reduced. The reason why the ZigBee transceiver needs this much time is because the communication is not synchronized. The transmitter has no information about the time when the receiver is activated, so it continuously transmits the information. The receiver does not know when the transmitter is sending data, so it must check for the presence of transmitted data. If the communication timing is specified and it is shared, synchronizing the two ZigBee transceivers in the controller and neural stimulator, the operating time of the ZigBee transceiver can be reduced by up to 83.4%, and the power consumption is also reduced proportionally. As a result, the total power consumption of the neural stimulator circuit can be reduced to 22.8 %.

Components	Pulse generation ASIC		Oscillator	ZigBee transceiver	DC-DC Converter	Regulator	Sum
	Analog part *	Digital part					
Power Consumption (mW)	0.506	0.33	0.0594	11.8	0.101	1.5	14.3

Table 4.4.3. Power consumption of the ICs that constituting the current version of neural stimulator circuit. *Maximum power consumption when applying stimulation parameters of this study.

The conventional 90 mAh lithium battery was the main reason for the increase in thickness of neural stimulator. Various researches have been conducted for thinning the battery. In Lui, 2017, a battery with a voltage of 3~4 V, a thickness of 474 μm and a power density of 3.09 mA/cm^2 was reported, and similar studies were also conducted in various ways [130-134]. When the above studies applied to here,

a capacity of about 11.7 mAh, which is about 13.0 % of the original battery capacity, can be obtained with the battery size of 179 mm^3 ($16.9 \times 12.8 \times 1.42 \text{ mm}^3$, 3 layers).

Coils can also be miniaturized using same microfabrication processes with PCBs. Two layer of the copper cladded LCP films can be patterned and laminated to make a flexible 2-layer coil with thickness of $350 \text{ }\mu\text{m}$. However, power transmission efficiency of the miniaturized coil can be reduced. Receiver coils were variously modeled according to their diameter and number of turns, and their effectiveness was verified through high-frequency structural simulation. Figure 4.4.2 (a) shows an example of the model used for the simulation. As shown in Figure 4.4.2 (b-c), the maximum power transmission efficiency was obtained when the number of turns of the receiver coil was 30 and the outer diameter was 10 mm. The calculated maximum power transfer efficiency is 45.3%, which is about 59.9% of the existing coil. Though the efficiency is reduced, the inductive link can charge the battery about 5 times faster than previous device, since the capacity of the newly designed battery is reduced. In the current design, the battery capacity is large (90 mAh), and it can power the device for 23.3 hours, with the device power consumption of 14.3 mW. In the new design, the battery capacity is reduced to 11.7 mAh, but the power consumption of the device is reduced to 3.27 mW, thus the device operation time is about 14.4 hour. Though the device operation time is reduce, it can be compensated with faster charging time. The charging time of the device used to be longer than expected, due to load mismatch between the inductive link design and the actual equivalent load of the circuit and the battery, which changes in time, resulting few hours of charging time. With the faster charging time, the time efficiency of the device usage can be improved.

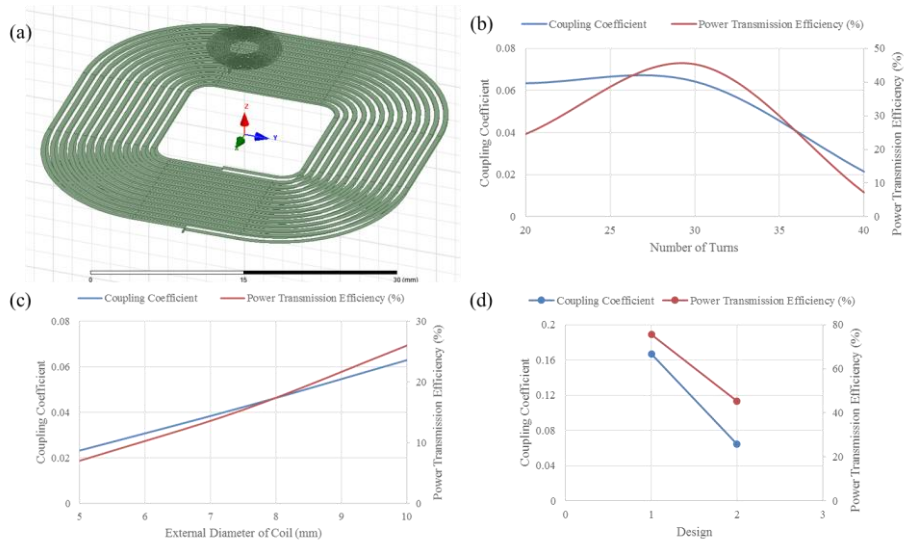


Figure 4.4.2. (a) Simulated models of the coils and simulated coupling coefficient and power transmission efficiency of the inductive link according to the design of the receiver coil: (b) the external diameter, (c) number of turns.

As a result, as shown in Table 4.4.4, the area of the circuit to be combined is $12.9 \times 9.8 \text{ mm}^2$ and the thickness is 2.7 mm in total, including 0.35 mm of coil, 1.42 mm of battery, 0.15 mm of PCB, and 1.25 mm of the maximum height of electrical components. Packaging margins of 2 mm at each corner and 0.5 mm at top and bottom side are added up to a total package size of $16.9 \times 13.8 \times 4.17$. The total volume is 863 mm³, which makes it possible to downsize to 16.1% of volume of the original devices.

Component s	Circuit				Coil	Battery	Packagi ng space	Sum (assemble)
	RLC s	ICs	Anten na	PCB				
Original Volume (mm ³)	12.0	122	11.0	144 (20×18×0. 4)	189	1200	4354	6032 (29×26×8)
Reduced Volume (mm ³)	9.16	10.7	11.0	19.0 (12.9×9.8 ×0.15)	27.5	179	716	973 (16.9×13.8× 4.17)

Table 4.4.4. Original volume of the electrical components that consist the circuitry of the neural stimulator.

4.4.2. Long-Term Reliability

Long-term reliability is an important issue for the implantable device. However, a long-term study could not be performed due to ethical issues suggested during *in vivo* experiments. Although the neural stimulation system was designed for minimizing discomfort of the rats, they sometimes showed the signs of discomfort such as scratching the sutured area, which resulted in the exposure of the implanted package in the worst case. We judged that it would be a more ethical and viable option at this stage to verify the feasibility of remote control of the rat movements with fully implanted stimulator as a proof-of-concept demonstration with the current version of the device and the surgical procedures. Therefore, the *in vivo* experiment was conducted for a single day during which the stimulation to S1 and MFB induced consistent and stable responses of the rats. In short, Contrary to our intention to miniaturize the device sufficiently, the size of the device still caused problems for long-term experiments. This problem will be eliminated if the device is significantly reduced in size through single-chip fabrication and improved battery and power efficiency as described in 4.4.1.

The bottleneck of our approach toward the long-term *in vivo* test was the animal reaction to the implantation, rather than the long-term reliability of the package of the neural stimulator. The long-term reliability of the LCP encapsulation including LCP-based electrode arrays and LCP packaging of electronics has been demonstrated in the previous studies. It was first investigated in [58] as an encapsulation material of the microelectrode array for retinal implants, resulting in 2 months of accelerated soak test at 75°C with no degradation in LCP-LCP adhesion, and 3 months of *in vivo* test in rabbit eyes with no chorioretinal inflammation. It was

demonstrated as an encapsulation of the radio frequency integrated circuit, showing stable RF characteristic *in vivo* more than 40 days, and an expected device lifetime of more than 2 years in *in vitro* accelerated soak tests [62]. It was also tested as a base material of the monolithic retinal prosthesis. At least 8 years of the device lifetime (LCP-LCP interface, LCP-metal interface, and LCP surface permeation included) was shown in *in vitro* accelerated soak tests, and stability in *in vivo* for 2.5 years [57]. Lastly, chronic reliability of as an encapsulation material of micro-electrocorticographic (μ ECoG) array were demonstrated, resulting in at least 3.4 years of lifetime in *in vitro* accelerated soak tests [60]. Also, fabrication method to enhance the adhesion of metal-polymer was studied, showing 21% enhanced mean time to failure in *in vitro* test [135].

These studies suggested that the lifetime of LCP encapsulation including all the possible water penetration paths, e.g., LCP-LCP adhesion, LCP-metal adhesion, and LCP surface permeation, is estimated to be at least a few years in the body temperature. The only interface that has not been addressed in the previous studies is the 4ch/12ch connectors sealed by dental cement. Accordingly, the reliability of the connector part was evaluated by soaking the connectors with flexible cable sealed by dental cement in 27 °C PBS while the cable ends were held above the water level for measurement. The resistance between each channel in the cable and the Pt reference electrode in PBS was monitored over time. The results showed drastic decrease in the resistance values of approximately 84.3 % after 21 days of the soaking test, but it was still 21 times larger than the resistance of the stimulation electrode used in this study. While the result suggests that the seal by the dental cement can be useful for semi-chronic test for a few weeks, the data still shows that the connector part is the weakest point in the entire system in terms of hermetic

encapsulation. The development of long-term reliable cable connectors based on monolithic LCP fabrication is required. It is expected to be applied to the general modularly designed biomedical implants.

Also, reliability of the device can be further improved by double encapsulating the metal lines. As shown in the previous study, LCP-metal adhesion is weaker than LCP-LCP adhesion [57]. An encapsulation layer that can form strong adhesion with both metal and LCP can be utilized to improve metal-LCP adhesion. There are various biocompatible coating materials that can be used as an anchoring to the underlying substrate and especially, coatings for metallic interface are being studied [136, 137]. Also, plasma treatment of substrate before the deposition, and other adhesive layer to enhance metal adhesion is an alternative solutions [138, 139].

Chapter 5

Conclusion

A remotely controlled, fully implantable neural stimulator for small animals was developed and evaluated *in vivo*. The system consists of a surface-type array for stimulating the S1 cortex for virtual sensation, a depth array for stimulating the MFB as a reward, a package encasing the stimulation electronics, and a ZigBee communication module, all of which were integrated on an LCP substrate. The stimulation parameters were optimized in a wired configuration with rats, followed by remote control of rat movement by means of the full implantation of the wireless stimulator. The device could successfully induce the rats to turn left or right and thus navigate through a 3D maze.

References

- [1] X.-Y. Kang, J.-Q. Liu, H.-C. Tian, B. Yang, Y. NuLi, and C.-S. Yang, "Fabrication and electrochemical comparison of SIROF-AIROF-EIROF microelectrodes for neural interfaces," in *2014 36th Annual International Conference of the IEEE Engineering in Medicine and Biology Society*, 2014: IEEE, pp. 478-481.
- [2] V. Di Lazzaro *et al.*, "Origin of facilitation of motor-evoked potentials after paired magnetic stimulation: direct recording of epidural activity in conscious humans," *Journal of neurophysiology*, vol. 96, no. 4, pp. 1765-1771, 2006.
- [3] A. K. Engel, C. K. Moll, I. Fried, and G. A. Ojemann, "Invasive recordings from the human brain: clinical insights and beyond," *Nature Reviews Neuroscience*, vol. 6, no. 1, p. 35, 2005.
- [4] G. Kozák, T. Földi, and A. Berényi, "Chronic Transcranial Electrical Stimulation and Intracortical Recording in Rats," *JoVE (Journal of Visualized Experiments)*, no. 135, p. e56669, 2018.
- [5] A. Dilshad and V. Uddin, "Development of efficient brain computer interface (BCI) system for stroke rehabilitation," in *17th IEEE International Multi Topic Conference 2014*, 2014: IEEE, pp. 311-313.
- [6] S. Kotov *et al.*, "Rehabilitation of stroke patients with a bioengineered "Brain-computer interface with exoskeleton" system," *Neuroscience and Behavioral Physiology*, vol. 46, no. 5, pp. 518-522, 2016.
- [7] G. S. Brindley and W. Lewin, "The sensations produced by electrical stimulation of the visual cortex," *The Journal of physiology*, vol. 196, no. 2, pp. 479-493, 1968.
- [8] R. Kanai, L. Chaieb, A. Antal, V. Walsh, and W. Paulus, "Frequency-dependent electrical stimulation of the visual cortex," *Current Biology*, vol. 18, no. 23, pp. 1839-1843, 2008.
- [9] M.-G. Lee *et al.*, "Operant conditioning of rat navigation using electrical stimulation for directional cues and rewards," *Behavioural processes*, vol. 84, no. 3, pp. 715-720, 2010.
- [10] S. K. Talwar, S. Xu, E. S. Hawley, S. A. Weiss, K. A. Moxon, and J. K. Chapin, "Behavioural neuroscience: Rat navigation guided by remote control," *Nature*, vol. 417, no. 6884, p. 37, 2002.
- [11] T. H. Moran, G. J. Schwartz, and E. M. Blass, "Organized behavioral responses to lateral hypothalamic electrical stimulation in infant rats," *Journal of Neuroscience*, vol. 3, no. 1, pp. 10-19, 1983.
- [12] B. Libet, W. W. Alberts, E. Wright, L. Delattre, G. Levin, and B. Feinstein, "Production of threshold levels of conscious sensation by electrical stimulation of human somatosensory cortex," in *Neurophysiology of Consciousness*: Springer, 1993, pp. 1-34.
- [13] D. R. Merrill, M. Bikson, and J. G. Jefferys, "Electrical stimulation of excitable tissue: design of efficacious and safe protocols," *Journal of neuroscience methods*, vol. 141, no. 2, pp. 171-198, 2005.
- [14] W. M. Chardack, A. A. Gage, and W. Greatbatch, "A transistorized, self-contained, implantable pacemaker for the long-term correction of complete heart block," *Surgery*, vol. 48, no. 4, pp. 643-654, 1960.
- [15] K. Eom *et al.*, "Enhanced infrared neural stimulation using localized surface plasmon resonance of gold nanorods," *Small*, vol. 10, no. 19, pp. 3853-3857, 2014.
- [16] W. J. Tyler, "Noninvasive neuromodulation with ultrasound? A continuum mechanics hypothesis," *The Neuroscientist*, vol. 17, no. 1, pp. 25-36, 2011.
- [17] L. Gavrilov, E. Tsurulnikov, and I. a. I. Davies, "Application of focused ultrasound for the stimulation of neural structures," *Ultrasound in medicine & biology*, vol. 22, no. 2, pp. 179-192, 1996.

- [18] W. Lee *et al.*, "Transcranial focused ultrasound stimulation of human primary visual cortex," *Scientific reports*, vol. 6, p. 34026, 2016.
- [19] H.-S. Han *et al.*, "Neural activity modulation via ultrasound stimulation measured on multi-channel electrodes," in *Proceedings of the World Congress on Engineering*, 2014, vol. 1.
- [20] G. Reich, "Near-infrared spectroscopy and imaging: basic principles and pharmaceutical applications," *Advanced drug delivery reviews*, vol. 57, no. 8, pp. 1109-1143, 2005.
- [21] K. Bennys, G. Rondouin, C. Vergnes, and J. Touchon, "Diagnostic value of quantitative EEG in Alzheimer's disease," *Neurophysiologie Clinique/Clinical Neurophysiology*, vol. 31, no. 3, pp. 153-160, 2001.
- [22] A. McGonigal, M. Oto, A. Russell, J. Greene, and R. Duncan, "Outpatient video EEG recording in the diagnosis of non-epileptic seizures: a randomised controlled trial of simple suggestion techniques," *Journal of Neurology, Neurosurgery & Psychiatry*, vol. 72, no. 4, pp. 549-551, 2002.
- [23] W. Wang *et al.*, "Human motor cortical activity recorded with Micro-ECoG electrodes, during individual finger movements," in *2009 Annual International Conference of the IEEE Engineering in Medicine and Biology Society*, 2009: IEEE, pp. 586-589.
- [24] G. Buzsáki, C. A. Anastassiou, and C. Koch, "The origin of extracellular fields and currents—EEG, ECoG, LFP and spikes," *Nature reviews neuroscience*, vol. 13, no. 6, p. 407, 2012.
- [25] S. E. Lee *et al.*, "A flexible depth probe using liquid crystal polymer," *IEEE Transactions on Biomedical Engineering*, vol. 59, no. 7, pp. 2085-2094, 2012.
- [26] S. Shin *et al.*, "High charge storage capacity electrodeposited iridium oxide film on liquid crystal polymer-based neural electrodes," *Sensor Mater*, vol. 28, no. 3, pp. 243-60, 2016.
- [27] P. Dario *et al.*, "Neural interfaces for regenerated nerve stimulation and recording," *IEEE Transactions on rehabilitation engineering*, vol. 6, no. 4, pp. 353-363, 1998.
- [28] R. E. Phillips and O. M. Youngren, "Brain stimulation and species-typical behaviour: activities evoked by electrical stimulation of the brains of chickens (*Gallus gallus*)," *Animal behaviour*, vol. 19, no. 4, pp. 757-779, 1971.
- [29] X. Chen, K. Xu, S. Ye, S. Guo, and X. Zheng, "A remote constant current stimulator designed for rat-robot navigation," in *2013 35th Annual International Conference of the IEEE Engineering in Medicine and Biology Society (EMBC)*, 2013: IEEE, pp. 2168-2171.
- [30] S. Xu, S. K. Talwar, E. S. Hawley, L. Li, and J. K. Chapin, "A multi-channel telemetry system for brain microstimulation in freely roaming animals," *Journal of neuroscience methods*, vol. 133, no. 1-2, pp. 57-63, 2004.
- [31] J. Yang, R. Huai, H. Wang, C. Lv, and X. Su, "A robo-pigeon based on an innovative multi-mode telestimulation system," *Bio-medical materials and engineering*, vol. 26, no. s1, pp. S357-S363, 2015.
- [32] R. E. Millard and R. K. Shepherd, "A fully implantable stimulator for use in small laboratory animals," *Journal of neuroscience methods*, vol. 166, no. 2, pp. 168-177, 2007.
- [33] D. Perry, D. Grayden, R. Shepherd, and J. Fallon, "A fully implantable rodent neural stimulator," *Journal of neural engineering*, vol. 9, no. 1, p. 014001, 2012.
- [34] J.-S. Lee, Y.-W. Su, and C.-C. Shen, "A comparative study of wireless protocols: Bluetooth, UWB, ZigBee, and Wi-Fi," *Industrial electronics society*, vol. 5, pp. 46-51, 2007.
- [35] Y. Zhang, X. Peng, L. Hou, J. Zhao, G. Sun, and R. Feng, "A design of hand-held remote controller for an implantable stimulator based on 51 MCU and WiFi," in *2016 13th IEEE International Conference on Solid-State and Integrated Circuit Technology (ICSICT)*, 2016: IEEE, pp. 376-378.

- [36] K. Matsushita *et al.*, "Development of an implantable wireless ECoG 128ch recording device for clinical brain machine interface," in *2013 35th Annual International Conference of the IEEE Engineering in Medicine and Biology Society (EMBC)*, 2013: IEEE, pp. 1867-1870.
- [37] N. Baker, "ZigBee and Bluetooth: Strengths and weaknesses for industrial applications," *Computing and Control Engineering*, vol. 16, no. 2, pp. 20-25, 2005.
- [38] G. Singh, R. Bhardwaj, and S. Mehla, "ZigBee: A Review 1," 2012.
- [39] P. Bogónez-Franco, R. Bragós, A. Bayés-Genís, and J. Rosell-Ferrer, "Implantable bioimpedance monitor using ZigBee," in *2009 Annual International Conference of the IEEE Engineering in Medicine and Biology Society*, 2009: IEEE, pp. 4868-4871.
- [40] P. Valdastrì *et al.*, "An implantable ZigBee ready telemetric platform for in vivo monitoring of physiological parameters," *Sensors and Actuators A: Physical*, vol. 142, no. 1, pp. 369-378, 2008.
- [41] C. M. Zierhofer and E. S. Hochmair, "Geometric approach for coupling enhancement of magnetically coupled coils," *IEEE transactions on Biomedical Engineering*, vol. 43, no. 7, pp. 708-714, 1996.
- [42] G. B. Hmida, H. Ghariani, and M. Samet, "Design of wireless power and data transmission circuits for implantable biomicrosystem," *Biotechnology*, vol. 6, no. 2, pp. 153-164, 2007.
- [43] R. R. Harrison, "Designing efficient inductive power links for implantable devices," in *2007 IEEE International Symposium on Circuits and Systems*, 2007: IEEE, pp. 2080-2083.
- [44] M. A. Hannan, S. Mutashar, S. A. Samad, and A. Hussain, "Energy harvesting for the implantable biomedical devices: issues and challenges," *Biomedical engineering online*, vol. 13, no. 1, p. 79, 2014.
- [45] G.-T. Hwang *et al.*, "Self-powered deep brain stimulation via a flexible PIMNT energy harvester," *Energy & Environmental Science*, vol. 8, no. 9, pp. 2677-2684, 2015.
- [46] K. M. Karkar, P. A. Garcia, L. M. Bateman, M. D. Smyth, N. M. Barbaro, and M. Berger, "Focal cooling suppresses spontaneous epileptiform activity without changing the cortical motor threshold," *Epilepsia*, vol. 43, no. 8, pp. 932-935, 2002.
- [47] M. Fujii *et al.*, "Application of focal cerebral cooling for the treatment of intractable epilepsy," *Neurologia medico-chirurgica*, vol. 50, no. 9, pp. 839-844, 2010.
- [48] A. Zebda *et al.*, "Single glucose biofuel cells implanted in rats power electronic devices," *Scientific reports*, vol. 3, p. 1516, 2013.
- [49] T. Miyake *et al.*, "Enzymatic biofuel cells designed for direct power generation from biofluids in living organisms," *Energy & Environmental Science*, vol. 4, no. 12, pp. 5008-5012, 2011.
- [50] D. D. Zhou, E. Greenbaum, and E. Greenbaum, "Implantable neural prostheses 2," *Biological and medical physics, biomedical engineering, ch. Technology Advances and Challenges in Hermetic Packaging for Implantable Medical Devices*, Springer London, Limited, 2010.
- [51] D. Armani, C. Liu, and N. Aluru, "Re-configurable fluid circuits by PDMS elastomer micromachining," in *Technical Digest. IEEE International MEMS 99 Conference. Twelfth IEEE International Conference on Micro Electro Mechanical Systems (Cat. No. 99CH36291)*, 1999: IEEE, pp. 222-227.
- [52] K. S. Ryu, X. Wang, K. Shaikh, and C. Liu, "A method for precision patterning of silicone elastomer and its applications," *Journal of microelectromechanical systems*, vol. 13, no. 4, pp. 568-575, 2004.
- [53] K. W. Meacham, R. J. Giuly, L. Guo, S. Hochman, and S. P. DeWeerth, "A lithographically-patterned, elastic multi-electrode array for surface stimulation of the spinal cord," *Biomedical microdevices*, vol. 10, no. 2, pp. 259-269, 2008.
- [54] J. H. Lee, "Direct Electroless copper plating on polyimide for FPCB applications," in *Materials science forum*, 2007, vol. 544: Trans Tech Publ, pp. 709-712.

- [55] H. Ning *et al.*, "Polyimide membrane based cell-electrofusion chip," *Chinese Journal of Analytical Chemistry*, vol. 37, no. 8, pp. 1247-1252, 2009.
- [56] C. P. Tan and H. G. Craighead, "Surface engineering and patterning using parylene for biological applications," *Materials*, vol. 3, no. 3, pp. 1803-1832, 2010.
- [57] J. Jeong, S. H. Bae, J.-M. Seo, H. Chung, and S. J. Kim, "Long-term evaluation of a liquid crystal polymer (LCP)-based retinal prosthesis," *Journal of neural engineering*, vol. 13, no. 2, p. 025004, 2016.
- [58] S. W. Lee, J.-M. Seo, S. Ha, E. T. Kim, H. Chung, and S. J. Kim, "Development of microelectrode arrays for artificial retinal implants using liquid crystal polymers," *Investigative ophthalmology & visual science*, vol. 50, no. 12, pp. 5859-5866, 2009.
- [59] J. Jeong, S. H. Bae, K. S. Min, J.-M. Seo, H. Chung, and S. J. Kim, "A miniaturized, eye-conformable, and long-term reliable retinal prosthesis using monolithic fabrication of liquid crystal polymer (LCP)," *IEEE Transactions on Biomedical Engineering*, vol. 62, no. 3, pp. 982-989, 2015.
- [60] V. Woods *et al.*, "Long-term recording reliability of liquid crystal polymer μ ECoG arrays," *Journal of neural engineering*, vol. 15, no. 6, p. 066024, 2018.
- [61] S. W. Lee, K. S. Min, J. Jeong, J. Kim, and S. J. Kim, "Monolithic encapsulation of implantable neuroprosthetic devices using liquid crystal polymers," *IEEE Transactions on Biomedical Engineering*, vol. 58, no. 8, pp. 2255-2263, 2011.
- [62] G.-T. Hwang *et al.*, "In vivo silicon-based flexible radio frequency integrated circuits monolithically encapsulated with biocompatible liquid crystal polymers," *Acs Nano*, vol. 7, no. 5, pp. 4545-4553, 2013.
- [63] K. S. Min *et al.*, "A Liquid Crystal Polymer-Based Neuromodulation System: An Application on Animal Model of Neuropathic Pain," *Neuromodulation: Technology at the Neural Interface*, vol. 17, no. 2, pp. 160-169, 2014.
- [64] T. Instruments, "CC2530 datasheet (Rev. B)," ed, 2012.
- [65] T. Instruments, "BQ25505 Datasheet," ed, 2015.
- [66] S. Shim *et al.*, "A handheld neural stimulation controller for avian navigation guided by remote control," *Bio-medical materials and engineering*, no. Preprint, pp. 1-11, 2019.
- [67] J.-I. Moon and S.-O. Park, "Small chip antenna for 2.4/5.8-GHz dual ISM-band applications," *IEEE Antennas and Wireless Propagation Letters*, vol. 2, pp. 313-315, 2003.
- [68] T. Yilmaz, T. Karacolak, and E. Topsakal, "Characterization and testing of a skin mimicking material for implantable antennas operating at ISM band (2.4 GHz-2.48 GHz)," *IEEE Antennas and Wireless Propagation Letters*, vol. 7, pp. 418-420, 2008.
- [69] Z. Duan, Y.-X. Guo, M. Je, and D.-L. Kwong, "Design and in vitro test of a differentially fed dual-band implantable antenna operating at MICS and ISM bands," *IEEE transactions on antennas and propagation*, vol. 62, no. 5, pp. 2430-2439, 2014.
- [70] E. Y. Chow, A. L. Chlebowski, S. Chakraborty, W. J. Chappell, and P. P. Irazoqui, "Fully wireless implantable cardiovascular pressure monitor integrated with a medical stent," *IEEE Transactions on Biomedical Engineering*, vol. 57, no. 6, pp. 1487-1496, 2010.
- [71] H. D. Yang, "Miniaturized printed wire antenna for wireless communications," *IEEE Antennas and Wireless Propagation Letters*, vol. 4, pp. 358-361, 2005.
- [72] J. Buckley, K. McCarthy, L. Loizou, B. O'flynn, and C. O'mathuna, "A dual-ISM-band antenna of small size using a spiral structure with parasitic element," *IEEE Antennas and Wireless Propagation Letters*, vol. 15, pp. 630-633, 2015.
- [73] Z. N. Chen and Y. Chia, "Impedance characteristics of trapezoidal planar monopole antennas," *Microwave and Optical Technology Letters*, vol. 27, no. 2, pp. 120-122, 2000.
- [74] S. K. Kelly *et al.*, "The Boston retinal prosthesis: A 15-channel hermetic wireless neural stimulator," in *2009 2nd International Symposium on Applied Sciences in*

- Biomedical and Communication Technologies*, 2009: IEEE, pp. 1-6.
- [75] H. Ali, T. J. Ahmad, and S. A. Khan, "Inductive link design for medical implants," in *2009 IEEE Symposium on Industrial Electronics & Applications*, 2009, vol. 2: IEEE, pp. 694-699.
- [76] M. Adeeb, A. Islam, M. Haider, F. Tulip, M. Ericson, and S. Islam, "An inductive link-based wireless power transfer system for biomedical applications," *Active and Passive Electronic Components*, vol. 2012, 2012.
- [77] S. Atluri, "A Wideband Power efficient inductive link for implantable biomedical devices using multiple carrier frequencies," 2006.
- [78] C. Fernandez, O. Garcia, R. Prieto, J. Cobos, S. Gabriels, and G. Van Der Borcht, "Design issues of a core-less transformer for a contact-less application," in *APEC. Seventeenth Annual IEEE Applied Power Electronics Conference and Exposition (Cat. No. 02CH37335)*, 2002, vol. 1: IEEE, pp. 339-345.
- [79] P. Vaillancourt, A. Djemouai, J. Harvey, and M. Sawan, "EM radiation behavior upon biological tissues in a radio-frequency power transfer link for a cortical visual implant," in *Proceedings of the 19th Annual International Conference of the IEEE Engineering in Medicine and Biology Society. Magnificent Milestones and Emerging Opportunities in Medical Engineering (Cat. No. 97CH36136)*, 1997, vol. 6: IEEE, pp. 2499-2502.
- [80] J. Seo, J. H. Wee, J. H. Park, P. Park, J.-W. Kim, and S. J. Kim, "Nerve cuff electrode using embedded magnets and its application to hypoglossal nerve stimulation," *Journal of neural engineering*, vol. 13, no. 6, p. 066014, 2016.
- [81] Z.-y. Feng *et al.*, "A remote control training system for rat navigation in complicated environment," *Journal of Zhejiang University-Science A*, vol. 8, no. 2, pp. 323-330, 2007.
- [82] L. W. Bosman *et al.*, "Anatomical pathways involved in generating and sensing rhythmic whisker movements," *Frontiers in integrative neuroscience*, vol. 5, p. 53, 2011.
- [83] Y. K. Cho *et al.*, "Neuromodulation methods for animal locomotion control," *Biomedical Engineering Letters*, vol. 6, no. 3, pp. 134-147, 2016.
- [84] M. Ciampa, *CWNA guide to wireless LANs*. Cengage Learning, 2012.
- [85] K. M. Silay *et al.*, "Load optimization of an inductive power link for remote powering of biomedical implants," in *2009 IEEE International Symposium on Circuits and Systems*, 2009: IEEE, pp. 533-536.
- [86] X. Ye *et al.*, "A portable telemetry system for brain stimulation and neuronal activity recording in freely behaving small animals," *Journal of neuroscience methods*, vol. 174, no. 2, pp. 186-193, 2008.
- [87] S. F. Cogan, "Neural stimulation and recording electrodes," *Annu. Rev. Biomed. Eng.*, vol. 10, pp. 275-309, 2008.
- [88] N. S. Davidovics, G. Y. Fridman, B. Chiang, and C. C. Della Santina, "Effects of biphasic current pulse frequency, amplitude, duration, and interphase gap on eye movement responses to prosthetic electrical stimulation of the vestibular nerve," *IEEE Transactions on Neural Systems and Rehabilitation Engineering*, vol. 19, no. 1, pp. 84-94, 2010.
- [89] S. W. Lee, D. K. Eddington, and S. I. Fried, "Responses to pulsatile subretinal electric stimulation: effects of amplitude and duration," *Journal of neurophysiology*, vol. 109, no. 7, pp. 1954-1968, 2013.
- [90] T. Rose and L. Robblee, "Electrical stimulation with Pt electrodes. VIII. Electrochemically safe charge injection limits with 0.2 ms pulses (neuronal application)," *IEEE Transactions on Biomedical Engineering*, vol. 37, no. 11, pp. 1118-1120, 1990.
- [91] D. B. McCreery, W. F. Agnew, T. G. Yuen, and L. Bullara, "Charge density and charge per phase as cofactors in neural injury induced by electrical stimulation," *IEEE Transactions on Biomedical Engineering*, vol. 37, no. 10, pp. 996-1001, 1990.

- [92] R. V. Shannon, "A model of safe levels for electrical stimulation," *IEEE Transactions on biomedical engineering*, vol. 39, no. 4, pp. 424-426, 1992.
- [93] S. Arcot Desai, J. D. Rolston, L. Guo, and S. M. Potter, "Improving impedance of implantable microwire multi-electrode arrays by ultrasonic electroplating of durable platinum black," *Frontiers in neuroengineering*, vol. 3, p. 5, 2010.
- [94] T. Chung, J. Wang, J. Wang, B. Cao, Y. Li, and S. Pang, "Electrode modifications to lower electrode impedance and improve neural signal recording sensitivity," *Journal of neural engineering*, vol. 12, no. 5, p. 056018, 2015.
- [95] E. Seker, Y. Berdichevsky, M. R. Begley, M. L. Reed, K. J. Staley, and M. L. Yarmush, "The fabrication of low-impedance nanoporous gold multiple-electrode arrays for neural electrophysiology studies," *Nanotechnology*, vol. 21, no. 12, p. 125504, 2010.
- [96] E. W. Keefer, B. R. Botterman, M. I. Romero, A. F. Rossi, and G. W. Gross, "Carbon nanotube coating improves neuronal recordings," *Nature nanotechnology*, vol. 3, no. 7, p. 434, 2008.
- [97] A. R. Harris, S. J. Morgan, J. Chen, R. M. Kapsa, G. G. Wallace, and A. G. Paolini, "Conducting polymer coated neural recording electrodes," *Journal of neural engineering*, vol. 10, no. 1, p. 016004, 2012.
- [98] S.-j. Paik and Y. Park, "Roughened polysilicon for low impedance microelectrodes in neural probes," *Journal of Micromechanics and Microengineering*, vol. 13, no. 3, p. 373, 2003.
- [99] U. GPO, "eCFR—Code of Federal Regulations," URL <http://www.ecfr.gov/cgi-bin/text-idx>.
- [100] K. Gosalia, J. Weiland, M. Humayun, and G. Lazzi, "Thermal elevation in the human eye and head due to the operation of a retinal prosthesis," *IEEE Transactions on Biomedical Engineering*, vol. 51, no. 8, pp. 1469-1477, 2004.
- [101] G. Elert, "The physics hypertextbook," *Found July*, vol. 9, p. 2008, 1998.
- [102] P. Hasgall *et al.*, "IT'IS Database for thermal and electromagnetic parameters of biological tissues. Version 4.0, May 15, 2018. doi: 10.13099, "VIP21000-04-0. Onl: www.itis.ethz.ch/database, 2018.
- [103] A. Kuhn, T. Keller, S. Micera, and M. Morari, "Array electrode design for transcutaneous electrical stimulation: a simulation study," *Medical engineering & physics*, vol. 31, no. 8, pp. 945-951, 2009.
- [104] S. Ramgopal *et al.*, "Seizure detection, seizure prediction, and closed-loop warning systems in epilepsy," *Epilepsy & behavior*, vol. 37, pp. 291-307, 2014.
- [105] C.-P. Young, S.-F. Liang, D.-W. Chang, Y.-C. Liao, F.-Z. Shaw, and C.-H. Hsieh, "A portable wireless online closed-loop seizure controller in freely moving rats," *IEEE Transactions on Instrumentation and Measurement*, vol. 60, no. 2, pp. 513-521, 2010.
- [106] S.-F. Liang, F.-Z. Shaw, C.-P. Young, D.-W. Chang, and Y.-C. Liao, "A closed-loop brain computer interface for real-time seizure detection and control," in *2010 Annual International Conference of the IEEE Engineering in Medicine and Biology*, 2010: IEEE, pp. 4950-4953.
- [107] S. Little *et al.*, "Adaptive deep brain stimulation in advanced Parkinson disease," *Annals of neurology*, vol. 74, no. 3, pp. 449-457, 2013.
- [108] P. J. Grahn *et al.*, "A neurochemical closed-loop controller for deep brain stimulation: toward individualized smart neuromodulation therapies," *Frontiers in neuroscience*, vol. 8, p. 169, 2014.
- [109] M. K. Hosain, A. Kouzani, and S. Tye, "Closed loop deep brain stimulation: an evolving technology," *Australasian physical & engineering sciences in medicine*, vol. 37, no. 4, pp. 619-634, 2014.
- [110] X.-J. Feng, E. Shea-Brown, B. Greenwald, R. Kosut, and H. Rabitz, "Optimal deep brain stimulation of the subthalamic nucleus—a computational study," *Journal of computational neuroscience*, vol. 23, no. 3, p. 265, 2007.

- [111] B. Ahrén and G. J. TABORSKY JR, "The mechanism of vagal nerve stimulation of glucagon and insulin secretion in the dog," *Endocrinology*, vol. 118, no. 4, pp. 1551-1557, 1986.
- [112] B. Ahren, R. C. VEITH, and G. J. TABORSKY JR, "Sympathetic nerve stimulation versus pancreatic norepinephrine infusion in the dog: 1) Effects on basal release of insulin and glucagon," *Endocrinology*, vol. 121, no. 1, pp. 323-331, 1987.
- [113] A. Kaneto, H. KAJINUMA, and K. KOSAKA, "Effect of splanchnic nerve stimulation on glucagon and insulin output in the dog," *Endocrinology*, vol. 96, no. 1, pp. 143-150, 1975.
- [114] E. A. Tanagho, "Neural stimulation for bladder control," in *Seminars in neurology*, 1988, vol. 8, no. 02: © 1988 by Thieme Medical Publishers, Inc., pp. 170-173.
- [115] E. A. Tanagho, R. A. Schmidt, and B. R. Orvis, "Neural stimulation for control of voiding dysfunction: a preliminary report in 22 patients with serious neuropathic voiding disorders," *The Journal of urology*, vol. 142, no. 2, pp. 340-345, 1989.
- [116] A. A. Elabbady, M. M. Hassouna, and M. M. Elhilali, "Neural stimulation for chronic voiding dysfunctions," *The Journal of urology*, vol. 152, no. 6 Part 1, pp. 2076-2080, 1994.
- [117] S. J. Majerus, S. L. Garverick, M. A. Suster, P. C. Fletter, and M. S. Damaser, "Wireless, ultra-low-power implantable sensor for chronic bladder pressure monitoring," *ACM Journal on Emerging Technologies in Computing Systems (JETC)*, vol. 8, no. 2, p. 11, 2012.
- [118] J. Melgaard and N. Rijkhoff, "Detecting the onset of urinary bladder contractions using an implantable pressure sensor," *IEEE Transactions on Neural Systems and Rehabilitation Engineering*, vol. 19, no. 6, pp. 700-708, 2011.
- [119] K. Tong and M. Granat, "Gait control system for functional electrical stimulation using neural networks," *Medical & biological engineering & computing*, vol. 37, no. 1, pp. 35-41, 1999.
- [120] R. Williamson and B. J. Andrews, "Gait event detection for FES using accelerometers and supervised machine learning," *IEEE Transactions on Rehabilitation Engineering*, vol. 8, no. 3, pp. 312-319, 2000.
- [121] J. Mantyjärvi, M. Lindholm, E. Vildjiounaite, S.-M. Makela, and H. Ailisto, "Identifying users of portable devices from gait pattern with accelerometers," in *Proceedings.(ICASSP'05). IEEE International Conference on Acoustics, Speech, and Signal Processing, 2005.*, 2005, vol. 2: IEEE, pp. ii/973-ii/976 Vol. 2.
- [122] F. Sepulveda, M. Granat, and J. A. Cliquet, "Gait restoration in a spinal cord injured subject via neuromuscular electrical stimulation controlled by an artificial neural network," *The International journal of artificial organs*, vol. 21, no. 1, pp. 49-62, 1998.
- [123] H. Lau and K. Tong, "The reliability of using accelerometer and gyroscope for gait event identification on persons with dropped foot," *Gait & posture*, vol. 27, no. 2, pp. 248-257, 2008.
- [124] M. Dimitrijevic and L.-E. Larsson, "Neural control of gait: clinical neurophysiological aspects," *Stereotactic and Functional Neurosurgery*, vol. 44, no. 1-3, pp. 152-159, 1981.
- [125] J. Olivo, S. Carrara, and G. De Micheli, "Energy harvesting and remote powering for implantable biosensors," *IEEE Sensors Journal*, vol. 11, no. 7, pp. 1573-1586, 2011.
- [126] P. Cinquin *et al.*, "A glucose biofuel cell implanted in rats," *PloS one*, vol. 5, no. 5, p. e10476, 2010.
- [127] A. Zolfaghari and B. Razavi, "A low-power 2.4-GHz transmitter/receiver CMOS IC," *IEEE Journal of Solid-State Circuits*, vol. 38, no. 2, pp. 176-183, 2003.
- [128] C. Y. Leung, P. K. Mok, and K. N. Leung, "A 1-V integrated current-mode boost converter in standard 3.3/5-V CMOS technologies," *IEEE Journal of Solid-State Circuits*, vol. 40, no. 11, pp. 2265-2274, 2005.

- [129] Y.-H. Lam, W.-H. Ki, and C.-Y. Tsui, "Integrated low-loss CMOS active rectifier for wirelessly powered devices," *IEEE Transactions on Circuits and Systems II: Express Briefs*, vol. 53, no. 12, pp. 1378-1382, 2006.
- [130] Z. Tehrani *et al.*, "Ultra-thin flexible screen printed rechargeable polymer battery for wearable electronic applications," *Organic Electronics*, vol. 26, pp. 386-394, 2015.
- [131] M. Koo *et al.*, "Bendable inorganic thin-film battery for fully flexible electronic systems," *Nano letters*, vol. 12, no. 9, pp. 4810-4816, 2012.
- [132] L. Hu, H. Wu, F. La Mantia, Y. Yang, and Y. Cui, "Thin, flexible secondary Li-ion paper batteries," *ACS nano*, vol. 4, no. 10, pp. 5843-5848, 2010.
- [133] Y. Wu *et al.*, "Entrapping electrode materials within ultrathin carbon nanotube network for flexible thin film lithium ion batteries," *Rsc Advances*, vol. 4, no. 38, pp. 20010-20016, 2014.
- [134] T. Liu *et al.*, "Ultrathin, Lightweight, and Wearable Li-O₂ Battery with High Robustness and Gravimetric/Volumetric Energy Density," *Small*, vol. 13, no. 6, p. 1602952, 2017.
- [135] T. M. Gwon, J. H. Kim, G. J. Choi, and S. J. Kim, "Mechanical interlocking to improve metal-polymer adhesion in polymer-based neural electrodes and its impact on device reliability," *Journal of materials science*, vol. 51, no. 14, pp. 6897-6912, 2016.
- [136] S. L. West *et al.*, "The biocompatibility of crosslinkable copolymer coatings containing sulfobetaines and phosphobetaines," *Biomaterials*, vol. 25, no. 7-8, pp. 1195-1204, 2004.
- [137] M. Fathi and A. Doostmohammadi, "Bioactive glass nanopowder and bioglass coating for biocompatibility improvement of metallic implant," *Journal of materials processing technology*, vol. 209, no. 3, pp. 1385-1391, 2009.
- [138] B. Wang, W. Eberhardt, and H. Kück, "Metal deposition on liquid crystal polymers for molded interconnect devices using physical vapor deposition," *Journal of adhesion science and technology*, vol. 18, no. 8, pp. 883-891, 2004.
- [139] L. Chen, M. Crnic, Z. Lai, and J. Liu, "Process development and adhesion behavior of electroless copper on liquid crystal polymer (LCP) for electronic packaging application," *IEEE Transactions on Electronics Packaging Manufacturing*, vol. 25, no. 4, pp. 273-278, 2002.
- [140] Y. Qin, M. M. Howlader, M. J. Deen, Y. M. Haddara, and P. R. Selvaganapathy, "Polymer integration for packaging of implantable sensors," *Sensors and Actuators B: Chemical*, vol. 202, pp. 758-778, 2014.
- [141] J. N. Campbell and R. A. Meyer, "Mechanisms of neuropathic pain," *Neuron*, vol. 52, no. 1, pp. 77-92, 2006.
- [142] R. Levy *et al.*, "Incidence and avoidance of neurologic complications with paddle type spinal cord stimulation leads," *Neuromodulation: Technology at the Neural Interface*, vol. 14, no. 5, pp. 412-422, 2011.
- [143] J. C. Oakley and J. P. Prager, "Spinal cord stimulation: mechanisms of action," *Spine*, vol. 27, no. 22, pp. 2574-2583, 2002.
- [144] D. D. Ohnmeiss, R. F. Rashbaum, and G. M. Bogdanffy, "Prospective outcome evaluation of spinal cord stimulation in patients with intractable leg pain," *Spine*, vol. 21, no. 11, pp. 1344-1350, 1996.
- [145] R. B. North, D. H. Kidd, J. C. Olin, and J. M. Sieracki, "Spinal cord stimulation electrode design: prospective, randomized, controlled trial comparing percutaneous and laminectomy electrodes—part I: technical outcomes," *Neurosurgery*, vol. 51, no. 2, pp. 381-390, 2002.
- [146] R. B. North, V. R. Recinos, F. J. Attenello, J. Shipley, and D. M. Long, "Prevention of percutaneous spinal cord stimulation electrode migration: a 15-year experience," *Neuromodulation: Technology at the Neural Interface*, vol. 17, no. 7, pp. 670-677, 2014.

- [147] V. M. Renard and R. B. North, "Prevention of percutaneous electrode migration in spinal cord stimulation by a modification of the standard implantation technique," *Journal of Neurosurgery: Spine*, vol. 4, no. 4, pp. 300-303, 2006.
- [148] "PRIMEADVANCED™ Multi-program neurostimulator Implant manual." Medtronic.
http://www.neuromodulation.ch/sites/default/files/pictures/prime_advanced_implant_manual.pdf (accessed 11/29, 2019).
- [149] "Precision™ M8 Adapter - Directions for Use." Boston Scientific Corporation.
https://www.bostonscientific.com/content/dam/Manuals/us/current-rev-en/90893429-09RevA_Precision_M8_Adapter_DFU_en-US_S.pdf (accessed 11/29, 2019).
- [150] J. He, G. Barolat, J. Holsheimer, and J. J. Struijk, "Perception threshold and electrode position for spinal cord stimulation," *Pain*, vol. 59, no. 1, pp. 55-63, 1994.
- [151] D. De Ridder, M. Plazier, N. Kamerling, T. Menovsky, and S. Vanneste, "Burst spinal cord stimulation for limb and back pain," *World neurosurgery*, vol. 80, no. 5, pp. 642-649. e1, 2013.
- [152] J. P. Van Buyten, A. Al-Kaisy, I. Smet, S. Palmisani, and T. Smith, "High-Frequency Spinal Cord Stimulation for the Treatment of Chronic Back Pain Patients: Results of a Prospective Multicenter European Clinical Study," *Neuromodulation: Technology at the Neural Interface*, vol. 16, no. 1, pp. 59-66, 2013.
- [153] A. Al-Kaisy, J.-P. Van Buyten, I. Smet, S. Palmisani, D. Pang, and T. Smith, "Sustained effectiveness of 10 kHz high-frequency spinal cord stimulation for patients with chronic, low back pain: 24-month results of a prospective multicenter study," *Pain Medicine*, vol. 15, no. 3, pp. 347-354, 2014.
- [154] "Physician Implant Manual 11051 Rev A." NEVRO CORP.
https://www.accessdata.fda.gov/cdrh_docs/pdf13/P130022d.pdf (accessed 11/29, 2019).
- [155] J. Jeong, S. W. Lee, K. S. Min, and S. J. Kim, "A novel multilayered planar coil based on biocompatible liquid crystal polymer for chronic implantation," *Sensors and Actuators A: Physical*, vol. 197, pp. 38-46, 2013.

Appendix

A Liquid Crystal Polymer (LCP) - Based Spinal Cord Stimulator

Abstract

Spinal cord stimulation is a therapy for the treatment of neuropathic pain. It is performed by the electrical stimulation of the spinal cord location where it is associated with the pain. Because the pain suppression persists only while the stimulation is being applied, the subject needs an implantable stimulator that can deliver continuous stimulation to the cord. Conventional devices are packaged in metal, battery operated, and with electrodes and implantable pulse generator (IPG) fabricated and implanted independently. They could operate stably in the body, but the devices have several disadvantages such as large and heavy IPG, limited implant location, and difficulty in applying wireless communication. It is mainly due to the metal package, which has large mass density and blocks electromagnetic waves.

In this study, a fully implantable spinal cord stimulator based on a biocompatible liquid crystal polymer (LCP) is suggested. Unlike conventional ones which use metal based packaging and manually assembled electrode array, the new one employs light weighted, polymer semi-hermetic packaging and microfabricated, ultrathin electrode arrays. Inductive link was utilized to transmit power and data to the implanted circuitry, and a pulse generation circuit is employed in the implanted circuits. Microfabricated electrode array and the circuitry are fabricated and monolithically encapsulated with LCP for stable *in vivo* operation and

miniaturization of the device.

To evaluate the fabricated stimulator, operation of the pulse generator circuit was examined and EIS measurement of the electrode array were performed. After the evaluation of the device functionality, the stimulator was implanted into the spared nerve injury model rats. Spinal cords of T11 level were stimulated to demonstrate the pain suppression effect of the spinal cord stimulator. Finally, several aspects of the fabricated device were discussed further.

1. Introduction

1.1. Neural Stimulator

Neural stimulator is a device that can activate of neurons to obtain physiological effects. There are a various methods to induce neuronal activation, including electrical stimulation, optical stimulation, magnetic field stimulation, ultrasonic stimulation, etc. However, most methods such as optical stimulation and ultrasonic stimulation have difficulty in daily use since a large device or high power for generating stimulation, or additional biological treatments are required to utilize these methods. In the case of electrical stimulation, highly developed semiconductor technology makes it possible to easily miniaturize the stimulation generating circuit, and small amount of power is consumed to generate the stimulation waveform. Also, effectiveness of the electrical stimulation in various fields has been evaluated for a long period, which led common use of the electrical stimulation. Electric stimulation is suitable for the stimulation method of implantable neural stimulators because of the advantages mentioned above. Implantable neural stimulator is a device that treats neuropathic diseases and complements impaired body function. The device must continuously apply stimulation to the neurons in the human body, thus it is designed

to be implanted into the body. Since the device should operate in the body, it should be miniaturized to reduce the burden and discomfort of the subject, should operate stably and safely in the body for a long time, and should be able to effectively stimulate the target site. In order to develop these parts, various researches such as miniaturization and fabrication technology of the circuitry, a biocompatible, long-term reliable packaging method, and an electrode structure depending on the position of the target location are being conducted [50, 53, 58, 59, 71, 140].

1.2. Spinal Cord Stimulator (SCS)

Spinal cord stimulation is a technique used to treat various diseases such as chronic pain, chronic mesenteric ischemia and allodynia, and it is particularly useful for the treatment of neuropathic pain. Neuropathic pain is caused by trauma or postoperative sequelae, and damage to the sensory nervous system [141]. Spinal cord stimulation delivers a stimulation current to the spinal cord location that is associated with the pain through an electrode inserted into the fat layer in the spine [142]. The delivered stimulation current suppresses nerves that conveys pain information or masks the pain with other sensory information [143]. Since the effects of pain suppression persist only while the stimulation is being delivered, the subject needs a neural stimulator, a spinal cord stimulator that can apply continuous stimulation to the cord. The spinal cord stimulator must meet following requirements. First, the insertion of the electrode into the spine should be easy, and the inserted electrode should be well fixed in order to maintain the inserted position for a long time. In implantation surgery, electrodes are inserted through a narrow gap between the vertebral bones and placed in the fat layer between the bone and the spinal cord [142].

In order for the insertion of the electrode to be successful, the electrode must be flexible so as not to damage the cord when the insertion, and it should also be rigidity to move through the fat layer to the target location. After insertion, the electrodes are located at the joint, and sporadic stresses is applied to the electrode for extended periods of time. Therefore, durability of the electrode is required to withstand it. In addition, it is necessary to develop the anchor and design the structure of the electrode so that the position of the electrode does not change during use.

According to the above requirements, the electrodes are designed in two directions: percutaneous electrode and surgical electrode. Percutaneous electrodes are designed to minimize damage to the body during insertion. It has a long insulated wire shape, and at each end, there are sites that interfacing with living bodies and openings for the connection to the circuits. The electrodes are fabricated to be flexible and also rigid, with a polymer insulation film that is thick enough to facilitate insertion through the gaps between the vertebral bones. This feature eliminates the need for intensive surgery, thus the operation of the electrode proceeds with the patient conscious. After the electrode is inserted, the stimulus is applied to check the patient's condition, and the position of the electrode is changed to find a proper location for the stimulation where shows pain relief effect [144]. For this process, the electrodes are designed to deliver stimulation current to a wide range. The disadvantage of this electrode is that dislocation occurs easily after surgery. The fat layer where the electrode is located is soft enough to be penetrated by the electrode, and the electrode is under sporadic stress due to the movement of the spine. One end of the electrode is fixed by the anchor at the bone, but the end near the cord is difficult to be fixed to the body and may be moved by external force. Indeed, dislocations of percutaneous electrodes are frequently reported, resulting in a change in the

stimulation site location and failure to stimulate the target position [145-147].

Surgical electrode is designed to compensate for the disadvantages of percutaneous electrode. Surgical electrode is an electrode designed with a large paddle-shaped head which stimulation sites are located. The paddle-shaped head expands the range that the electrode can stimulate and acts as an anchor in the spine, preventing the implanted electrode from being dislocated. However, unlike the percutaneous electrode, the surgical electrode cannot be implanted by a simple percutaneous insertion procedure due to its large-sized head. It requires laminectomy which involves bone incision for the insertion of the surgical electrode.

In common, the implantation surgery involves risk of complication such as infection or local pain. Though the cause of the complication can vary, it is known that the pressure of the electrode plate against the spinal cord which increases in proportion to the volume of the electrode has quite an impact on the occurrence [142]. Development of an electrode that is thin enough, while its mechanical properties are also similar with conventional ones is expected.

1.3. Conventional device

The efficacy of spinal cord stimulation has been demonstrated in several clinical studies, and commercial spinal cord stimulators have been developed for human use. Medtronic has developed a spinal cord stimulator combining electrodes for spinal cord stimulation with a universal implantable pulse generator (IPG; PrimeAdvanced, Medtronic, USA). The IPG is packaged in titanium, battery operated and capable of constant voltage stimulation from 2 Hz to 130 Hz and 0 V to 10.5 V [148]. The electrodes are polyurethane-insulated Pt-Ir electrodes with wire diameter of 1.3 mm

and various structures have been developed [149]. Up to two 8-channel electrodes can be connected to the IPG. Nevro Corporation has developed a spinal cord stimulation system called Senza System. It consists of two 8-channel percutaneous electrodes, an IPG and an anchor. The system is characterized by kilohertz stimulation. In general, spinal cord stimulation has a parameter of 40 ~ 60 Hz pulse rate [150, 151]. Its effect is masking pain in the target area by the paresthesia so-called tickling sensation. It is known that kilohertz stimulation desensitizes the neurons in the target nerve, which can remove pain without interlocking with other senses [152]. This effect has been proven in clinical trials [152, 153]. The IPG of the Senza System is capable of constant current stimulation in the range of 0 mA to 15 mA with frequencies up to 10 kHz [154].

The devices have common characteristics that they are packaged in metal, battery operated, with electrodes and IPG fabricated and implanted independently. They succeeded in developing a device that operates stably in the body, but the developed devices have some disadvantages. First, IPG is big and heavy. The IPGs packaged in metal have a volume of approximately 50 cm³ and a weight of about 70 g [148]. While these devices are burdensome to implant in the body, their size also limits the locations where they can be implanted. In fact, the location where the devices can be implanted are limited to the hip or abdomen, which is very different from the actual stimulation position [148, 154]. This difference causes problems such as lengthening of the electrode and tunnel under the skin created during the surgery. In addition, metal packages have limitations in implementing functions that may be useful for implanted devices such as wireless communication or wireless power transmission due to its characteristics that impedes electromagnetic waves. Another disadvantage is the separate design of the system. The system takes the form of

electrodes and IPGs that are made independently and connected through connectors after implantation. The connector is encapsulated by a silicone cover after connecting the electrodes. It is an inevitable design considering the limitation of implantable location of IPG. However, this configuration makes it vulnerable to the moisture penetration. Silicone has a significantly higher moisture penetration rate than metal packages, and the moisture passing through the cover can infiltrate through the gap between the electrode and the circuit. In this case, the channels of the electrodes are short-circuited, and in the worst case, the circuit may be affected.

1.4. Liquid crystal polymer (LCP)

LCP is a biocompatible material and has been studied as an insulating material for implantable medical devices. A semiconductor processes that can deposit a metal pattern on the film-type LCP were developed, and a neural electrodes fabricated using this process were studied [25, 58]. In particular, a depth probe that can be inserted through a dura without a guide by using the flexible and strong mechanical properties of the LCP, does not bend during insertion, and is compatible with living organisms has been developed [25, 26]. There are two types of LCPs depending on their melting point (HT/LT-LCP; 280 °C/330 °C, Vecstar CTF/CTZ series, Kuraray, Japan). Using the difference in melting point, a lamination process for attaching two objects made of LCP has been developed, and research on packaging radio communication circuits and neural prosthesis using this process has been conducted [59, 62]. The long-term reliability of the LCP encapsulation was evaluated in various study, resulting in at least 8 years of estimated lifetime [57, 60, 61].

1.5. Objective of the study

We present an implantable neural stimulator using polymer, for spinal cord stimulation. Unlike conventional ones, which use metal based packaging and manually assembled electrode array, the new ones employ light weighted, polymer semi-hermetic packaging and microfabricated, ultrathin electrode arrays. Inductive link was utilized to transmit power and data to the implanted circuitry. A pulse generation circuit is employed in the implanted circuits. Microfabricated electrode array is integrated with pulse generation circuitry by a biocompatible material called liquid crystal polymer, which has very low moisture absorption rate compared to conventional polymers such as polyimide, parylene or silicon elastomers, thereby minimizing the size of the implanted device.

2. Methods

2.1. System Overview

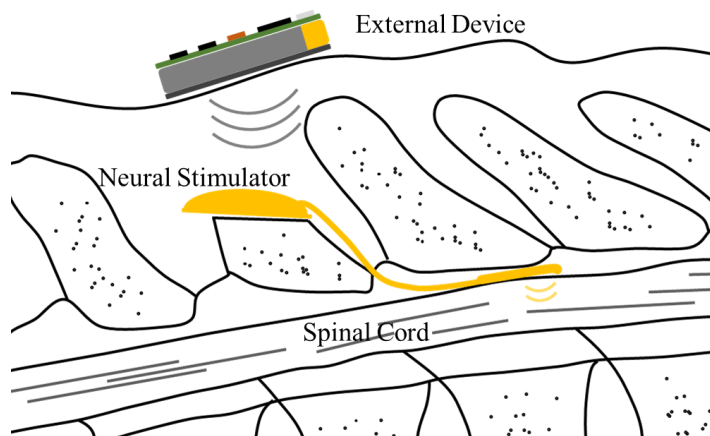


Figure 2.1.1.S. A fully-implantable neural stimulation system: electrode array part inserted in the epidural space, the package connected to the electrode is placed outside the vertebra, and an external device attached on the skin.

The Spinal cord stimulator system consists of an implantable neural stimulator

(internal device) and an external device, as shown in Figure 2.1.1.S. The implanted stimulator includes pulse generating electronics and electrode. The circuitry for wireless power/data transmission, voltage level adjustment, and neural stimulation is enclosed in the package of the internal device. The implanted electronics is encapsulated by an LCP package with a microfabricated electrodes. Figure 2.1.2.S shows the block diagram of the spinal cord stimulator system. The external device includes wireless transceiver for stimulation parameter/amplifier control, and the class-E amplifier with transmitter coil send power and data to the receiver coil in the internal device.

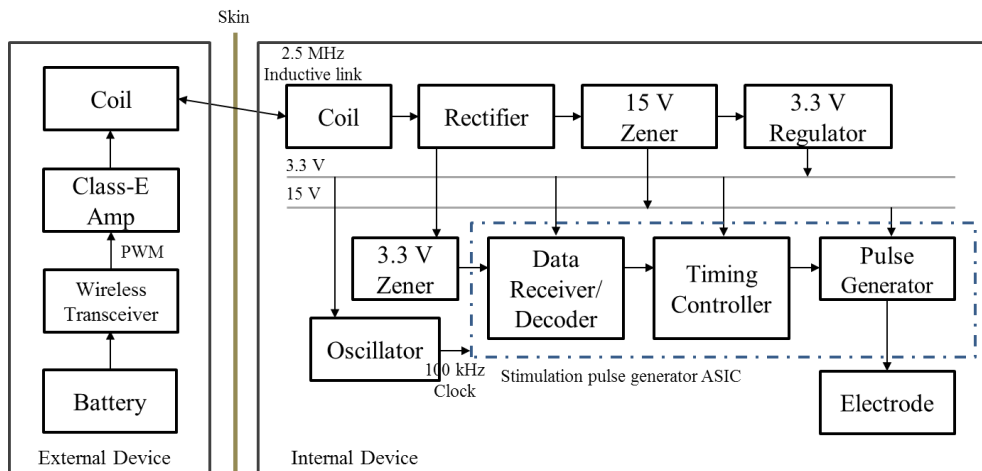


Figure 2.1.2.S. A block diagram of the neural stimulator and the external device.

2.1.1. Implantable Neural Stimulator

A pulse generator application specific integrated circuit (ASIC) is used to generate electrical stimulation pulses, and the ASIC is controlled by the received data from the external device. The data contains stimulation parameters (channel configuration, pulse amplitude, pulse width and pulse rate) and on/off commands. It is sent in form of pulse-width-modulated sinusoidal signal via the inductive link. The

received signal is first rectified, generating constant voltage to power the circuitry. The constant voltage is clamped to 15 V by a Zener diode and a capacitor. The 15 V constant voltage is fed to a regulator (NCP71533, On Semiconductor, USA) to generate 3.3V constant voltage to power an oscillator (LTC6906, Linear Technology, USA) and the digital circuitry of the ASIC. Rectified signal also go through 3.3 V Zener diode to make half-sinusoidal, pulse-width-modulated signal whose peak voltage is clamped at 3.3 V. The ASIC consists of digital circuit parts, including data receiver, data decoder and timing controller, and analog circuit part of pulse generator. The data receiver retrieve the signal, and count the number of peaks to measure the length of a pulse to reconstruct a command. The measured length represents the bit information of the pulse, 75 % as '1'. 50 % as frame bit, and 25 % as '0'. A command consists of 16 bit of '1's, '0's, and a frame bit at the end. First 3 bits represent the requested operation, and next 12 bits are operands. Last bit is an even parity bit for error detection, and the frame bit is a marker that shows where a command ends. When a non-error command is reconstructed, the data receiver decoder identify the command and extract parameters to send to the timing controller. The timing controller stores the parameters, and control the pulse generator circuit according to the stored parameters. The pulse generator is a large set of digital-analog converters (DAC). A reference current source exists, and the other DACs generate a current corresponding to a multiple of the reference current according to the control signals from the timing controller. The pulse amplitude, pulse width, and pulse rate of the generated current is controlled by the timing controller, in the range of 20~230 Hz, 10~630 μ s, 0.01~10.23 mA respectively, with ASIC input clock of 100 kHz.

A liquid crystal polymer (LCP) is used as packaging material for stimulation electronics and substrate material for electrode array. It is featured with low moisture

absorption rate, moderate flexibility, and compatibility with batch process. The circuit, the receiver coil, and the electrode is fabricated based on the LCP flexible printed circuit board, and integrated to make a monolithic package. The electrode was designed to be thin and moderately flexible for the easier insertion in the surgery.

2.1.2. Surrounding Circuitries

Surrounding circuitries include a ZigBee transceiver and a class-E amplifier that are powered by a 1300 mAh lithium battery (TW-103440, The Han, Korea). The ZigBee transceiver has a programmable flash memory that can be easily reprogrammed through C language-based interface (IAR Embedded Workbench for 8051, IAR Systems, Sweden) such that a user can change the operation algorithm of the Integrated Circuit (IC) usefully according to the intention. The ZigBee transceiver is a mixed signal circuit which consists of an RF transceiver module and an MCU (Microcontroller Unit) that controls RF communication according to the ZigBee protocol. Here we utilized commercial transceiver CC2530 model (Texas Instruments, USA). It can control various peripheral circuit integrated in the IC, including general-purpose input/output (GPIO), Analog-Digital Converter (ADC), universal asynchronous receiver-transmitter (UART), etc. In this application, the transceiver is programmed to output serially through a GPIO as PWM. The generated PWM signal is 2.5 MHz-frequency-modulated with the class-E amplifier, sent to the stimulation ASIC through the coils.

2.2. Antenna Design

2.2.1. Design of Coil Antenna

The size and the structure of the receiving coils are important factors that determines the power transmission efficiency of the inductive link. In this study, the coil for the implantable neural stimulator is fabricated based on the LCP. The characteristics of the LCP-based coil was investigated in previous study [155]. However, efficiency drop due to the misalignment of the coils were not evaluated, while it is happens easily because the location of the implanted internal coil cannot be identified. Also, new coil design was required to fit the elongated shape of the stimulator. In designing a receiver coil, shape of the coil were first determined. Oval coils that is similar with the shape of the neural stimulator were compared with rectangular coils. The coils with higher self-inductance were selected, and their power transmission efficiency with shared transmitter coil was evaluated.

2.2.2. FEM Simulation

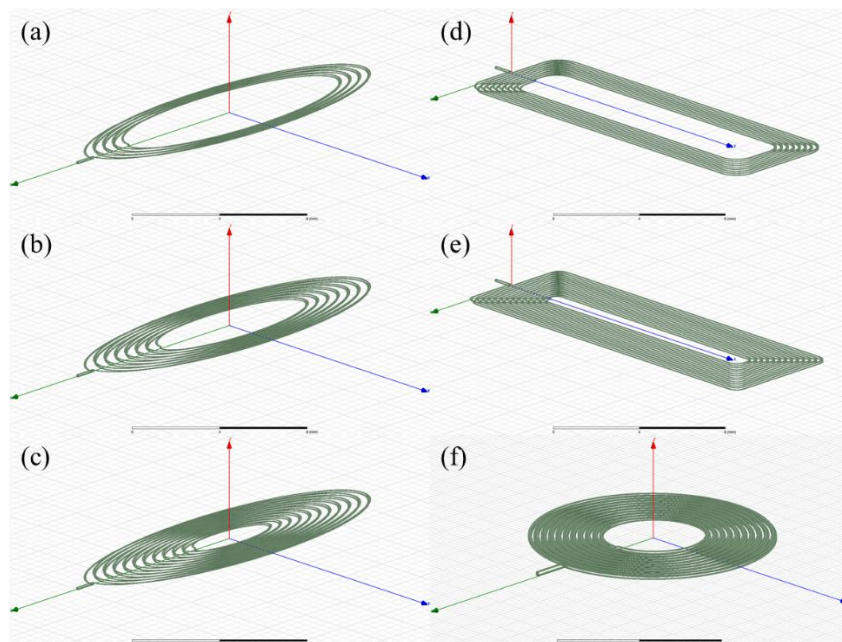


Figure 2.2.1.S. Simulation models of the coils with varying shapes and number of turns: (a) oval, 8 turns, (b) oval, 14 turns, (c) oval, 22 turns, (d) rectangular, 16 turns, and (e) rectangular, 26 turn, (f) reference coil of circular, 40 turn [155].

The characteristics of the coils according to the structure were analyzed by computer simulation software (ANSYS Electronics Desktop, ANSYS Inc., USA).

The models used for the simulation of the coil shapes are shown in Figure 2.2.1.S.

Shape	Number of Turns	Self-Inductance (μH)	Resistance (Ω)	Q-factor
Oval	8	0.145	0.829	2.75
Oval	14	0.395	1.39	4.46
Oval	16	0.22	1.19	2.90
Oval	22	0.324	1.18	4.31
Oval	24	0.104	0.656	2.49
Rectangular	16	4.89	2.88	26.7
Rectangular	18	5.66	3.19	27.9
Rectangular	20	6.4	3.5	28.7
Rectangular	22	7.08	3.79	29.3
Rectangular	26	8.36	4.47	29.4

Table 2.2.1.S. Simulated characteristics of the designed coils.

The Table 2.2.1.S. shows that the square coils have superior self-inductance and Q-factor. Rectangular coils were selected, and the coils were simulated with shared transmission coil to find their coupling coefficients. Reference coil was also simulated to compare the functionality of the newly designed coil. The receiver coils were modeled to be aligned with the transmitter coils, and misaligned models with 10 mm vertical shift from the center line, shown in Figure 2.2.2.S, were also simulated. As shown in Figure 2.2.3.S, rectangular coil with 9 turn showed the highest power transmission efficiency when misaligned. Its efficiency was even higher than the well-aligned one. Though the efficiency of the reference coil was highest when well-aligned, its drop rate were largest. It is shown that the elongated

rectangular coil can operate most stably when coil alignment is inexact.

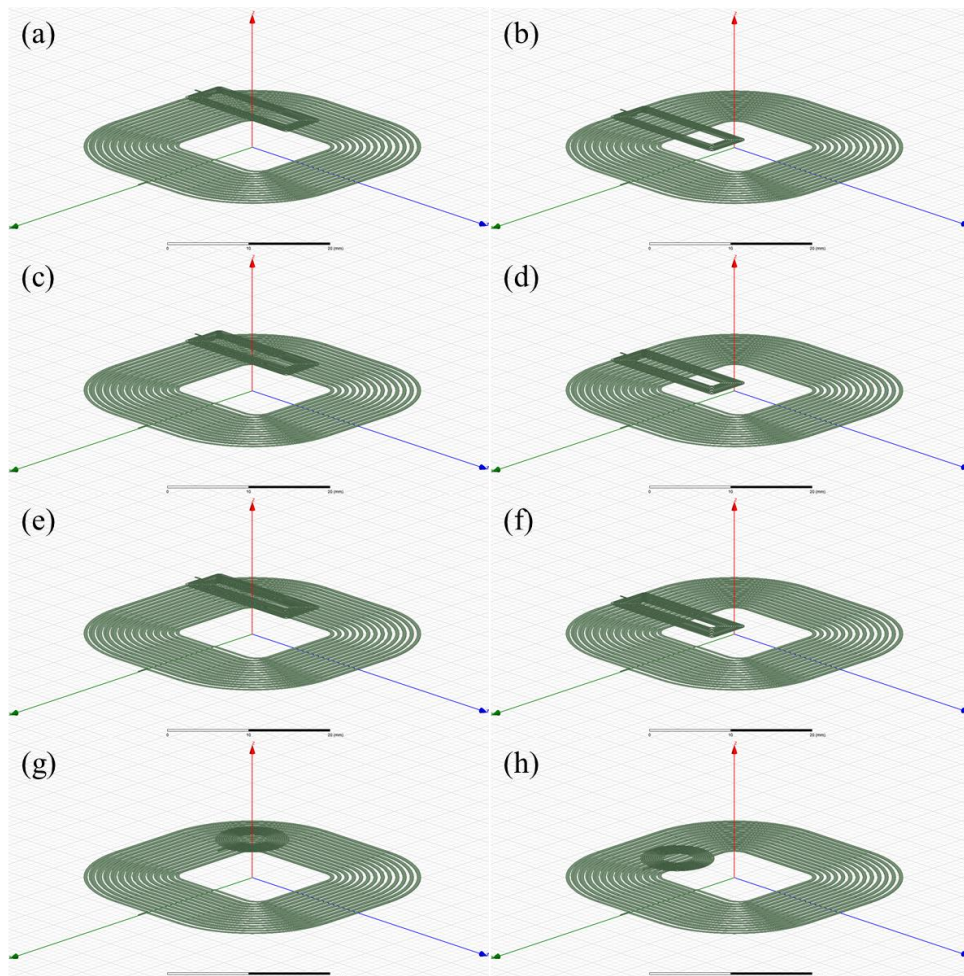


Figure 2.2.2.S. Simulation models of the coils with varying number of turns and 10 mm vertical misalignment adjusted: (a) aligned, 18 turns, (b) misaligned, 18 turns, (c) aligned, 22 turns, (d) misaligned, 22 turns, (e) aligned, 26 turns, (f) misaligned, 26 turns, (g) aligned, 40 turns (reference coil), (h) misaligned, 40 turns (reference coil) [155].

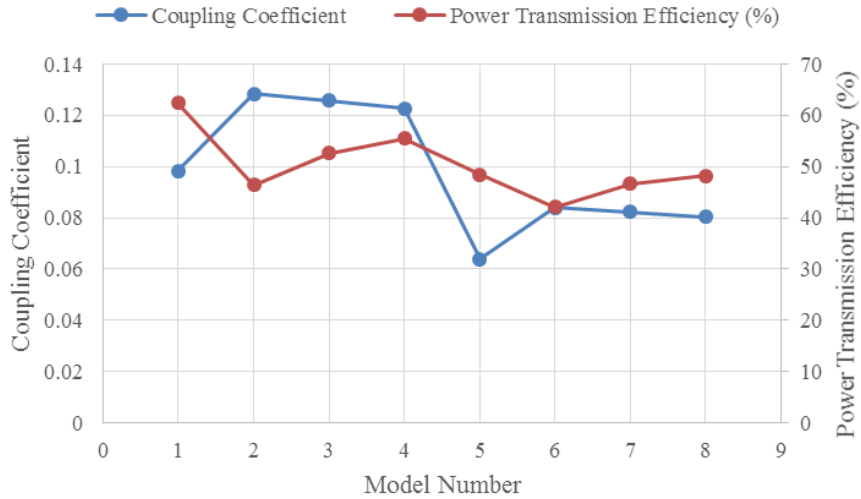


Figure 2.2.3.S. Simulated coupling coefficient and power transmission efficiency of the inductive link according to the receiver coil design: model number 1, 3, 5, 7 for well-aligned coils with 18, 22, 26, 40 (reference coil) turns, and 2, 4, 6, 8 for misaligned coils with 18, 22, 26, 40 (reference coil) turns.

2.3. Device Fabrication

2.3.1. Electrode Fabrication

The electrode arrays were microfabricated using LCP films generally following the procedures in previous publications on LCP-based neural interfaces [26, 80]. First, LCP substrate for the microfabrication was prepared. An elastomer (MED 6233, Nusil Silicone Technology, USA) layer was spin-coated on a 4-inch silicon wafer. A 25- μm -thick LCP film (HT-LCP; 330 °C, Vecstar CT-Z series, Kuraray, Japan) was cut into a 4-inch-wafer-sized pieces by using a UV laser system (Samurai System, DPSS, USA). The LCP piece is attached to a 4-inch silicon wafer using a roller. As the first procedure of metal patterning, the LCP substrate is placed under O_2 plasma condition for 180 seconds using an etcher (Oxford Etcher 80Plus, Oxford Instruments, UK); then a 50-nm-thick titanium layer and a 100-nm-thick gold layer

were deposited on the prepared LCP substrate by evaporation. A photoresist layer (AZ4620, Clariant, Switzerland) was spin-coated on the metal layer, and patterned using an aligner (MA6/BA6, SUSS MicroTec, Germany) and a developer (AZ300, AZ Electronic Materials, Luxembourg). An 8- μm -thick gold layer was electroplated on the areas without photoresist. The photoresist was removed with a stripper (AZ700, AZ Electronic Materials, Luxembourg). Remaining thin metal layer on the LCP was etched with aqua regia and HF. The outlining process were performed by lasers-machining using the UV laser system for post-lamination processes.

2.3.2. Circuit Assembly

A single-layer flexible printed circuit board and two-layer elongated-rectangular coil was fabricated with 100 μm -thick copper-cladded LCP films with a high melting temperature (HT-LCP; 330 °C, ULTRALAM 3850, Rogers Corporation, USA). The FPCB and the coil layout contain circle markers connected to the circuitry for post via generation process. The fabricated coil layer, a 25 μm -thick low-temperature LCP (LT-LCP; 280 °C, Vecstar CT-F series, Kuraray, Japan), the fabricated electrode array, 25 μm -thick low-temperature LCP, and the fabricated circuit layer were alternately aligned as shown in Figure 2.3.1.S in a pair of custom-designed aluminum jig and laminated at 285 °C for 10 min with a load of 2 kg/cm^2 in a heat press (Model 4330, Carver, USA). Two via holes were made at the markers on the circuit, and electrode parts were thinned by the laser machining. The via holes were filled with conductive epoxy (H20E, Epotek) to connect coil to the circuitry. On the fabricated circuitry, a stimulation generator ASIC was wire-bonded and the other electronics including regulator, Zener diode, oscillator, and rectifier were

mounted using conductive epoxy, baked in the oven at 100 °C for 1 hour to harden the epoxy. The outlining process were performed by lasers-machining using the UV laser system for the packaging process.

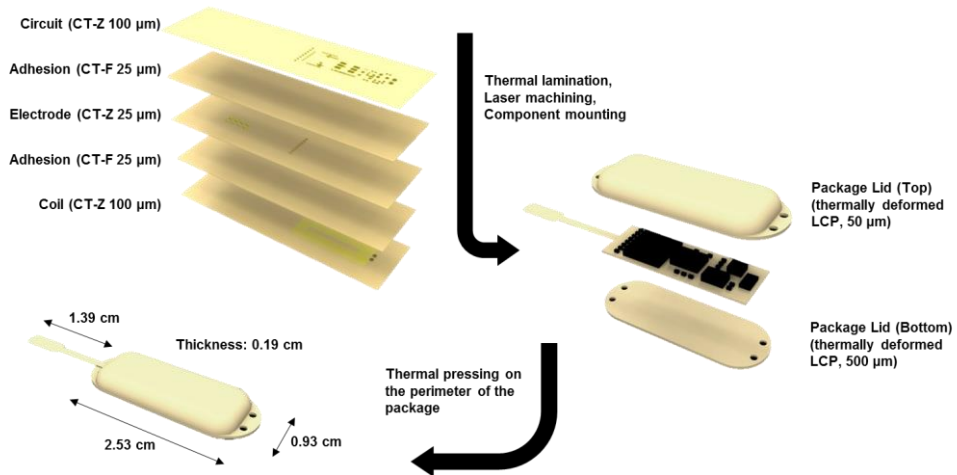


Figure 2.3.1.S. Fabrication process of the designed neural stimulator.

2.3.3. Packaging

100 μm-thick low temperature LCP and 100 μm-thick high temperature LCP films were cut in size of 20 mm × 40 mm with a laser machine. Four HT-LCP films and four LT-LCP films were alternately aligned in a pair of custom-designed aluminum jig with two slots, laminated and deformed at 290 °C for 10 min with a load of 2 Kg/cm² in the heat press to prepare two 400 μm-thick LCP package lids in desired shapes, as shown in Figure 2.3.1.S. The assembled stimulator circuit board was placed between two LCP package lids with the electrode extruded at the center of a rounded lid corner. The circuit board was fixed at the bottom lid by locally applied heat at the rim of the board. This was followed by thermal pressing on the edge of the package with a 2 mm margin for biocompatible encapsulation of the electronics to protect them from body fluids. The edge of the package was trimmed

by a laser.

2.4. Evaluation

2.4.1. Circuit Examination

The tests were conducted using a fully assembled stimulator and electrode array but without packaging to have the access to the voltage nodes for measurement. First, wireless power transmission was tested. The stimulator circuit was placed 5 mm away from the on the transmitter coil that was connected to the class-E amplifier. Voltage applied to the transmitter coil and the receiver coil, and rectified voltage (VDDH) were measured, and the capacitor connected to the receiver coil in parallel was changed according to the VDDH to maximize the received power. Then, the output voltage of the regulator, oscillator, and the 3.3 V Zener diode was measured. Finally, generated stimulation pulse waveform of the ASIC was measured.

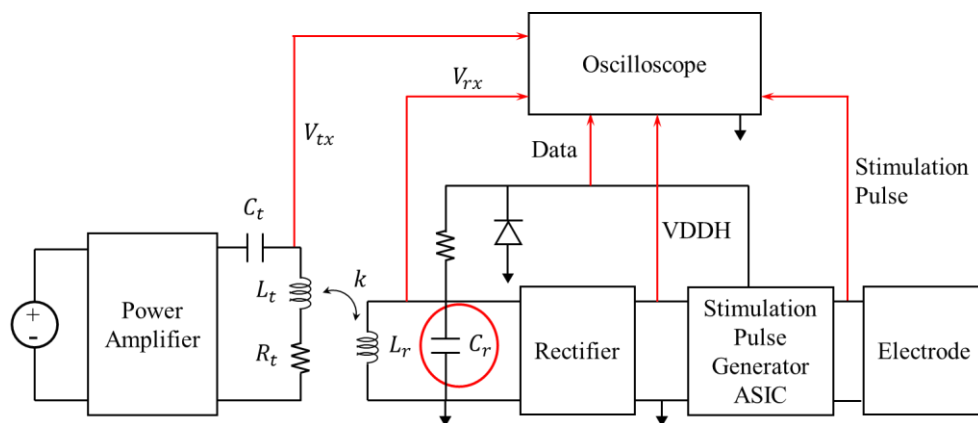


Figure 2.4.1.S. Simplified schematic of inductive link and neural stimulator. Voltage waveform measuring points are specified in the figure.

2.4.2. *In Vitro* Evaluation

The EIS of the stimulating electrode arrays was measured using a potentiostat

(SI 1287/Si1260, Solatron, UK) for frequencies ranging from 1 Hz to 100 kHz. Sinusoidal waves with a varying amplitude of 10 mV, ranging -0.8~0.6 V were applied in a phosphate buffered solution (PBS; 1X, Gibco) and the current flowing through the electrode was recorded.

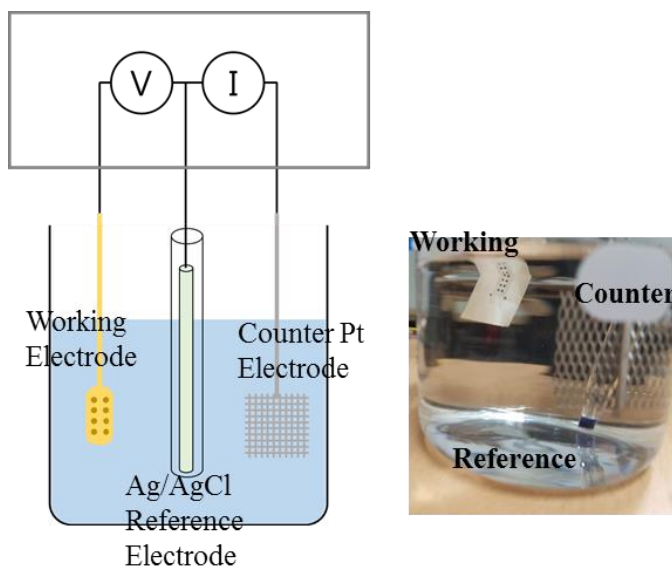


Figure 2.4.2.S. Experimental setup of the EIS measurement.

2.4.3. *In Vivo* Evaluation

Four male adult Sprague-Dawley rats (200–250 g) (Orientbiod, Osan, Korea) were individually housed in polycarbonate cages with wood chip bedding while free access to food and water was allowed. A 12 h light/dark cycle (08:00 to 20:00) was maintained at $24 \pm 2^\circ$ and $55 \pm 5\%$ humidity. The Institutional Animal Care and Use Committee of Yonsei University (IACUC no. 2016-0161, date of approval 2016.09.26.) approved the study. Spared nerve injury (SNI) model was chosen as a neuropathic pain model. Rats were anesthetized via an intraperitoneal injection of pentobarbital (40 mg/kg) (Hanlim Pharm, South Korea). The rats were injected with

0.1 mL of atropine (Huons, South Korea) 10 min before the injection to insure the stability of anesthesia. Left sciatic nerve was exposed, and the three major divisions of the sciatic nerve (tibial, sural, and common peroneal nerves) were clearly separated. To generate an efficient neuropathic pain model, the tibial and sural nerves were completely ligated and transected except peroneal nerve. Hemostasis was completed and the cut was closed with muscle and skin sutures. Implantation of the neural stimulator was performed a week after the SNI modeling. A midline skin incision was made, and laminectomy was performed to expose the spinal cord. The electrode was implanted epidurally at the T11 level. Caution was taken to avoid penetrating the dura while the insertion of the electrode. The package part connected to the electrode was placed in line with the vertebra and fixed with sutures. The wounds were closed with sutures and the stimulation test commenced three days thereafter.

Rats were placed inside acrylic cages (8×10×20 cm) on a wire mesh grid, and the external device was attached to the back of the rats. Innocuous mechanical stimulation was applied with a von Frey filament to the lateral edge of the left hind paw to measure the thresholds of the flexion withdrawal reflex in response to mechanical stimulation of the hind-limb. As a control experiment, the threshold was measured while no electrical stimulation was applied. Then, electrical stimulation of pulse rate 38.8Hz, pulse duration 120 μs, amplitude varied between 100 μA to 500 μA was applied, and the threshold varying with stimulation amplitude was determined. Each stimulation was performed in 15 minute period.

3. Results

3.1.1. Fabricated System

The fabricated implantable neural stimulator is shown in Figure 3.1.1.S. The package of the fabricated neural stimulator was 0.4 g in weight, and 2.53 cm × 0.93 cm × 0.19 cm in width, length, and thickness, respectively. The electrode was fabricated in length of 1.39 cm, 100 μm thick, shank width of 700 μm and its stimulation site area was 0.442 mm². The coil size was 1.75 cm × 0.6 cm, with self-inductance of 9.9 μH and resistance of 0.46 Ω. Two 1 mm-diameter suture holes were made on each end of the package.

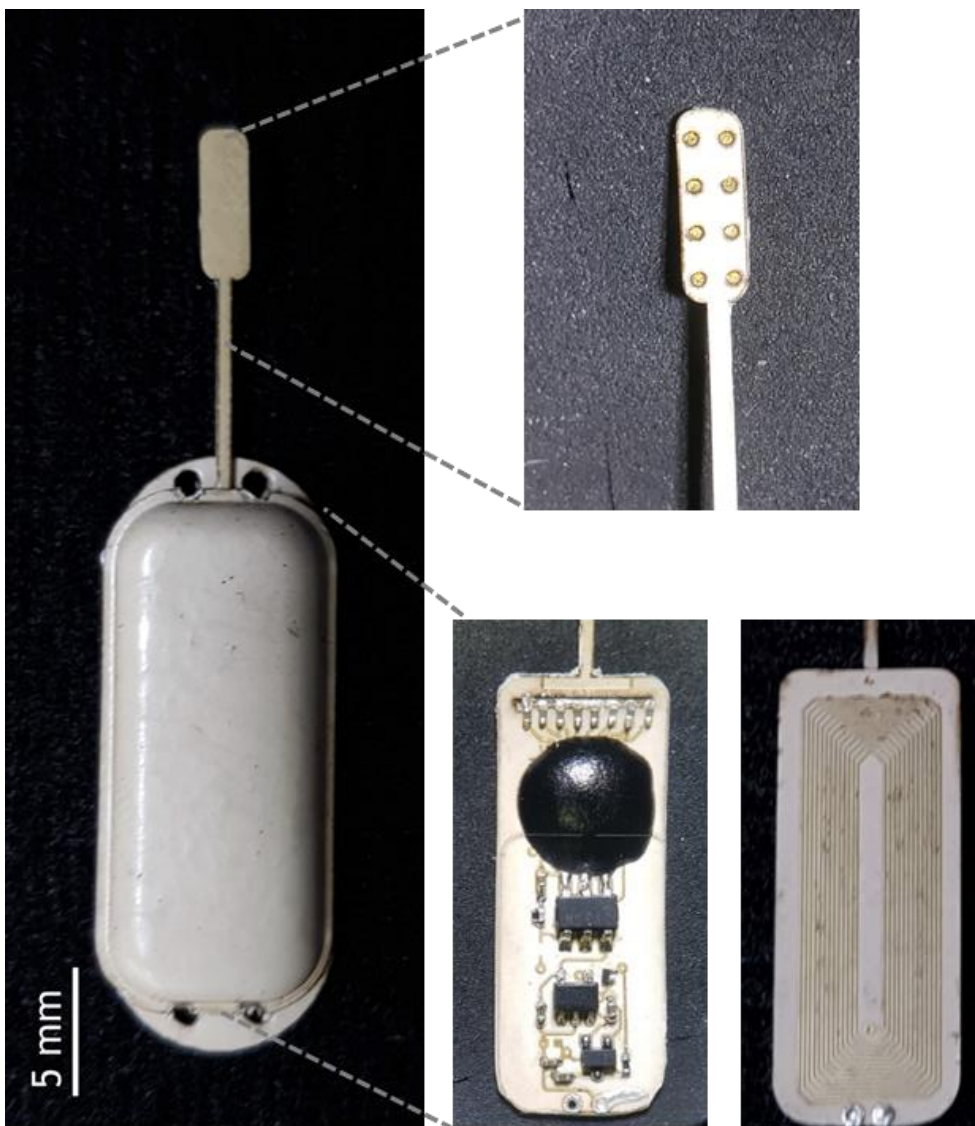


Figure 3.1.1.S. Fabricated implantable neural stimulator.

3.2.1. Circuit Examination

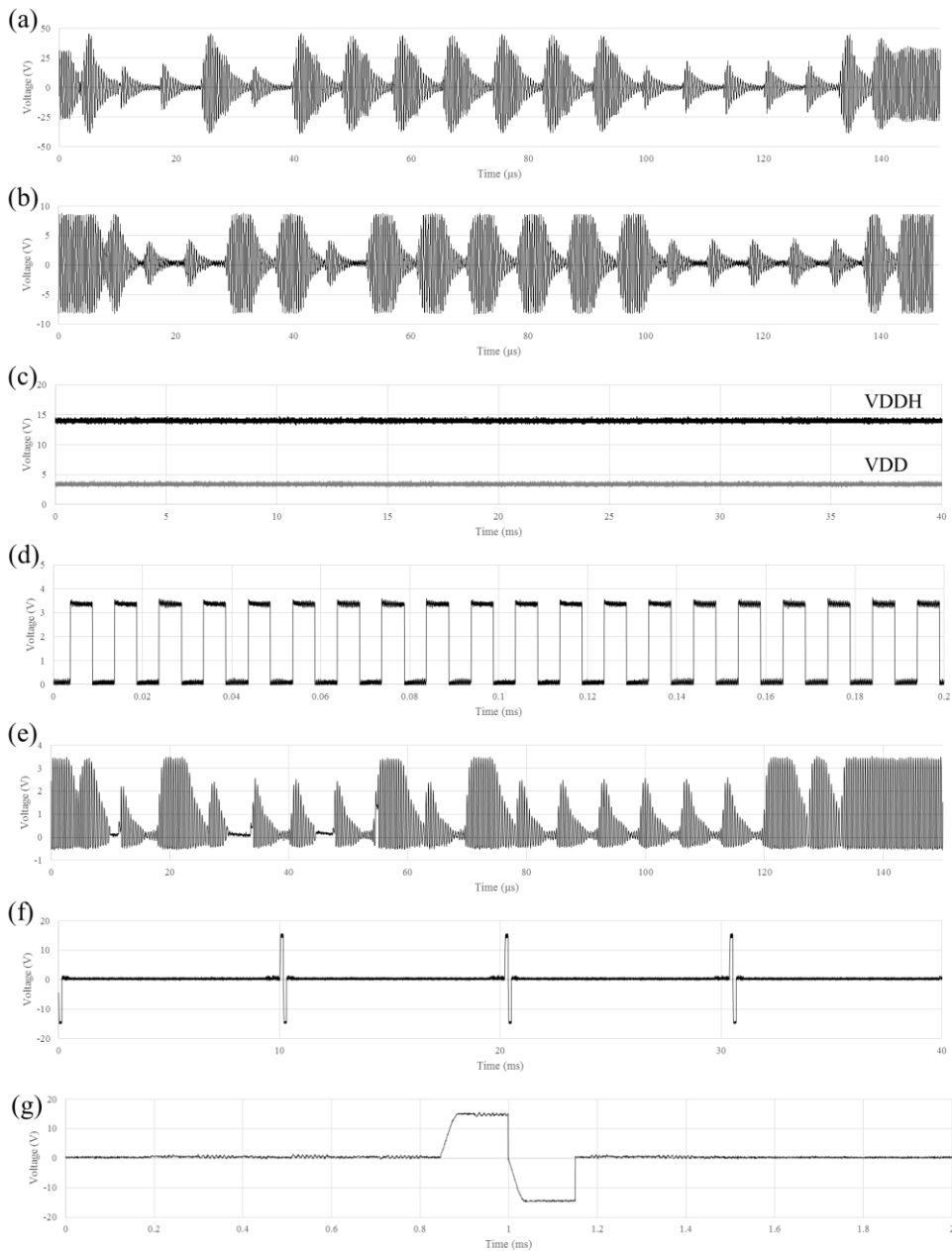


Figure 3.2.2.S. Circuit examination results: measured voltage across (a) transmitter coil, (b) receiver coil, measured output voltage of (c) 15 V Zener diode/3.3 V regulator, (d) oscillator, (e) 3.3 V Zener diode, (f, g) stimulation generator ASIC.

Figure 3.2.1.S. shows the peak voltage of the receiver coil, which is maximized

when the capacitor in parallel was 240 μF . In this condition, the operation of the stimulator circuitry was examined. The coil voltages and output voltage of the rectified, Zener diode, regulator, oscillator, and stimulation pulse generation ASIC is shown in Figure 3.2.2.S, which confirm their normal operation.

3.2.2. Electrochemical Measurements *In Vitro*

The means and the standard deviations of the EIS measurements are plotted in Figure 3.2.3.S for the magnitude and phase (a) at each frequency in the range from 0.1 Hz to 100 kHz, and a representative CV curve (b). The average impedance magnitude and charge storage capacity (CSC) of the fabricated electrodes were $166 \pm 21.9 \Omega$ at 1 kHz, and $21.2 \pm 15.7 \text{ mC}$.

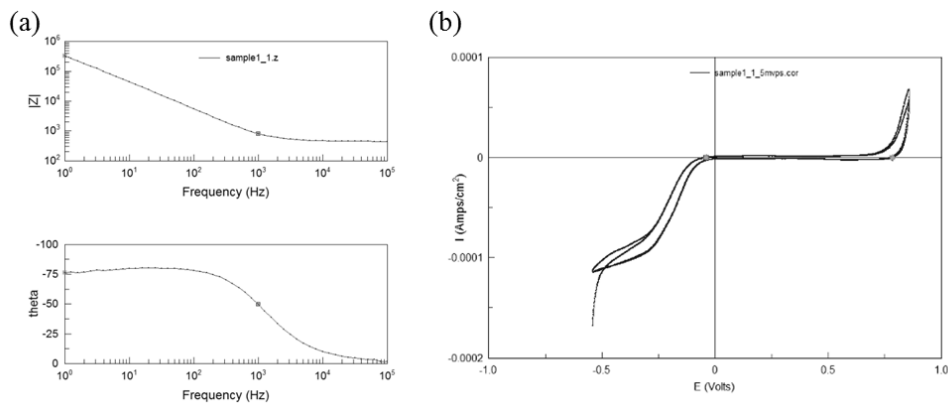


Figure 3.2.3.S. EIS measurements of the two types of fabricated electrode arrays: (a) magnitude and phase of the electrode impedance, (b) representative CV plot.

3.2.3. Animal Testing *In Vivo*

Animal care and surgical procedure were performed by Chin Su Koh, and test procedures were performed by Chin Su Koh and Minkyung Park in Department of Neurosurgery, College of Medicine, Yonsei University. Figure 3.2.4.S shows the

surgical implantation of the neural stimulator and experimental setup for Von Frey test. In the control experiment, behavioral responses of rats were observed while no electrical stimulation was applied. Paw withdrawal response was induced with small mechanical stimulation of 1.47 ± 0.623 g (Figure 3.2.5.S, PRE). After electrical stimulation of $100 \mu\text{A}$, the response threshold abruptly increased, showing the highest value of 12.7 ± 4.00 g (Figure 3.2.5.S, 100). When the stimulation intensity was increased, response threshold to the mechanical stimulation was slightly reduced.

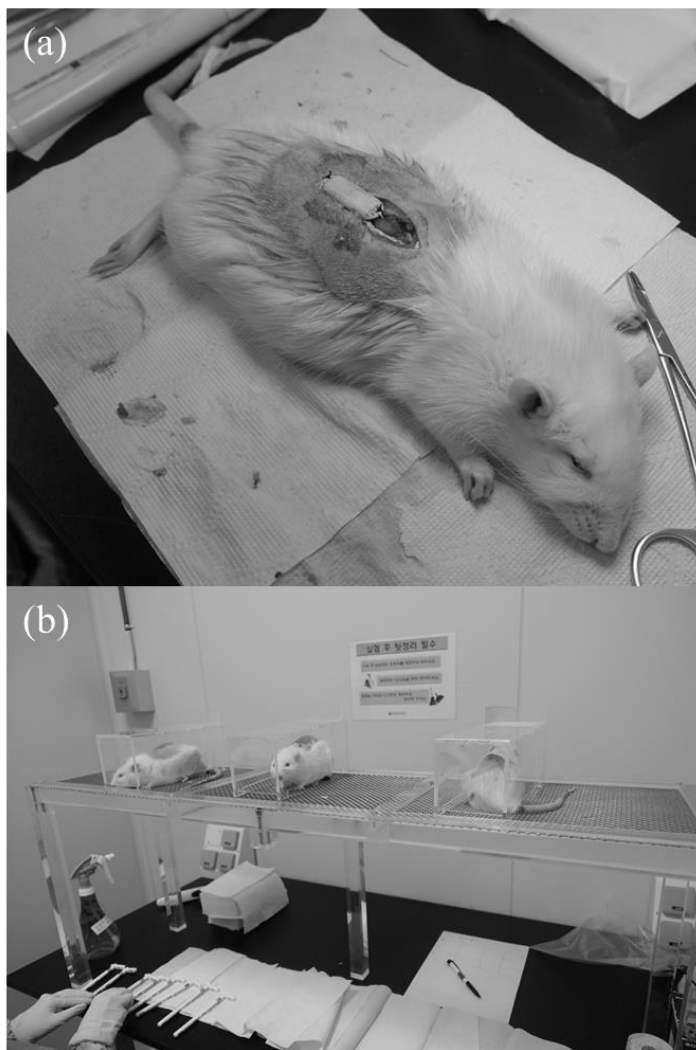


Figure 3.2.4.S. (a) Surgical implantation of a neural stimulator in a rat and (b) experimental setup for Von Frey test to determine thresholds of the flexion withdrawal reflex in response to mechanical stimulation of the hind-limb.

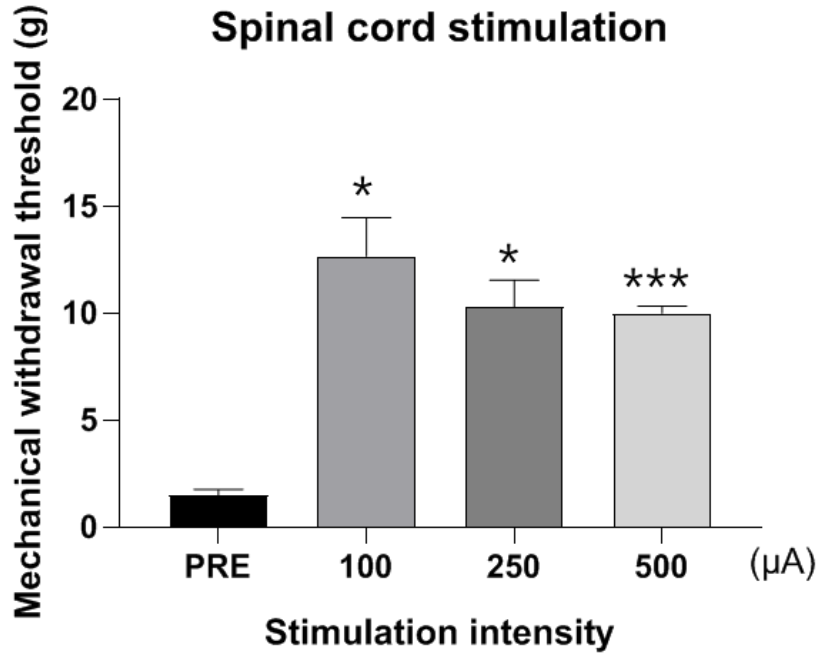


Figure 3.2.5.S. Verification of the spinal cord stimulation effect. Measured mechanical withdrawal threshold according to the stimulation intensity (* $p < 0.05$, *** $p < 0.005$).

4. Discussion

A fully implantable neural stimulator was developed for spinal cord stimulation. The fabricated neural stimulator was packaged with LCP, a biocompatible polymer, for reliable *in vivo* operation, complete implantation to animals, and device miniaturization. The whole device, including package and electrode, was monolithically fabricated based on LCP, which enabled microfabrication of 100 µm-thick electrode and small package (0.447 cm³). The device is designed to generate electrical stimulation according to the data and power sent through the inductive link, which is a key functionality of neural prosthetics. It can be readily extended and utilized for a much wider range of implantable neural interfaces such as those used

in deep-brain stimulation (DBS), for BMI and other sensory and motor prosthetics.

4.1. Comparison with Conventional Devices

Most devices that has been developed for spinal cord stimulation have metal package, and modular configuration of electrode and the package. While this configuration is inevitable for its large package, it can cause a problem in the long term stability of the device. In this study, we utilized LCP, a biocompatible polymer, to fabricate the designed spinal cord stimulator. LCP packaging lightens the device weight, and its compatibility with electromagnetic waves facilitate the use of inductive link for power and data transmission. Also, the electrode and the package of the device can be monolithically fabricated to further miniaturize the device, therefore its implantation procedure can be simplified. The volume of the fabricated device is 0.447 cm^3 , which is approximately 0.9 % of the conventional ones [148]. Monolithically fabricated device also has an advantage in long-term reliability of the device, since it has less leakage paths comparing to the device that uses connector. LCP-based devices also have several advantages in terms of electrode fabrication. First, microfabrication can be utilized such that the electrode can be fabricated in high precision and a plurality of electrodes can be easily manufactured. Also, the electrode can be custom designed according to specific need such as peripheral nerve stimulation, surface (cortex) stimulation, or deep brain stimulation by replacing only the mask used in the photolithographic process. In addition, mechanical properties of the LCP facilitate surgical insertion of the electrode. Another characteristic of the designed device is the use of inductive link. Conventional spinal cord stimulators uses battery to power the stimulation generating circuit. Since the battery capacity is

limited, the device life time is also limited, thus it requires battery replacing surgery when it is depleted. The power source of the inductive link is located outside the body, and its power is transmitted via the coils, resulting unlimited power supplement to the implanted device.

4.2. Long-term reliability

The long-term reliability of the LCP encapsulation including LCP-based electrode arrays and LCP packaging of electronics has been demonstrated in the previous studies. It was first investigated in [58] as an encapsulation material of the microelectrode array for retinal implants, resulting in 2 months of accelerated soak test at 75°C with no degradation in LCP-LCP adhesion, and 3 months of *in vivo* test in rabbit eyes with no chorioretinal inflammation. It was demonstrated as an encapsulation of the radio frequency integrated circuit, showing stable RF characteristic *in vivo* more than 40 days, and an expected device lifetime of more than 2 years in *in vitro* accelerated soak tests [62]. It was also tested as a base material of the monolithic retinal prosthesis. At least 8 years of the device lifetime (LCP-LCP interface, LCP-metal interface, and LCP surface permeation included) was shown in *in vitro* accelerated soak tests, and stability in *in vivo* for 2.5 years [57]. Lastly, chronic reliability of as an encapsulation material of micro-electrocorticographic (μ ECoG) array were demonstrated, resulting in at least 3.4 years of lifetime in *in vitro* accelerated soak tests [60]. Also, fabrication method to enhance the adhesion of metal-polymer was studied, showing 21% enhanced mean time to failure in *in vitro* test [135].

4.3. Further improvements

A kilohertz electrical stimulation can be adopted to the device. The efficacy of this method was proven in clinical studies, showing the pain reduction effect with no masking sensation. The current version of the device has maximum pulse rate of 230 Hz. The pulse rate of the electricals stimulation is controlled by the timing controller in the ASIC. Therefore, if the timing controller is revised to generate kilohertz-speed control signals, kilohertz electrical stimulation can be implemented. An ASIC was fabricated in 0.35 μm HV-CMOS process. The analog part of the ASIC was designed by Shinyong Shim in Department of Electrical and Computer Engineering, College of Engineering, Seoul National University. The ASIC was similarly designed, which consists of data receiver, data decoder, timing controller, pulse generator. The ASIC was designed to operate assuming that the data is sent through an inductive link in the form of PWM. Instruction set and the timing controller was modified. An instruction consists of 2-bit op code, 14-bit operand, single-bit even parity, and end-of-frame, as shown in Table 4.3.1.S. Four instruction that sets pulse rate, pulse duration, pulse amplitude, and stimulation on/off was designed. Especially, high/low frequency stimulation mode was designed to support electrical stimulation with pulse rate of 3.05 ~ 12.5 kHz, 34~490 Hz, respectively. The timing controller was carefully designed to update signals that controls pulse generator by single clock cycle to meet timing constraints for high frequency stimulation. The area of the fabricated ASIC was 10.2 mm² (3.2 mm \times 3.2 mm, Figure 4.3.1.S (b)) including 3.3 V regulator and frequency-tunable oscillator. The fabricated ASIC was wire-mounted on a customized PCB to test its functionality. As shown in Figure 4.3.1.S (c-d), electrical stimulation with pulse rate of over whole design range was normally

generated, and the output of the oscillator was also confirmed.

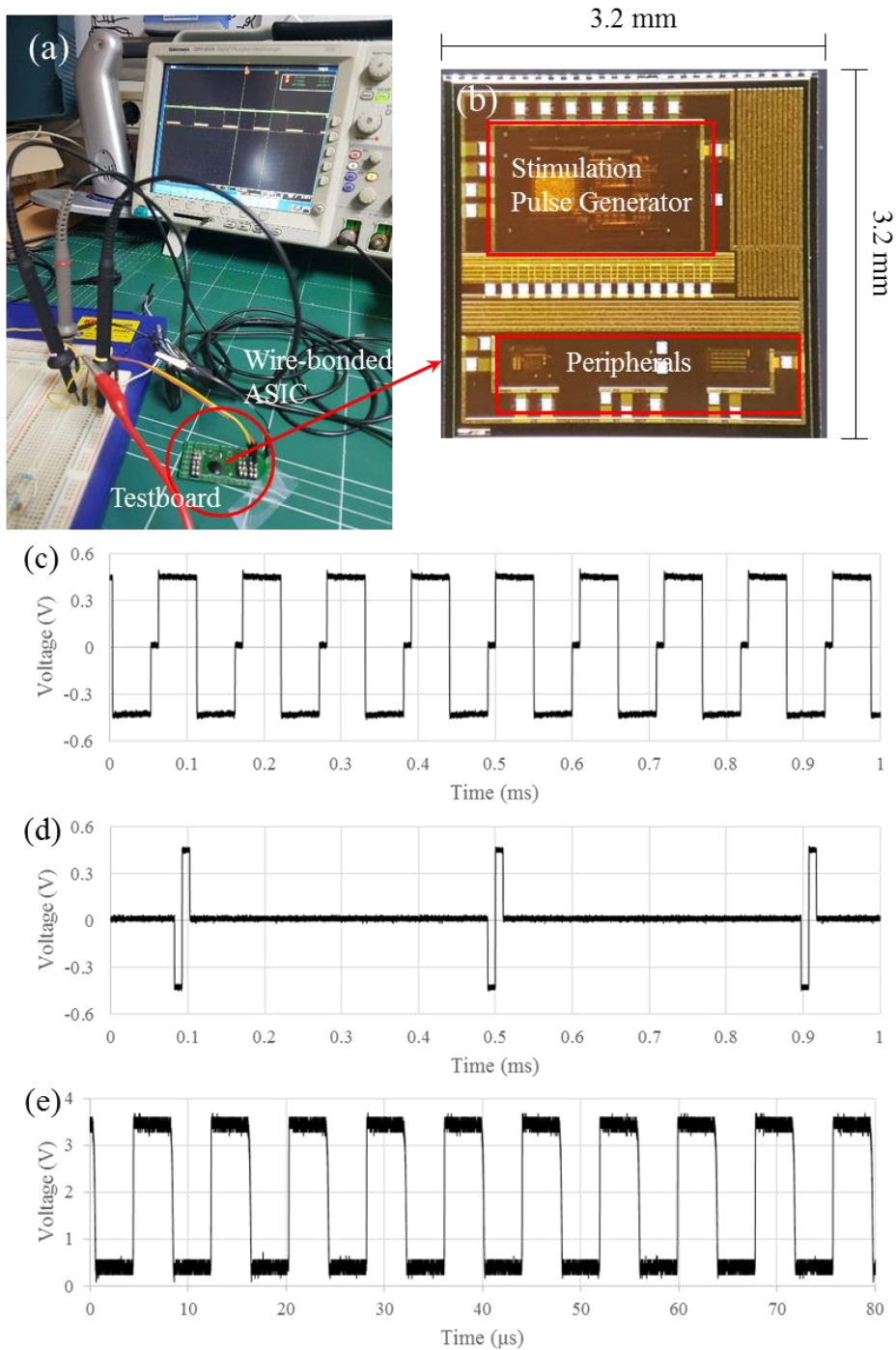


Figure 4.3.1.S. (a) Experimental setup of testing fabricated ASIC, (b) chip die of fabricated ASIC, output electrical stimulation pulse in high frequency stimulation mode with (c) maximum pulse rate, maximum pulse duration and (d) minimum pulse rate, minimum pulse duration, and (e) output of frequency-tunable oscillator.

Operation	Op Code	Operand
Pulse Rate Setting	00	MOD (1-bit), PR (6-bit)
Pulse Duration Setting	01	CH (1-bit), DR (6-bit)
Pulse Amplitude, Stimulation Site Setting	10	CH (1-bit), AM (8-bit), S (4-bit)
Stimulation On/Off	11	SW (1-bit)

Table 4.3.1.S. Instruction configuration of the fabricated ASIC. (MOD: high/low frequency stimulation mode, PR: pulse rate, CH: Channel selection, DR: pulse duration, AM: pulse amplitude, S: stimulation site setting, SW: stimulation on/off).

Utilizing the fabricated ASIC, the designed stimulator can be further miniaturized. The current version of implanted stimulator has a package with size of 25.3 mm long, 9.3 mm wide, and 1.9 mm thick. The package area is mostly determined by the circuit board area. Multiple ICs are mounted, and their package, routing space occupies most board areas. Single-chip integrated version of the ICs except the rectifier is the fabricated ASIC. The ASIC can save at least 17.0 mm² of the area from removed ICs, resulting in reduction of total package area of about 9 %. Integration of more circuit elements into single chip is expected to reduce the circuit area further.

5. Conclusion

A miniaturized fully implantable neural stimulator was developed for spinal cord stimulation. It was fabricated using LCP, a biocompatible polymer for reliable in vivo operation, complete implantation to animals, and device miniaturization. The whole device, including package and electrode, was monolithically fabricated based on LCP, which enabled microfabrication of 100 μm-thick electrode and small

package (0.447 cm³). Efficacy of the fabricated device was demonstrated *in vitro* EIS measurement and behavior test *in vivo*.

국문초록

본 연구에서는 소형 동물의 두뇌를 자극하기 위한 완전 이식형 신경자극기가 개발되었다. 소형 동물의 전기자극은 전임상 연구, 신경과학 연구를 위한 행동연구 등에 활용된다. 특히, 자유롭게 움직이는 동물을 대상으로 한 행동 연구는 자극에 의한 감각 및 운동 기능의 조절을 관찰하는 데 유용하게 활용된다. 행동 연구는 두뇌의 특정 관심 영역을 직접적으로 자극하여 동물의 행동반응을 조건화하는 방식으로 수행된다. 이러한 적용을 가능케 하는 핵심기술은 이식형 신경자극기의 개발이다. 이식형 신경자극기는 동물의 움직임을 방해하지 않으면서도 그 행동을 조절하기 위해 사용된다. 따라서 동물 내에서의 안정적인 동작과 장치의 크기가 이식형 신경자극기를 설계함에 있어 중요한 문제이다. 기존의 신경자극기는 두뇌에 이식되는 전극 부분과, 동물의 등 부분에 위치한 회로부분으로 구성된다. 회로에서 생산된 전기자극은 회로와 전선으로 연결된 전극을 통해 목표 지점으로 전달된다. 장치는 배터리에 의해 구동되며, 내장된 마이크로 컨트롤러에 의해 제어된다. 이는 쉽고 간단한 접근방식이지만, 짧은 동작시간, 이식부위의 감염이나 장치의 기계적 결함, 그리고 동물의 자연스러운 움직임 방해 등 여러 문제점을 야기할 수 있다. 이러한 문제의 개선을 위해 무선통신이 가능하고, 저전력, 소형화된 완전 이식형 신경자극기의 설계가 필요하다.

본 연구에서는 자유롭게 움직이는 동물에 적용하기 위하여 원격 제어가 가능하며, 크기가 작고, 소모전력이 최소화된 완전이식형 자극기를 제시한다. 설계된 신경자극기는 목표로 하는 두뇌 영역에 접근할 수 있는 표면형 전극과 탐침형 전극, 그리고 자극 펄스 생성 회로를 포함하는 패키지 등의 모듈들로 구성되며, 각각의 모듈은 독립적으로 제작되어 동물에 이식된 뒤 케이블과 커넥터로 연결된다. 패키지 내부의 회로는 저전력 무선통신을 위한 지그비 트랜시버, 리튬 배터리의 재충전을 위한 인덕티브 링크, 그리고 신경자극을 위한 이상성 자극파형을 생성하는 ASIC으로 구성된다. 전력 절감을 위해 두 개의

모드를 통해 사용률을 조절하는 방식이 장치에 적용된다. 모든 모듈들은 이식 후의 생물학적, 화학적 안정성을 위해 액정 폴리머로 패키징되었다. 제작된 신경자극기를 평가하기 위해 무선 동작 테스트가 수행되었다. 지그비 통신의 신호 대 잡음비가 측정되었으며, 해당 통신의 동작거리 및 데이터 스트리밍 성능이 검사되었고, 장치의 충전이 수행될 때 코일간의 거리에 따라 전송되는 전력의 크기가 측정되었다. 장치의 평가 이후, 신경자극기는 쥐에 이식되었으며, 해당 동물은 이식된 장치를 이용해 방향 신호에 따라 좌우로 이동하도록 훈련되었다. 또한, 3차원 미로 구조에서 쥐의 이동방향을 유도하는 실험을 통하여 장치의 기능성을 추가적으로 검증하였다. 마지막으로, 제작된 장치의 특징이 여러 측면에서 심층적으로 논의되었다.

주요어 : neural interface, electrical stimulation; wireless telemetry; implantable neural stimulator; polymer packaging, energy harvesting

학 번 : 2015-20952

감사의 글

심사 전까진 이 글을 쓰게 되는 순간을 기대하면서 지냈는데, 막상 쓰려니 어떤 말로 시작해야 될지 모르겠네요. 돌이켜보면 참 너무나 감사한 부분이 많았던 시간이었습니다. 처음 대학원에 들어올 때, 저는 모든 것이 맘 먹은 대로, 계획한 대로 될 줄 알았던 머리에 잉크가 덜 마른 학부생이었습니다. 하지만 5년동안 제가 진행했던 일들은 모두 한결같이 제 생각 밖에서 놀았던 것 같습니다. 처음 제작했던 회로는 기초적인 실수들로 인해 동작하지 않았고, 처음 발표했던 연구계획은 실행 불가능한 것들만 가득 차 있었으며, 제가 처음 참여했던 과제 제안 계획은 제안서 제출도 하지 못한 채 거꾸러졌고, 제가 처음 주도적으로 수행했던 연구는 제대로 된 결과를 얻지 못해 흐지부지 되었습니다. 하지만 생각지도 못했던 것을 만들어 새로 실험을 하게 되었고, 논문이 될 수 없을 거라 생각했던 것을 논문으로 작성했으며, 할 수 없을 거라 생각했던 졸업도 이제 눈 앞에 두고 있네요. 제 우물 안만 들여다볼 줄 알던 제가 이런 결과를 얻은 건 정말 다른 많은 분들의 도움이 없었다면 불가능했을 일입니다. 그분들에의 감사에 감히 우선순위를 매길 수 없어 어떻게 글을 써야 할지 난감한 마음입니다.

그래서, 일단 생각나는 순서대로 써 보려 합니다. 이 글을 쓰며 마음에 자꾸 맴도는 분은 교수님입니다. 처음 뵈었을 때 당신을 아버지처럼 생각하라 하셨던 교수님. 그리고 실제로 최근 5년동안 연구실원들 외에 자주 뵈고, 또 제게 가장 많은 영향을 주셨던 분입니다. 교수님 말씀 중 계속 생각나는 말씀이 하나 있습니다. 교만하지 말아라. 언젠가 소통이 잘 되지 않던 저를 꾸중하시며 해 주신 말씀입니다. 저는 참 자기중심적인 면이 있어서, 무언가가 마음속에서 맞다 싶으면 주변 얘기를 잘 안 듣게 되면서 마냥 밀고 나가는 성향이 있었습니다. 지금도 잘 고쳐진 것 같지는 않지만, 이 말씀을 해주시던 순간이 이러한 제 자신을 자각하고, 또 경계하게 된 순간이었습니다. 교수님께 감사했던 일들은 참 많지만, 그 중에서 이렇게 학문적인 부분과 동시에 그 외적인

부분에서도 모난 곳을 짚어주시고, 보살펴주시면서 성숙한 방향으로 나아가도록 이끌어주신 점이 지금 돌아볼 때 가장 감사한 부분인 것 같습니다. 존경하고 사랑합니다 교수님.

바쁘신 와중에 심사를 맡아주신 박병국 교수님, 장진우 교수님, 서종모 교수님, 그리고 정준수 교수님께도 감사의 말씀을 드립니다. 제가 간과한 부분들을 말씀 주시고 잘 지도해주셔서 보다 나은 논문을 쓸 수 있었습니다.

생각해보면 신용이, 광진이는 연구실에 들어오기로 결심한 순간부터, 졸업하는 순간까지 함께했네요. 대학원 지원하던 당시엔 영화 매트릭스에 나오는 시스템을 만들어보고 싶다는 디스토피아적인 꿈이 있었는데... 덕분에 연구실을 알게 되고, 들어와 같이 연구하면서 약간 비슷한 걸 만들어 보고 졸업하게 되었네요. 사실 이것 외에도 고마웠던 점이 참 많습니다. 자잘한 것들로 괴롭힌 적도 정말 많았고, 그만큼 알게 모르게 많이 기대왔던 것 같네요. 5년이라는 짧지 않은 기간 동안 일상을 함께 보내줘서 고맙고, 이제 다들 찾아 떠나는 새로운 곳에서 잘 적응하길 바랍니다.

승희형은 같은 DBS 팀으로 시작해서 연구실에서 걸어온 길이 비슷한 것 같아요. 힘들 때 같이 힘들고, 놀 때 같이 놀고, 그래서 약간 동지 같은 느낌이 있긴 해요. 그러면서도 선배로서, 혹은 형으로서 많이 의지한 것 같아요. 돌아보면 참 많은 이야기가 있지만, 어떤 걸 적어야 될지 모르겠네요. 힘들 때 위로해주신 거, 옆에서 자꾸 까불거려도 귀엽게 봐주신 거, 못난 후배 하나라도 더 챙겨주신 거, 다 고맙습니다. 그리고 마지막 심사까지 같이 준비하면서 바쁘실 때도 저 도와주신 거 고마웠어요. 삼성 가서서도 자주 봐요!

2018년을 국방부 팀으로 같이 했던 정민이형, 파워미터... 얘기를 써달라고 하셨지만 넘어갈게요. 같이 일하는 게 가장 편했고, 많이 배려해주시는 게 느껴졌었던 형. 계실 땐 몰랐지만 가시고 난 뒤엔 빈 자리가 되게 컸어요. 근데 아직도 논문 쓰는 것이 즐거우셨다는 말씀은 공감이 잘 안 갑니다 ㅎㅎ. 돌아보면 스쿼시, PT 등 운동도 같이 하고,

팩도 같이 까고 (턱으로), 이것 저것 추억이 참 많네요. 그리고, 보면서 정말 많은 걸 배운 사람이었던 것 같아요. 똑똑하게, 효율적으로 일하는 것, 가끔은 옆에서 보면서 이런 분이 박사구나 싶을 때도 있고. 연구실 생활에서 제 롤모델이었어요. 여러모로 감사하고, 행복하세요!

먼저 졸업하신 선배님들 중에도 고마운 분들이 참 많습니다. 연구실에서 처음 적응하는 것을 도와주셨던 성은이형, 항상 유쾌한 모습으로 챙겨주셨던 진호형, 연구실 자리를 챙겨주셨던 정훈이형, 연구적으로 많이 가르쳐주시고 고생해주신 태목이형, 수원누나, 연구실 분위기를 띄워주시던 정환이형, 연구 가르쳐주시고 잘 챙겨주신 경식이형, 많이 도와주셨던 채빈이형, 그리고 논문에서 심사까지 도와주신 준수형까지 참 많은 도움을 받았습니다. 다시 한번 감사드립니다.

그리고 연구하는 과정에서 도움을 주셨던 연세대학교 고진수, 신재우, 공찬호, 박민경, 그리고 이화여자대학교 조운경, 황서영, 졸업해 학교를 떠나신 김순영, 정혜선, 그리고 서울대학교 정승희, 이다혜 선생님들께 감사의 말씀을 드립니다.

사랑하는 부모님께도 감사의 말씀을 드립니다. 바쁘다는 핑계로 자주 찾아 뵈지도 않고, 많이 신경 써드리지 못해 죄송해요. 이런 불효자라도 항상 무엇을 해도 믿고 응원 해주셔서 감사합니다. 어머니 아버지, 저를 생각해주는 절반만큼이라도 되돌려드릴 수 있도록 노력할게요. 사랑해요.

마지막으로, 제가 편히 연구를 진행할 수 있었던 다른 모든 것에 감사합니다. 선배들이 구비해 놓은 연구실 실험 도구들, 학교/학부에서 지원해주는 라이선스, 연구할 목표와 연구생활을 이어나갈 인건비를 지원해 준 과제, 그리고 많은 참고가 된 선행논문들. 무엇 하나라도 없었더라면 제 연구과정은 보다 많이 험난했었을 것입니다. 이처럼 제 박사 논문은 참 많은 도움을 받아 완성되었습니다. 논문뿐만 아니라, 제가 이루어 온 다른 것들도 마찬가지로이겠지요. 앞으로 보다 겸손한 마음으로, 보답하는 마음으로 살아가겠다고 다짐하며 이 글을 마치려고

합니다.

2020년 1월 17일

윤승현 올림.